Sustained Release of Growth Factors from Hyaluronic Acid Hydrogels and Polyethylene-Glycol Microparticles for Axonal Growth

Pablo Ramos Ferrer

A dissertation submitted in partial fulfillment of the

requirements for the degree of

Doctor of Philosophy

University of Washington

2023

Reading Committee:

Chair: Shelly Sakiyama-Elbert

Elizabeth Nance

Miqin Zhang

Program Authorized to Offer Degree:

Chemical Engineering

University of Washington

Abstract

Sustained Release of Growth Factors from Hyaluronic Acid Hydrogels and Polyethylene-Glycol Microparticles for Axonal Growth

Pablo Ramos Ferrer

Chair of the Supervisory Committee:
Shelly Sakiyama-Elbert
Bioengineering Department

The central nervous system, unlike other tissues, lacks the ability to spontaneously regenerate. During spinal cord injury, the disruption of axonal pathways is one of the main causes of functional loss. Neurotrophin-3 (NT-3) and insulin-like growth factor-1 (IGF-1) are two growth factors that have been shown to improve axonal growth and functional recovery in several studies, but there is a lack of effective delivery methods capable of maintaining their biological activity. In this work, we explored the feasibility of using injectable hyaluronic acid (HA) hydrogels and polyethylene glycol-diacrylate (PEG-DA) microparticles as platforms for sustained delivery of bioactive NT-3 and IGF-1, respectively. HA hydrogels were successfully synthesized using a polyethylene-glycol (PEG) dimaleimide crosslinker and characterized chemically and mechanically. The stiffness of the hydrogels was tuned to match that of central nervous tissue. Similarly, PEG-DA MPs were fabricated with acrylic acid as a comonomer and characterized. In the case of HA and NT-3, the drug release was measured, and the delivery mechanism was found to be controlled by electrostatic interactions between the negatively

charged HA and the positively charged NT-3. IGF-1 showed a similar interaction when loaded onto and released from the PEG-DA MPs, displaying higher binding when the concentration of acrylic acid present was increased. The presence of affinity binding between the negatively charged polymeric systems and cationic proteins enabled control over the loading and release of the growth factors. The biological activity of the released NT-3 and IGF-1 was confirmed using a dorsal root ganglion assay. The concentration of both growth factors in the media was correlated to the axonal growth of primary sensory neurons, as well as that of stem cell-derived motoneurons and interneurons to more closely match the type of cells that are present in the spinal cord. A synergistic effect on neurite outgrowth was found for the combination of NT-3 and IGF-1, confirmed via phosphorylation of ERK1/2 in the shared downstream signaling pathway of both growth factors. The hydrogel provided an attractive platform for tissue sparing and neural fiber sprouting when neurons were cultured within the scaffolds and were shown to extend neurite processes. The MPs showed high cytocompatibility, suggesting their potential to be translated from *in vitro* to *in vivo*. This dual delivery system presents a promising alternative to current treatments for SCI but further work is needed to confirm their effect on *in vivo* axonal growth and functional recovery.

Table of Contents

List of Figures

Acknowledgements

To begin, I would like to thank everyone that I have had the pleasure of working with both at The University of Texas at Austin and the University of Washington during my work on this project. First and foremost, I want to thank Dr. Sakiyama-Elbert for her continuous guidance, mentorship, and encouragement throughout these 5 years. You inspired me and pushed me to become a better scientist, a better scholar and a better writer. Thank you for letting me explore my interests and supporting me to find my own path. I also extend my sincere appreciation to the members of my thesis committee at UW, and my old committee at UT, for their constructive feedback and insightful suggestions that significantly enhanced the rigor and quality of this work.

Working in the Sakiyama-Elbert lab has provided me with a number of amazing relationships. I am grateful to Thomas Wilems, Nick White and Jennifer Pardieck for their unselfish advice, teaching me how to think critically and showing me what to strive for as a graduate student. To my lab mates Sanju Vardhan, Tyler Jordan, and Hayley Lyndsay, thank you for keeping the lab running and making Seattle a new home after moving across the country. To the rest of my colleagues: Bill Wang, Jaewon Lee, Mary Salazar, Lori Won and Alaynah Murphy, you made the Sakiyama-Elbert lab a great environment to work in.

To my girlfriend Laura, my best friend and my biggest supporter during this past half decade. Your constant patience and love have carried me through the ups and downs of this journey. I could not hope for a better companion for life and look forward to our future.

To my graduate school roommates and friends Giannis, Edwin and Yiannis. Living abroad is never easy but you made our house a welcoming, friendly place to call home in Austin and Seattle.

To my managers and colleagues at GSK and Merck, I am grateful for your mentorship, career guidance and advice. Working with and learning alongside scientists with decades of experience in the pharmaceutical industry helped me understand the big picture and the importance of developing new drugs. My time in Boston showed me there is a whole city passionate about biotech and convinced me to move back after graduation.

To all my previous teachers and professors, thank you for instilling in me a sense of curiosity and encouraging me to ask questions. Special thanks to Ms. Bachman, my high school chemistry teacher at SAS, who taught me that science was awesome and inspired me to choose my career.

Por último, quería dar las gracias a mi familia. Gracias a mi padre, César y a mi madre, Lola. Vuestro apoyo, paciencia y cariño incondicional ha hecho posible que viva esta aventura y siga luchando por mis sueños. Vosotros me enseñasteis la importancia de la educación y la formación, y estaré siempre agradecido por los sacrificios que habéis hecho por mi. A mi hermano, Carlos, por inspirarme, cuidarme, y empujarme a ser mejor cada día. No querría haber crecido y compartido todos mis éxitos y fracasos con nadie más.

Pablo Ramos Ferrer

University of Washington

October 2023

"We're still pioneers, we've barely begun. Our greatest accomplishments cannot be behind us, because our destiny lies above us."

Chapter 1

Introduction

1.1 Overview

Spinal cord injury (SCI) is a severe medical condition with devastating consequences for the patients resulting in the partial or total loss of sensory and motor function below the site of injury. The tissue damage disrupts axonal pathways and the surrounding vasculature, while the cell death results in inflammation and the formation of a fluid-filled cystic cavity surrounded by a glial scar. This lesion environment has been shown to be inhibitory to axon growth and is one reason for the impaired ability of the central nervous system (CNS) to regenerate (Lu et al., 2015; O'Shea et al., 2017). Experimental approaches to treat SCI include the use of scaffolds or biomaterials for cell transplantation or delivery of therapeutic agents. One example is the implantation of polymeric scaffolds in the site of injury. These are meant to fill the injury defect and provide support for cell infiltration into the lesion after SCI (Austin et al., 2012; Johnson et al., 2010; Koffler et al., 2019; Lampe et al., 2013; J. Park et al., 2010; Seidlits et al., 2010; S. J. Taylor et al., 2004; Thompson et al., 2018; Wilems & Sakiyama-Elbert, 2015; Ziemba & Gilbert, 2017). However, scaffolds alone are not sufficient to achieve functional recovery, and the biomaterials must be able to present physical or chemical cues to promote cell migration and axonal extension within the scaffold and ultimately back into the host tissue. Extracellular matrix proteins or binding motifs can serve as biochemical cues to increase host cell adhesion and ingrowth (Deister et al., 2007; Hou et al., 2005; Ishihara et al., 2018). Another focus area is the use of the scaffolds as platforms for drug delivery of therapeutic molecules (Ansorena et al., 2013; Burdick et al.,

2006). The neuroregenerative and neuroprotective capability of neurotrophins and other growth factors can be exploited to increase axonal growth and improve functional recovery in several preclinical studies. Two growth factors that have gained increased attention due to their neuroregenerative potential are neurotrophin-3 (NT-3) and insulin like growth factor-1 (IGF-1) (Anderson et al., 2018; Rao et al., 2018). For these therapeutic agents to exert the right effect on injured neurons in the spinal cord, the delivery mechanism must be controlled, and their biological activity must be maintained following encapsulation and release. Local delivery using hydrogels has shown promise as drugs can reach the injection or implantation lesion microenvironment and be released with temporal control by finely tuning the characteristics of the hydrogel scaffold.

In this work, we have developed two distinct but combinatory drug delivery systems that exploit affinity-based release of growth factors. We first tuned a hyaluronic acid-based scaffold to deliver biologically active NT-3 *in vitro*. We synthesized methylfuran-functionalized hyaluronic acid, crosslinked with polyethylene glycol-dimaleimide and characterized the chemical and mechanical properties of the resulting hydrogels. We carried out release studies to evaluate the sustained release of bioactive molecules, including NT-3. We have also tested the biological activity of the NT-3 that is encapsulated and released using neurite outgrowth experiments from both primary neurons and stem cell-derived neurons *in vitro*. Alternatively, we also developed a microparticle-based drug delivery system based on polyethylene glycol-diacrylate. Using precipitation polymerization, we synthesized PEG-Diacrylate-based microparticles that were capable of encapsulating IGF-1. By incorporating acrylic acid into the formulation, we developed an affinity-based release system in which the amount of IGF-1 bound and released could be controlled. This study presents controlled

delivery of NT-3 from HA-based hydrogels and IGF-1 from PEG-DA microparticles as a promising approach to promote axonal growth.

1.2 Spinal Cord Injury

Spinal cord injury is a severely debilitating condition of the central nervous system that currently affects over 290,000 people just in the United States, with a range between 250,000 to 380,000 (Lasfargues et al., 1995; *National Spinal Cord Injury Statistical Center, Traumatic Spinal Cord Injury Facts and Figures at a Glance. Birmingham, AL: University of Alabama at Birmingham*, 2023). There are approximately 17,500 new cases every year, with an average incidence of 54 cases per one million people in the US, excluding the instances where the patient dies at the SCI incident location, based on analysis of survey data from the US Nationwide Inpatient Sample databases (Jain et al., 2015).

As it is characteristic of this type of injury, most SCI cases involve traumatic events. The most common cause is vehicle and car crashes, representing almost 40% of SCI cases, followed by falls (accidental or physiological) at 30% of the total. Violent acts, including physical altercations and gunshot wounds, account for almost 15%, while the remaining causes are split between accidents during recreational or sports events, and other accidents during medical and surgical procedures (*National Spinal Cord Injury Statistical Center, 2019*).

SCI patients suffer from a wide range of complications that often impair their ability to carry out daily activities. Depending on the severity, location and type of injury, individuals suffering from SCI may experience from loss of sensory perception and muscle weakness, to full paralysis in the most severe cases. Other indications include improper bladder function, abnormal sweating, and pain and spasticity due to improper function of

neural circuits. Due to the complex and multifaceted nature of SCI, a comprehensive approach to management and treatment of the condition is required. As mentioned, SCI results primarily from traumatic events and its severity is heavily dependent upon the initial forces received by the tissue as well as the level where the injury occurs. The majority of cases can be divided into complete and incomplete SCI, with the most common outcomes are paraplegia or tetraplegia, and partial loss of sensory and motor function, respectively. The specific type of injury is dictated by the spinal cord section affected. The spinal cord is divided into four sections, from top to bottom: cervical, thoracic, lumbar and sacral. Cervical injuries affect the neck and head region (vertebrae C1 – C7) and are the most severe type of SCI, often resulting in tetraplegia or complete loss of feeling and movement below the shoulders. Damage to the thoracic region (T1 – T12) may result in paraplegia along with loss of bladder function, but most patients tend to retain arm and hand function. Lumbar (L1 – L5) and sacral (S1 – S5) injuries are less severe, affecting the hips and legs. In many cases individuals are still able to walk, in some instances with the help of braces or other aids.

In addition to these symptoms that can significantly impact an individual's quality of life, this condition incurs serious financial and societal costs. According to the National SCI Statistical Center, lifetime healthcare costs of a 25 year old SCI patient can reach $5 million, with an initial cost exceeding $1 million the first year and an average yearly cost of $200,000 in cases of high tetraplegia. In less severe cases such as paraplegia and injuries where the patient maintains motor function, yearly costs range from $50,000 to $80,000 and total lifetime costs exceed $1 million. These include the ongoing medical expenses for medication, rehabilitation and physical therapy, and specialized equipment such as wheelchairs. However, patients and their families are not the only ones who must carry the

burden of SCI, as healthcare systems and society in general are also affected. Indirect costs mainly consist of lost wages, fringe benefits and lower productivity, and should also be accounted for when estimating lifetime costs.

From the early days of neuroscience, the main theory was that neurons, nerves, and axonal connections were fixed, immutable and not capable of regrowth once development was over. However, current advances in the field are shedding some light on the molecular mechanisms of central nervous system regeneration that may pave the way for clinically relevant cures for SCI patients. For this reason, it is important to have a thorough understanding of the pathological and molecular mechanisms that follow SCI to develop successful therapies and treatments.

1.2.1 Physiology and tissue response

A combination of intrinsic (cell specific) and extrinsic (microenvironment) factors is the reason for the lack of inherent regeneration in central nervous tissue. The pathophysiology of SCI involves a complex cascade of events that can be broadly divided into primary and secondary injury mechanisms. Primary injury occurs with the physical force of the initial trauma in the shape of a contusion, compression, laceration, shearing or stretching. Contusions are the most common form of SCI and result from direct impact to the spinal cord. They can be focal or diffuse, and the severity depends on the force and duration of the impact. Compression injuries occur when the spinal cord is compressed or pinched, leading to loss of blood supply and subsequent tissue damage. Laceration injuries occur when the spinal cord is cut or torn, resulting in immediate loss of function and in shearing injuries the spinal cord may be stretched and ruptured. Overall, the physical damage received by the spinal cord may cause disruption of nervous connections and vasculature present in the site

of injury as well as the blood-spinal cord barrier (BSCB), directly affecting the integrity of the tissue and causing hemorrhage and edema.

The secondary injury occurs in a delayed fashion and lasts from hours to months, beginning with an immediate immune response that involves infiltration of immune cells into the damaged tissue and is followed by a complex process of biological responses that often result in further damage. Inflammatory cells including microglia, macrophages, T-cells and neutrophils enter the injury site through the disrupted, more permeable BSCB and contribute to the expansion of the neural tissue injury (Nakamura et al., 2003).

This inflammatory response can exacerbate tissue damage by releasing pro-inflammatory cytokines, chemokines, and reactive oxygen species (ROS) (Dizdaroglu et al., 2002; Hausmann, 2003; Waxman, 1989). Tumor necrosis factor-alpha (TNF-α) and interleukins (IL-1 and IL-6 most notably) are both pro-inflammatory cytokines that get released and upregulated following SCI, increasing the permeability of the BSCB and inducing the expression of other cytokines and chemokines that may result in further inflammation and axonal regeneration inhibition. The highest concentration levels of these molecules peak around 6 - 12 hours after injury and remain elevated for days. Necrosis and apoptosis may be induced by this process, driven by protein and lipid peroxidation, and DNA oxidative damage from the ROS released by phagocytic pro-inflammatory cells. Cellular excitotoxicity after SCI is caused by the accumulation of neurotransmitters such as glutamate in the extracellular space, which can activate N-methyl-D-aspartate (NMDA) receptors on neurons and lead to altered calcium influx, oxidative stress, and cell death (Hausmann, 2003). Overall, several chemical pathways and cues are activated in the injury microenvironment and have both benefits and may be detrimental to recovery. The most notable case of this is the formation of the glial scar. The upregulation of astrocytes

following injury and their interactions with microglia, pericytes, fibroblasts and oligodendrocyte progenitor cells (OPCs) lead to the formation of a fibrotic/glial scar that physically separates the injury site from the rest of the tissue. A dynamic process occurs at this stage, where these cells cooperate to secrete and remodel the extracellular matrix space, restricting and isolating the lesion epicenter to reduce neuroinflammation. However, this same scar poses a physical and chemical barrier to the affected region and prevents axonal regeneration. Historically, the astrocytic glial scar has been considered one of the main barriers to tissue regrowth in spinal cord. Several recent studies have challenged this theory, showing that contrary to popular belief, glial scar formation does not prevent CNS axonal regrowth but actually plays a role in regeneration. For example, using loss of function experiments in adult mice, fully preventing glial scar formation, attenuating the formation of reactive astrocytes or directly ablating chronic astrocytic scars all resulted in failure of spontaneous regrowth of axons through severe SCI lesions (Anderson et al., 2016). While sustained, local delivery of axon-growth promoting growth factors via a hydrogel depot resulted in robust, axonal regrowth past the lesion site, preventing, ablating or attenuating the formation and function of astrocytes or the glial scar all failed to promote spontaneous regrowth of previously transected axons through severe SCI.

These aspects of SCI pathophysiology are critical to the development of effective therapies and treatments. Targeting the underlying mechanisms of the injury and response of the tissue through advances in drug delivery, biomaterials and regenerative medicine has the potential to promote the highest levels of repair and regeneration as well as mitigating the secondary injury mechanisms.

1.2.2 Spinal cord structure and biomechanics

The spinal cord is the connection between the brain and the rest of the body, sending motor commands from the motor cortex to the muscles and sensory information from the afferent fibers to the sensory cortex. In some cases, the spinal cord may independently coordinate reflexes using reflex arcs and thus function without signals from the brain, allowing the body to respond to sensory information without waiting for brain input. A reflex arc begins with a signal from a sensory receptor, which travels to the spinal cord through sensory nerve fibers that connect synapses to interneurons and then to motor neurons, stimulating effector muscles and organs (Atkinson & Atkinson, 1996).

A critical part of the CNS, the spinal cord is contained within the spinal column. Anatomically, it extends from the brainstem at the medulla oblongata down to the lower back, ending in a conical shape known as the conus medullaris. In adults, it measures approximately 50 cm long and 1 to 1.5 cm in diameter. It is composed of both white and grey matter, organized in an H-shaped area. The cross-sectional structure is mostly maintained over the whole length of the cord. The grey matter contains the cell bodies of neurons (motor and sensory as well as interneurons), and glia, integrating signals within each segment (Czervionke et al., 1988; Savio & Schwab, 1989). On the other hand, white matter contains the axons and fibers, mostly myelinated and unmyelinated motor and sensory axons, that are in charge of transmitting signals from and to the brain.
It is organized in tracts, which in turn can be ascending or descending. Ascending tracts include the dorsal column and lateral/anterior spinothalamic tracts and carry signals from the sensory receptors up to the brain, while descending tracts (such as the corticospinal and vestibulospinal tracts) carry information from high levels of the CNS down to the periphery (Nathan & Smith, 1955; Rexed, 1952; Tan et al., 2023; Wheeler-Kingshott et al., 2002).

Three distinct layers cover the spinal cord, namely the dura mater, arachnoid mater and pia mater, in order from outer to inner layers, and their role is mainly protective (Harrow-Mortelliti et al., 2023; Ozawa et al., 2004; Vandenabeele et al., 1996). Cerebrospinal fluid (CSF) surrounds the spinal cord and plays a crucial role in CNS homeostasis. It fills the ventricular space between the arachnoid and dura mater. It is a water-based fluid that contains proteins, neurotransmitters, ions and other molecules and is renewed four to five times a day (Wichmann et al., 2022). The main function of CSF is maintaining equilibrium in the CNS, clearing out waste products resulting from the highly metabolic regions both in the brain and spinal cord. The mechanism by which waste clearance occurs is the glymphatic system, even though there is not complete agreement in the literature (Jessen et al., 2015). This recently reported system is made up by conduits that circulate and mediate fluid-exchange of CSF, and is formed by astroglial cells. Some of the waste products originated in the CNS have neurotoxic effects, such as β-amyloid.

One aspect often overlooked in many SCI therapies studies is spinal cord biomechanics. By definition, this is the study of how mechanical forces affect the overall and molecular structure of the spinal cord, as well as the effect that these may have on its function. These factors become extremely relevant in the context of SCI mechanisms, and how those affect the approach to prevention, diagnosis, treatment and rehabilitation. There are several important parameters that affect the spinal cord from a biomechanics perspective including tissue composition, mechanical stiffness, and viscoelasticity (Mattucci et al., 2019).

Mechanical stiffness is a measurement of the amount of deformation an object incurs when a force is applied onto it. The spinal cord, due to its composition and location, must remain structurally sound to properly function. There are several methods for measuring

and reporting mechanical stiffness, varying in the sample collection and handling, to the way the spinal cord is probed. These methods can be broadly classified as ex vivo and in-situ. “Ex vivo” techniques involve taking out or removing the tissue part from the body and are the most commonly used. They include uniaxial tensile testing, compression testing, and atomic force microscopy. Uniaxial tensile testing involves attaching a section of spinal cord tissue to a testing jig and applying a uniaxial tensional force, while compression testing involves either testing whole specimens or using AFM to map topographical changes across the surface of a material down to the cellular level (Bartlett et al., 2016). On the other hand, in-situ techniques involve testing spinal cord tissue while it is still functioning and in place. These techniques are less commonly used because they require specialized equipment and are more difficult to perform. Some in-situ techniques include magnetic resonance elastography, shear wave elastography, and indentation-based methods.

Obtaining accurate measurements of the mechanical properties of spinal cord tissue is challenging because of the soft viscoelastic nature of the tissue. Proper tissue dissection, whether from animal or human samples, requires highly specific skills in surgical technique and overall CNS anatomy. There are two main sources of variation in measurement values: intrinsic differences in the tissue itself and variations in external measurement parameters. Pre-conditioning, which involves the cyclical straining of samples by small amounts prior to the final measurement, is one technique that has been used to reduce inter-sample variability. However, the number of preconditioning cycles performed can potentially influence final modulus measurements (Cheng et al., 2009).

It is worth noting that there are significant differences between species, and there is not a robust alignment in terms of scientific studies when it comes to reporting biomechanical data. Factors such as specimen age, sex, tissue collection method, storage

conditions and even time between collection and testing all affect the resulting measurements. Logically, using healthy or injured tissue will yield significantly different results. The presence of inflammation, edema, scarring, axonal or vasculature damage will affect the integrity of the tissue and alter the biomechanical properties. These factors must be accounted for or at least reported so that result heterogeneity in the literature can be reduced, and direct comparison between groups and studies can be made. However, much of the literature agrees on a storage modulus for CNS tissue (both brain and spinal cord) in the range of 0.1 -1 kPa (Austin et al., 2012; Geissler et al., 2018; Hou et al., 2005).

The spinal cord acts as a crucial conduit between the brain and the body, facilitating motor control and sensory integration. Its intricate composition of white and grey matter, organized tracts, and protective layers demonstrates its complexity and importance. The role of biomechanics in understanding the spinal cord's behavior and function cannot be understated. Accurately measuring the mechanical properties, such as stiffness, of the spinal cord tissue presents challenges, but efforts to standardize measurement techniques and report relevant factors are vital. By deepening our understanding of spinal cord biomechanics, we can make significant advancements in the field of spinal cord injury research and develop innovative approaches for prevention, diagnosis, treatment, and rehabilitation, ultimately improving the quality of life for individuals with spinal cord-related conditions. In the field of tissue regeneration, accounting for these physical properties along with the molecular and cellular features is critical for developing successful clinical treatments. This is especially relevant in the context of this work, where the hydrogels used must be biomechanically compatible with the target tissue, in this case the spinal cord.

1.2.3 Regulation of axonal growth and regeneration following SCI

Cellular composition in the spinal cord is highly diverse, as previously discussed. There is general consensus that a strong correlation between number of neurons, and not body mass, and cognitive and behavioral capabilities exists (Herculano-Houzel, 2017). Bahney et al used stereology and isotropic fractionation methods to determine the cellular composition of human spinal cord based on morphological criteria. They estimated that human spinal cords contain 1.5-1.7 billion cells, with 197-222 million being neurons (13.4% of cells). Endothelial cells accounted for 12.2%, while glial cells were the largest portion at 74.8%, resulting in a glia-neuron ratio of 5.6-7.1. The ratio of non-neuronal to neuron cells was 6.5 in humans and 3.2 in cynomolgus monkeys, indicating a previously overestimated ratio. No significant variance in cellular composition was observed between cervical, thoracic and lumbar levels. The glia-neuron ratio in the spinal cord gradually increased with increasing brain mass, similar to the cerebral cortex and the brainstem (Bahney & Von Bartheld, 2018).

Like other organs, the SC microenvironment is highly dynamic after injury. Recent advances in sequencing have allowed researchers to probe and map tissues at the single cell level, giving insight into the spatial localization of specific cells within a given tissue. Matson et al. created a single cell atlas of the injured spinal cord using single nucleus RNA sequencing to profile the molecular and anatomical changes of several cell populations at the lumbar level (Matson et al., 2022). They reported that oligodendrocytes make up almost 35% of the cells, with neurons following closely at 30%, astrocytes at 10% and finally microglia and hematopoietic cells at 4%. Following injury, the overall cell composition of the samples remained relatively stable except for the number of astrocytes decreasing to almost half and a significant increase in both neurons and microglia. One important

limitation of this study is that instead of using whole cells for transcriptional profiling they extracted cell nuclei, potentially leading to composition bias in terms of gene expression.

At the microenvironment level, cells are surrounded by the extracellular matrix. Its primary role is providing a 3-dimensional network that supports both neural and non-neural cells (which in turn secrete other ECM components), dictating their function and fate via several mechanisms. These include regulating signaling through specific cell receptors, sustaining proper axon guidance and synaptogenesis, and preventing aberrant structure remodeling. This highly complex, intricate network of macromolecules provides structural support and a number of biochemical cues to cells, effecting tissue development, repair and maintenance (Haggerty et al., 2017). The ECM is composed of several macromolecules, including collagen types, noncollagenous glycoproteins, glycosaminoglycans (GAGs), and proteoglycans. Collagen types I, II, and III are the interstitial collagens and make up a large proportion of the ECM. Each collagen molecule consists of three alpha chains with specific amino acid sequences that form a triple-helical domain. Procollagens are larger, more soluble precursors of collagens that are cleaved to form the fibrils of triple-helical collagens. Noncollagenous glycoproteins, such as laminin and fibronectin, are relatively large compounds and play important roles in cell attachment and adhesion. GAGs and proteoglycans, such as chondroitin sulfate proteoglycans (CSPGs), are critical to regulating cellular behavior in the CNS (Lau et al., 2013; Rutka et al., 1988). For this reason, in the tissue engineering field, collagen, fibronectin and laminin are often used as therapeutics. Their biocompatibility, accessibility and ease of use, make them great systems for drug and cell delivery, either directly as hydrogel scaffolds, or functionalizing these proteins onto the biomaterials to promote specific cell behavior, such as adhesion or growth (Deister et al., 2007; Ishihara et al., 2018; Mullen et al., 2015).

Axonal regeneration is the process through which damaged or severed axons in the CNS attempt to regrow and reconnect with their target cells. This regrowth is crucial for functional recovery after injury, as it enables the restoration of neural circuits responsible for controlling movement, sensation, and other essential functions. For many decades, it was widely believed that neurons in the adult CNS were not capable of regeneration. Nevertheless, several recent key studies have challenged this notion by making significant progress in the understanding of the molecular basis of axonal regeneration, the factors that limit it, and developing strategies to enhance and promote regrowth (Anderson et al., 2018; Zheng & Tuszynski, 2023).

One important focus has been on identifying and characterizing inhibitory factors within the CNS microenvironment that impede or present a barrier to axonal regeneration. This process is complex and can be hindered by the presence or absence of specific factors. By understanding and targeting these factors, researchers aim to recreate a more conducive environment for axonal regrowth through advances in molecular biology, protein chemistry and gene therapy. The development of successful strategies will require overcoming these limitations and using the latest techniques to manipulate at the molecular level axonal regeneration, especially in the context of CNS injury (Tuszynski & Steward, 2012). Following injury, damaged neurons need to establish new connections with their target cells in order to restore function. However, the absence of suitable, conducive substrates results in the failure to form cellular attachments that support axonal elongation across the target area. Researchers are actively exploring the development of artificial substrates or bridges, capable of guiding regeneration of neurons and axons across injury sites.

Environmental, inhibitory factors are also responsible for limiting proper axonal regeneration, including specific molecules present within the ECM. Following injury, the composition of the CNS ECM is dramatically altered. Besides the migration of glia and immune cells such as macrophages, the spatial organization of the tissue is also changed (Burnside & Bradbury, 2014). Scar matrix deposition and upregulation of chondroitin sulphate proteoglycans (CSPGs) also negatively impact and restrict axonal growth. More specifically, these CSPGs accumulate at the injury site following SCI and, among other actions, impair oligodendrocyte function and remyelination, which in turn inhibit axonal regeneration (Lau et al., 2013; Waxman, 1989).

In addition to environmental factors, intraneuronal mechanisms also play a key role axonal regulation and growth. Namely, the presence of distinct, highly intricate intracellular signaling pathways that control and modulate neuronal ability to grow and regenerate. Multiple genetic regulators of axonal growth have been identified in neurons, including mTOR, MAPK, STAT3 and PTEN (Ding & Chen, 2022; Hammarlund et al., 2009; K. Liu et al., 2010; K. K. Park et al., 2008; Sun et al., 2011). The disruption or inhibition of these signaling pathways may prevent neurons from initiating a regenerative response. Thus, the activation and promotion of these pathways may provide a promising avenue to enhance axonal regeneration.

Due to the multifaceted barriers to axonal regeneration, strategies to promote regrowth encompass molecular, cellular and combination therapies. Molecular approaches include using small molecule drugs or gene therapy vectors to elicit a specific response, such as promoting growth or reducing inflammation. Small molecule therapeutics target specific signaling pathways within neurons while gene therapy introduces exogenous genes into damaged neurons, in both cases to promote their regenerative capacity. On the other hand,

cellular approaches offer another potential avenue to aid in neuronal regeneration. Several types of cells have been and are actively being investigated, more details can be found in Section 1.4.3. It is important to note that due to the complex nature of axonal regeneration, successful approaches will most likely be a combination of therapies that target multiple factors simultaneously. By utilizing a mixture of approaches, the overall treatment effectivity may show higher effectivity than single interventions alone. For instance, combining gene therapy, stem cell transplantation and tissue engineering with biomaterials may have a synergistic effect on axonal regeneration.

In the context of SCI, it is worth noting that treatment personalization is of utmost importance. The type, location, severity, and longevity of the injury results in different symptoms and factors such as age, sex, preexisting conditions all play a role in making most spinal cord injuries unique in their characteristics. Therefore, it is crucial to customize each treatment to the unique needs of the patient. This may mean adjusting dosages, formulations, cell types or intervention location, in order to optimize the therapy to maximize the recovery.

1.3 Drug delivery as a therapeutic approach for SCI

Out of all the therapeutic approaches to SCI, drug delivery is one of the most extensively studied. The use of drugs such as proteins or growth factors provides a plethora of potential targets to elicit a beneficial cell response. In the SCI field, these drugs can have several objectives: increasing cell survival, enhancing neuronal regeneration via neurite outgrowth, reducing inflammation, or driving specific differentiation of progenitor cells into the target neuronal or glial population. Successful treatments often use a combination of these goals,

aiming to get a more comprehensive response following the multifaceted nature of CNS tissue injury.

Studies have explored many avenues to deliver these drugs into the spinal cord, varying in complexity, route of administration, dosage and tunability. Some examples are direct injections, implantable pumps, using scaffolds such as hydrogels, micro and nanoparticles and using viral delivery of gene vectors to overexpress the desired protein (Nguyen et al., 2017; Papa et al., 2019). Each of these methods has benefits and disadvantages, and the correct choice for a given treatment depends on many factors including the lesion type, time elapsed from the injury, severity, and overall therapeutic objective.

One factor that is often overlooked in the field of drug delivery is biological activity. Most assays used to measure protein concentration detect proteins indiscriminately, regardless of their bioactivity. Conditions such as its three-dimensional structure, group modification, and microenvironment (in most cases the solution in which the protein is dissolved) all affect the overall biological activity of the molecule. Commonly used protein assays such as UV absorption and Biuret methods (BCA, Lowry) only require the presence of certain amino acids or polypeptides to read out a specific measurement of protein, regardless of its conformation. Since stability plays a large role in whether a growth factor retains its biological function, simple protein assays must be accompanied by specific, functional assays related to the relevant biological function of such molecule. This becomes critical in studies where release experiments span weeks, where small traces of protein will be detected weeks or even months after encapsulating the protein, but the bioactivity aspect tends to be ignored at longer timeframes, assuming that the whole amount of growth factor that is measured is still biologically active.

1.3.1 Drug delivery mechanisms

To maximize therapeutic effects in any treatment, the pharmacological agent must reach the target tissue or organ at the right concentration, the right time and be biologically active at the time of delivery. At the macroscopic level, this means designing materials that are capable of encapsulating drugs and maintaining their physical integrity, while reducing potential off-target and immunological responses. At the molecular level, drug delivery systems can be tuned to have fine control over the specific interactions between the therapeutic agents and the materials, allowing to modify the specific properties that control when and where the drug gets released. There are many mechanisms by which therapeutic agents are delivered, depending on the platform and application. Passive methods rely on intrinsic, physical properties of the drug delivery platform and include diffusion, swelling and erosion. Here, parameters such as pore size, swelling ratio and degradability drive the rate of drug release. Alternatively, more active methods can be used, taking advantage of specific interactions or stimuli-responsive materials (**Figure 1.1**).

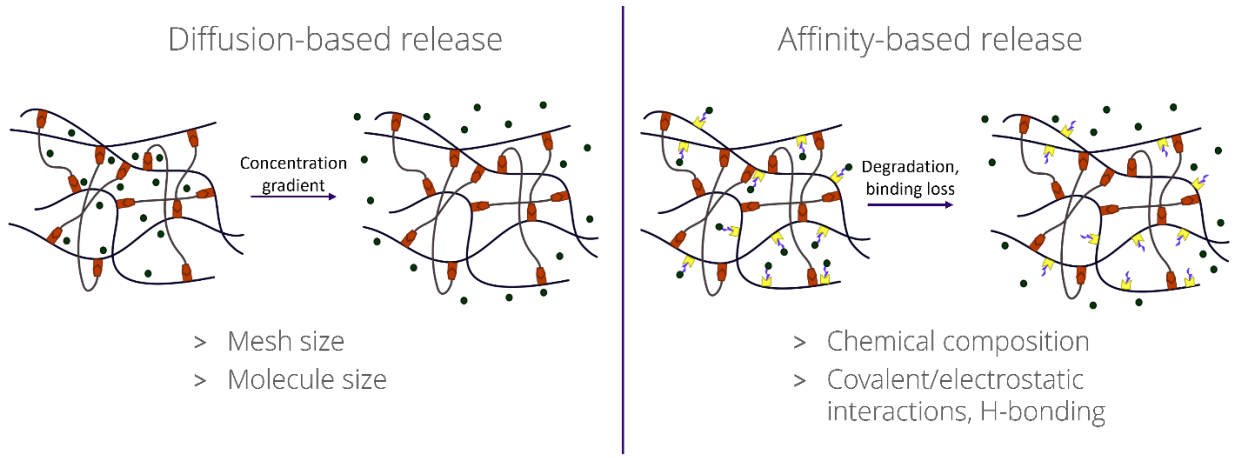

Figure 1.1. Drug delivery mechanisms and relevant design parameters.

Amongst the passive methods, diffusion and swelling controlled release are the most common. In the case of hydrogels, Fick's laws of diffusion can be used to describe quite accurately the release behavior of proteins (Peppas et al., 2000; Wagner et al., 2018). In this case, the proteins are encapsulated by physical entrapment within the hydrogel chains. The concentration gradient between the hydrogel and the environment drives the diffusion as the gel starts swelling. In other cases, the rate limiting step for this process is the degradation of the hydrogel structure. The main drawback of diffusion-based release systems is the "burst effect", which is characterized by a rapid, often significant release of protein in the first seconds or minutes. The majority of the amount released at this point is often protein that was not properly encapsulated or that it adhered to the surface of the hydrogel. Ideally, drug delivery systems should allow for complete control over the release rate, including the initial stages. Different approaches can be used to reduce the burst effect, and perhaps the most effective one is increasing protein sequestration within the hydrogels via specific binding.

More recent efforts have focused on affinity-based mechanisms of release (Delplace et al., 2016). These systems take advantage of molecular recognition, and exploit distinct, often highly specific interactions, between the protein of choice and other ligands. Instead of a purely diffusional mechanism, there is a reaction present governing release, namely the binding between the proteins and ligands. A binding equilibrium exists between both molecules, with an equilibrium constant and binding affinity that is dependent on the concentration and accessibility of both proteins and ligands. The overall release is often also driven by diffusion, with the added binding reaction that, through chemical conjugation, decreases the concentration of free protein and tends to decrease the release rate. However, it is also possible that swelling, degradation of certain ligands or moieties, and other factors

such as pore interconnectedness and mesh size may affect protein release. All of these parameters are inherently related to each other (Abune & Wang, 2021; Wang & von Recum, 2011). For example, by increasing swelling of a hydrogel, pore size increases and polymer volume fraction decreases. It is important to account for the relationship between these factors when designing a delivery system in order to have maximum control over the release mechanism.

1.3.2 Neurotrophins

Neurotrophins are growth factors that modulate the behavior of cells in the nervous system (Kolbeck et al., 1994; Labouyrie et al., 1999). They have been extensively studied for their potential therapeutic benefits in various neurological disorders, including SCI. While preclinical studies have shown promising results, translating these findings to the clinical setting has been challenging. Different factors, such as the type of neurotrophic factor, dosage, route of administration, and duration of treatment, may affect the efficacy and safety of neurotrophic factor therapy in SCI. Neurotrophic factors exert their effects by binding to specific receptors on the surface of neurons and other cells in the nervous system. This binding activates intracellular signaling pathways that regulate gene expression, protein synthesis, and other cellular processes (Ramer et al., 2002). In SCI, neurotrophic factors can promote axonal regeneration by stimulating axon outgrowth, reducing scar formation, and modulating inflammation. They can also enhance neuronal survival and function by protecting neurons from cell death, promoting synaptic plasticity, and modulating neurotransmitter release.

One of the key mechanisms of neurotrophic factors in SCI is the promotion of axonal regeneration. Following SCI, the disruption of the spinal cord tissue and the formation of a

glial scar create a hostile environment for axonal growth (Silver & Miller, 2004). Neurotrophic factors can stimulate the sprouting and elongation of axons by activating intracellular signaling pathways that promote cytoskeletal rearrangement and protein synthesis. In addition, neurotrophic factors can modulate the inflammatory response to SCI by regulating the expression of cytokines, chemokines, and other immune factors (Nakamura et al., 2003). This can help to reduce the secondary damage to the spinal cord tissue and create a more favorable environment for axonal growth and regeneration. Another important mechanism of neurotrophic factors in SCI is the enhancement of neuronal survival and function. SCI can cause neuronal death, synaptic loss, and altered neurotransmitter release, leading to impaired motor and sensory function. Neurotrophic factors can protect neurons from cell death by activating anti-apoptotic signaling pathways, which prevent the activation of pro-apoptotic factors and promote cell survival (Javvaji et al., 2021; Zhou et al., 2003). Additionally, neurotrophic factors can promote synaptic plasticity by modulating the expression and localization of synaptic proteins, such as neurotransmitter receptors and vesicles. This can improve the communication between neurons and restore the function of the damaged neural circuits.

Nerve growth factor (NGF), brain derived neurotrophic factor (BDNF) and neurotrophin-3 (NT-3) are members of this family of proteins that exist as dimers and share a cystine knot motif. These factors can be classified into different families based on their chemical structure and biological activity. The neurotrophin family, which includes NGF, BDNF, NT-3, and neurotrophin-4/5 (NT-4/5), plays a critical role in the development, maintenance, and plasticity of the nervous system. NGF, for example, supports the survival and growth of sympathetic and sensory neurons, while BDNF is involved in the regulation of synaptic plasticity and learning. The glial cell line-derived neurotrophic factor (GDNF)

family, which includes GDNF, neurturin, persephin, and artemin, promotes the survival and differentiation of motor neurons. Other neurotrophic factors, such as ciliary neurotrophic factor (CNTF) and insulin-like growth factor (IGF), have also been investigated for their potential therapeutic benefits in SCI (Allen et al., 2013; Keefe et al., 2017).

CNTF and IGF bind to their respective receptors and activate downstream signaling pathways that promote neuronal survival, growth, and differentiation (Ciucci et al., 2007; Eleftheriadou et al., 2016). On the other hand, NGF binds to the tropomyosin receptor kinase A (TrkA) receptor, which is expressed by sympathetic and sensory neurons, while BDNF binds to the TrkB receptor, which is expressed by a variety of neurons, including motor neurons. GDNF, on the other hand, binds to the GDNF family receptor alpha (GFRα) and activates the RET tyrosine kinase receptor, which is expressed by motor neurons (Ansorena et al., 2013).

Out of all the neurotrophins, NT-3 has been shown to increase axonal growth and promote functional recovery *in vivo* by attracting endogenous neural stem cells and driving proliferation, differentiation into neurons and formation of neuronal networks (Baumann et al., 2009; Oudega et al., 2019; S. J. Taylor et al., 2004). Overexpression of NT3 in lumbar motor neurons resulted in increased growth of intact corticospinal tract (CST) axons across the midline into the denervated side in animals with a SCI lesion, likely responding to denervation via axonal plasticity (Zhou et al., 2003). NT-3 activates intracellular signaling pathways by binding to the TrkC receptor with high affinity, as well as the p75 receptor with lower affinity (Labouyrie et al., 1999; Urferl et al., 1994). Different methods have been used to deliver NT-3 to the CNS, including microparticles (Elliott Donaghue et al., 2015, 2016; Stanwick et al., 2012), affinity-based systems (Ishihara et al., 2018; S. J. Taylor et al., 2004),

and encapsulation in hydrogels (Baumann et al., 2009; Designed Research; J, 2018; Johnson et al., 2009; Oudega et al., 2019; Tang et al., 2014).

Despite the potential therapeutic benefits of neurotrophic factors in SCI, several challenges remain in translating these findings to the clinical setting. One major challenge is the limited ability of neurotrophic factors to cross the blood-brain barrier (BBB) and blood-spinal cord barrier (BCSB), which restrict their access to the brain and spinal cord tissue, respectively. This has led to the investigation of different strategies to enhance the delivery of neurotrophic factors to the site of injury (Blanco et al., 2015). Another challenge is the potential adverse effects of neurotrophic factor therapy, such as systemic toxicity, inflammation, and abnormal growth of neural tissues (Hellenbrand et al., 2019). The optimal dosage, duration, and frequency of neurotrophic factor administration need to be carefully evaluated to maximize their therapeutic benefits while minimizing their side effects. In addition, the combination of different neurotrophic factors and other therapies, such as cell transplantation and rehabilitation, may offer synergistic effects in promoting functional recovery after SCI.

1.3.3 Micro and nanoparticles

Over the past decades, particulate drug release systems have transitioned from laboratory experiments to having massive scale societal impact as part of the formulation in COVID-19 vaccinations. Lipid nanoparticles (LNPs) were used in both Pfizer's Comirnaty and Moderna's Spikevax mRNA-1273 to protect and deliver nucleic acid cargo, increasing immunogenicity and ultimately efficacy. Micro- and nanoparticles provide a tunable platform to encapsulate therapeutic agents, enhancing their efficacy by protecting their biological activity and allowing for targeted, temporal control over the release (Blanco et al.,

2015). Microparticles are between 1 – 1000 um in diameter, while nanoparticles are in the nanometer range. Their composition can be synthetic or have plant or animal biopolymer origin. Polysaccharides, proteins, lipids, and other excipients are selected, modified, combined, and sometimes supplemented with yet more excipients to tune the properties of the particle formulation depending on its purpose. The nature of the therapeutic agent, namely whether it is a growth factor, a small molecule, a nucleic acid or some other type of response-causing drug dictates the overall parameters required for efficient encapsulation, stabilization and finally delivery to the right target organ with minimal immune and tissue response. The target organ is also relevant, as it is the delivery route (oral, nasal, parenteral or transdermal) and the particle formation process. Nanoparticles have been used to target and overcome biological barriers, including tumors and cancers (Sau et al., 2018; Yoon et al., 2018). Methods such as spray drying, extrusion and the use of microfluidic devices are the most common techniques used to synthesize and manufacture particles of different formulations.

In the context of CNS disease, MPs and NPs have been extensively explored both as therapeutics and as a diagnostic tool. For example, NPs can be designed to have a small size and high permeability to cross the BBB. Once inside, these particles can be used as probes in molecular imaging, facilitating the visualization of amyloid-beta plaques in Alzheimer's disease, or to aid in biomarker detection using magnetic NPs for several neurological diseases (Fernández-Cabada & Ramos-Gómez, 2019; Y. Zhao et al., 2014). For SCI, MPs and NPs have mostly been used to locally deliver payloads. Zuidema et al. embedded porous silicon NPs within PLGA nanofiber scaffolds and delivered a PTEN inhibitor, an RNA aptamer for the trkB receptor and the neurotrophin NGF resulting in increased axonal extension in a DRG explant assay (Zuidema et al., 2020). Other groups have also used PLGA

nanoparticles dispersed in a hydrogel to deliver NT-3 and anti-NogoA to an impact SCI rat model, showing improved locomotor function and increased axonal density in the site of injury post implantation (Elliott Donaghue et al., 2016; Stanwick et al., 2012).

One of the key advantages of certain NP or MP formulations is their ability to reach target areas often challenging to access, the most notorious one being crossing the BBB. Characterization of MPs must also be accounted for when designing novel delivery systems. Particle size and shape are two of the most critical parameters and can be measured directly using microscopy or light scattering methods such as DLS. Here, the polydispersity index (PDI) indicates the overall size distribution of a microparticle solution and gives insight into the homogeneity of a formulation. Drug delivery systems may use several transport mechanisms to cross biological barriers, including transcytosis, paracellular transport and transcellular diffusion. To be able to accomplish this, the material properties of the delivering material must be tuned. Size, shape, charge, hydrophobicity/hydrophilicity, stiffness and even the addition of specific ligands all influence the adsorption, distribution and clearance of particulate systems following administration in the CNS (Nance et al., 2022).

1.4 Biomaterials for SCI

Sustained systemic delivery of biologically active molecules to the spinal cord remains a major challenge due to the presence of the blood spinal cord barrier (BSCB) and the rapid clearance of drugs caused by the continual exchange of cerebrospinal fluid (Pakulska et al., 2012). The BSCB prevents therapeutic agents from being administered systemically by inhibiting the transport of drugs to the spinal cord from the blood stream. To overcome this barrier, local drug delivery methods have been used, including intrathecal delivery and

direct injection (Ramer et al., 2002), as well as the implantation of minipump delivery devices (Namiki et al., 2000). Biomaterials present a promising alternative for local sustained release of molecules at the site of injury. The encapsulation of proteins and growth factors that promote axon growth either in hydrogels or micro/nanoparticle systems allows for spatio-temporal control of drug release while providing extra protection and enhancing protein stability compared to drugs dissolved in solution. Biomaterials may also be used as a platform to transplant cells into the SC, by maintaining a biologically relevant microenvironment that maximizes cell survival, adhesion and growth. This can be done by finely tuning the stiffness and chemical composition of the material, aiming to replicate as finely as possible the complexity of the natural extracellular matrix (Haggerty et al., 2017). Additional complexity can be implemented into biomaterials in the form of magnetic fibers for anisotropic alignment of the biomaterial nanostructure, which allow to spatially direct axonal growth in the optimal direction (Nguyen et al., 2017; Rose et al., 2018). Finally, biomaterials may also be simply used to fill up the injury defect volume, providing mechanical stability for the tissue and a conducive environment for cells to migrate and regenerate in the injury site.

1.4.1 Hydrogel scaffolds

Hydrophilic polymers are a class of biomaterials that in their crosslinked form are known as hydrogels. These macromolecules contain a high amount of water, approximately 70 – 99% due to their hydrophilicity. Their physical structure contains a chemically or physically crosslinked network with water penetrating between the polymer chains, causing swelling and giving the gels their typical shape and, in many cases, translucent color (J. Li & Mooney, 2016; Peppas et al., 2006). This high water content makes hydrogels physically similar to

human tissues and gives them the capability to encapsulate hydrophilic drugs with ease. Hydrogel systems used in tissue engineering applications can be synthetic or natural. Artificial materials are those that are synthetically developed, such as PLGA, PEG, and other polymeric compounds. On the other hand, natural hydrogels such as gelatin, collagen, hyaluronic acid or fibrin have a physiological origin (Khademhosseini & Langer, 2007; Lee & Mooney, 2001). Each type of material has benefits and advantages and the choice of one versus another often depends on the specific application for which the material is being designed. For example, synthetic polymers tend to have more tunability and thus there is more control over the physical and chemical characteristics. However, their synthesis may include the use of non-cytocompatible compounds such as organic solvents. On the other hand, natural polymers are usually highly biocompatible since they are already found through tissue and extracellular matrix. The downside is that the ability to control their properties is limited.

Again, when developing specific hydrogel systems for tissue engineering applications, there are several factors that must be considered. These include biocompatibility, biodegradability, ability to seamlessly integrate with the host tissue and mechanical properties. Hydrogels, whether they have a natural or synthetic origin, are formed via crosslinking, which in turn can be physical or chemical. The bonds that create the matrix within the scaffolds can be covalent or non-covalent, and their strength and type often dictate the overall properties of the final hydrogel. One of the most important parameters used to characterize hydrogels is swelling behavior. This refers to the amount of water content that hydrogels uptake, which in turn directly affects the porosity and permeability of the gels. Stiffness and viscoelasticity are also impacted by these parameters, more information regarding these parameters in the spinal cord can be found in Section

1.2.2. Not surprisingly, the release behavior of proteins or growth factors from hydrogels is dictated by a combination of all these factors. Namely, for a drug delivery system based on diffusion and in absence of any other binding or interactions between protein and scaffold, the pore size of the gel and the size of the protein will drive a faster or slower release kinetics based on the relative sizes of each. To control or slow down the release, chemical or biochemical cues including other proteins or reactive groups can be functionalized onto the hydrogels. These materials are often developed and designed such that they elicit a response when exposed to physical external factors (light, magnetic fields, enzymes). Other approaches introduce specific chemistries to control the degradation kinetics and therefore this dynamic environment can only release drugs in the presence of specific molecules. For example, systems have been developed to degrade scaffolds in a controlled manner in the presence of certain metalloproteinases, such as MMP-1 and MMP-2, by introducing protease-sensitive peptides (Patterson & Hubbell, 2010; Seliktar et al., 2004). Similarly, environmental factors such as pH and temperature can also be exploited by introducing molecules or chemical groups that respond to high or low pH and temperature environments. Examples of these stimuli-responsive hydrogels include polyacrylic acid, polyacrylamide and polylactic acid (Rizwan et al., 2017; Xu et al., 2018).

1.4.2 Hyaluronic acid applications in neural tissue engineering

Hyaluronic acid (HA) is a glycosaminoglycan formed by repeating units of D-glucuronic acid and N-acetyl-D-glucosamine linked by a glycosidic bond. It is ubiquitously present in the extracellular matrix (ECM) throughout the body and acts as an essential component in the nervous system, providing structural support and a range of physical and biochemical cues to surrounding cells (Wolf & Kumar, 2019). It can be covalently modified to form hydrogels

via chemical or physical crosslinking methods, allowing for a high degree of tunability in terms of chemical and mechanical properties. When compared to other carbohydrate-based polymers, HA is available in a wide range of sizes (with molecular weights from the low thousands to millions) and contains a few readily accessible sites susceptible to chemical modification. The carboxylic acid in the glucuronic acid unit can be modified via esterification, amidation and carbodiimide based reactions; the hydroxyl groups, both primary and secondary, can be etherified, esterified, or crosslinked; and the N-acetyl group can also be chemically modified but requires additional reactions due to its low reactivity (Figure 1.1) (Hu et al., 2019; Seidlits et al., 2010; Tsaryk et al., 2015; Yu et al., 2014).

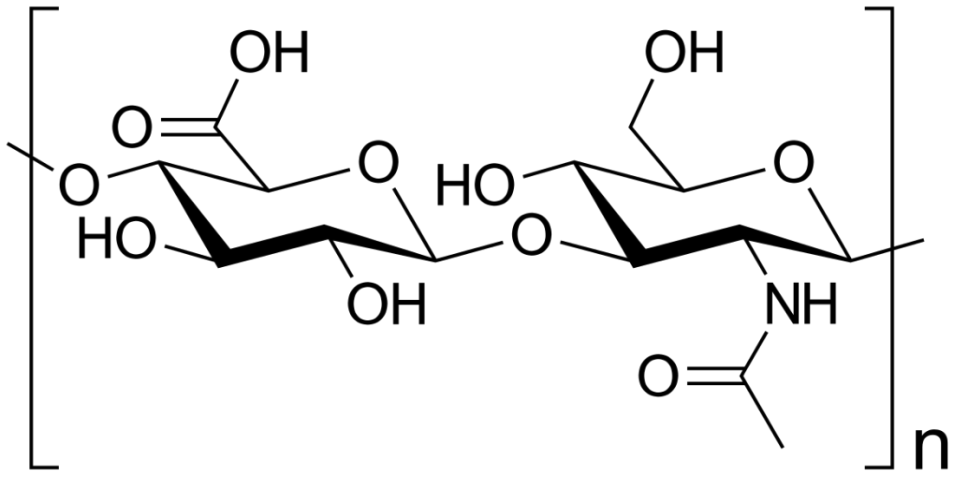

Figure 1.2 Molecular diagram of a repeating unit of hyaluronic acid.

Several studies have used HA scaffolds in the central nervous system showing that it effectively reduces the host inflammatory response, working as a scaffold that can support cell infiltration and angiogenesis (Austin et al., 2012; Deister et al., 2007; Hou et al., 2005; Nih et al., 2018). HA has also been used to promote differentiation of neural progenitor cells and as a matrix for magneto-mechanical neuromodulation of primary neurons (Geissler et al., 2018; Seidlits et al., 2010; Tay et al., 2018). Previous work from our laboratory and

collaborators has shown that HA hydrogels supplemented with astrocyte-derived ECM and containing V2a interneurons effectively reduced the size of the glial scar, reduced macrophage infiltration, and led to an increase in axonal and neuronal processes both within and surrounding the lesion site (Thompson et al., 2018).

1.4.3 Cell transplantation and delivery

Hydrogels have not only been used to deliver therapeutic agents to the CNS but they are also extensively exploited as a platform to support cell transplantation. Within the context of injury in the CNS, several cell types have been explored to provide support after SCI. Mature neurons, neural stem cells, astrocytes, oligodendrocyte progenitor cells (OPCs) and microglia have all been transplanted into animal models (Davies et al., 2008; Iyer et al., 2017; Shibata et al., 2023; Wuttke et al., 2018). Each cell type provides specific support and benefits to the injury site, from undifferentiated stem cells that can replace dead neurons and regenerate axonal pathways, to OPCs that provide the factors necessary to remyelinate injured cells.

The temporal element of SCI gives scientists the challenge and opportunity to develop therapies that can have the most optimal effect tailored to the injury phase. For example, neuroprotective and anti-inflammatory interventions would have relatively higher efficacy when delivered quickly within the first few hours or days of the acute phase following injury. The goal in these is to prevent the spread of secondary injury and protect the left-over tissue and cells that remain intact, and this occurs right after the acute trauma has occurred. Replacing lost neural cells and lost axonal circuitry would also be useful in the initial stages of injury. Alternatively, in the case of subacute and chronic SCI, cell types such as neural stem cells and Schwann cells would be beneficial due to their ability to promote

and drive axonal growth, myelinate other cells and potentially bridge the injury site through amplification of neuron plasticity (Zipser et al., 2022). Further understanding the molecular mechanisms and efficacy of treatments across each injury phase will allow us to design better treatments finely tuned to specific therapeutic windows.

Clinical translation of these types of therapies is held back by several distinct issues. Stem cell transplantation still presents challenges that span from ethical concerns related to cell sourcing to issues with tumorigenicity and de-differentiation of stem cells. The rise and progress of stem cell reprogramming permits us to move away from embryonic tissue origins and source cells from the own patient's tissue, opening the door for true autologous therapies. Another one is transplantation efficiency, often measured by engraftment survival and cell differentiation into the intended lineage (Iyer et al., 2017). To this day, neural induction of stem cells is still lower than desirable, differentiation of adult stem cells into neurons often require induction and maturation periods of weeks to months and cell survival following injection and transplantation must be improved to achieve significant improvements over current therapies.

Overall, the complexity of SCI requires cell transplantation to be highly efficient and selective, with a clear therapeutic objective to use the most appropriate cell type and delivery vehicle. The choice of what cell type to use depends on the objective of the therapy and the injury phase at which transplantation would occur. Furthermore, an optimal treatment will most likely include a combination of several cell types as no single population would be capable of tackling all the multifaceted issues and symptoms present in SCI patients.

1.5 Research objectives and hypotheses

In this introduction, I have attempted to discuss critical concepts regarding the multifaceted aspects of SCI, emphasizing several potential therapeutic avenues that are being explored by research groups all over the globe. SCI is a highly complex, patient-dependent condition of which we still ignore some of the molecular mechanisms that follow injury. Only through a deep understanding of the injury events, the role of each specific cell population, signaling cascades and the relationship between local, axonal regeneration with overall functional recovery will we develop an effective SCI therapy. Despite the rise in popularity of electrical stimulation and brain/spine machine interfaces, the development of a true regenerative approach to SCI is still worthwhile. Epidural electrical stimulation (EES) has shown promise in studies helping individuals with chronic tetraplegia to stand, walk and climb stairs by using a digital bridge between the brain and the spinal cord, overcoming the physical interruption of axonal connections through the spine that allow for movement (Angeli et al., 2018; Lorach et al., 2023). These technologies might provide an alternative and temporary solution to regain motor and sensory function, but the underlying symptoms of SCI are not directly tackled. Even though there are reports of neurorehabilitation by itself supporting neurological recovery, a regenerative, long term therapy for SCI will likely include the delivery of pharmacological agents to promote axonal regeneration and cells to replenish the population affected by the injury. The Sakiyama-Elbert lab has been continuously working on drug delivery approaches targeting the spinal cord, focusing on the

use of hydrogels to release growth factors and as a platform for cell transplantation (**Figure 1.3**).

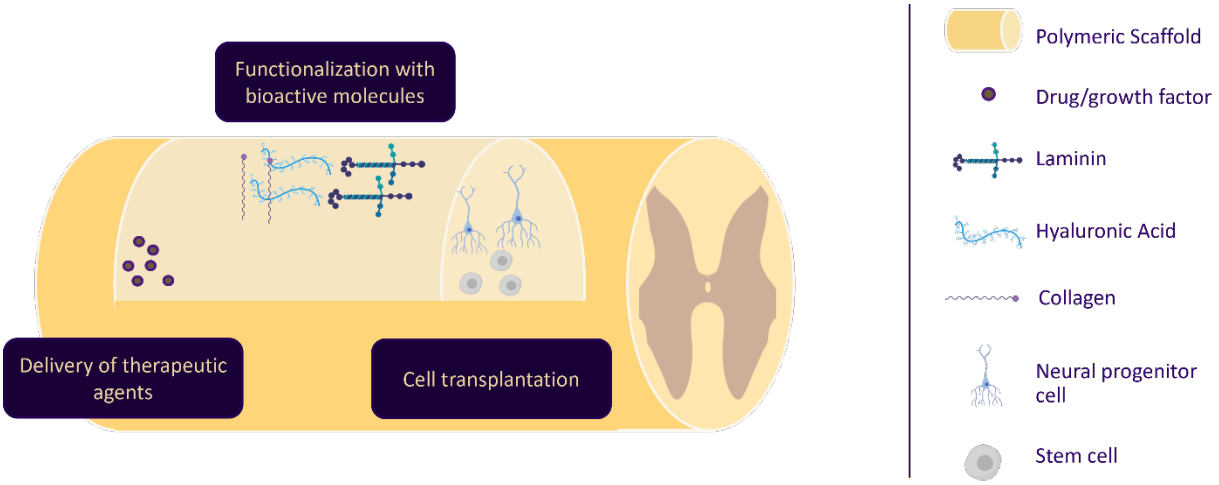

Figure 1.3 Schematic of spinal cord with a polymeric scaffold in the site of injury. The three approaches to treat SCI are highlighted: the scaffold can be functionalized with bioactive molecules (such as laminin, collagen); therapeutic agents/growth factors can be encapsulated for controlled release; the scaffold can be used as a platform for cell transplantation of stem cells, neural progenitor cells and mature neurons.

Initially, fibrin scaffolds were developed and binding sequences specific to heparin were incorporated to control protein binding and release (Johnson et al., 2009; S. J. Taylor et al., 2004). The most recent system is the hyaluronic acid-based hydrogel platform that is described herein. HA hydrogels were previously used as an implant containing extracellular matrix, harvested from astrocytes derived from mouse embryonic stem cells, and V2a interneurons, also mESC-derived (Thompson et al., 2018). Our group found a significant difference in regenerative potential between ECM harvested from white matter or fibrous astrocytes, and that of grey matter or protoplasmic astrocytes. In a rat SCI model, protoplasmic-derived ECM incorporated into the HA hydrogels resulted in a reduction of the glial scar size, increased axonal penetration into the injury site, and reduced

microglia/macrophage staining. The hydrogel was also conducive to V2a interneuron transplantation, with an increase in neuronal processes both within and surrounding the lesion site. However, no additional neurotrophic factors were delivered along the ECM and cells, leaving room to further improve this hydrogel system to tackle the regeneration aspect of SCI by incorporating controlled drug release. Since both NT-3 and IGF-1 have been shown to increase axonal regrowth and improve functional recovery in some SCI rodent models, we aimed to tune this HA scaffold system for sustained delivery of biologically active NT-3. Since a successful therapy will be multifactorial, we also aimed to develop a microparticle-based growth factor delivery system that could be used in combination with the current model. For this, we chose to follow up on work from the Elbert group and modified PEG-diacrylate based precipitated microparticles to allow for controlled encapsulation and sustained release of bioactive IGF-1. In both aims, the biological activity and role of the growth factors was studied on both primary sensory neurons, in the form of DRGs, and more specific neuronal populations that more represent the SC environment we are tackling. We developed drug potency assays with mouse embryonic stem cell derived motoneurons and V2a interneurons, both as single cells and in an aggregated form. This was to ensure that the growth factors released from the delivery systems are not only detectable via protein quantification assays, but also perform their expected biological function, in this case increasing axonal extension. Even though no in vivo studies were carried out for this work, we expect that both drug delivery platforms will be tested in a SCI rodent model by other laboratory members in the near future.

Chapter 2

A Hyaluronic Acid Hydrogel System as a Drug Delivery Platform for Neurotrophin-3

2.1 Abstract

Neurotrophin-3 has been shown to increase axonal growth both in vitro and in vivo models of spinal cord injury, resulting in improved functional outcomes. Its activity promotes neuronal survival and enhances neurite outgrowth via activation of the TrkC receptor. Hyaluronic acid hydrogels have been extensively used in tissue engineering applications due to its high degree of tunability and biocompatibility. Here, we have developed an injectable hyaluronic acid scaffold drug delivery system to deliver biologically active NT-3 locally to the spinal cord. HA hydrogels were synthesized in two steps and crosslinked via click chemistry. The stiffness of the gels could be tuned by controlling the ratio of reactive groups, methylfuran and maleimide, allowing to develop gels that match the stiffness of native rat spinal cord tissue. NT-3 was loaded onto the scaffolds by rehydrating freeze-dried HA scaffolds in a solution containing the growth factor. Release studies showed that the gels were capable of sustained release of NT-3 over a period of at least 4 weeks. The mechanism of release was driven by electrostatic interactions between the positively charged growth factor and negatively charged HA chains with carboxyl groups at physiological pH. In addition, the bioactivity of the encapsulated and released NT-3 was confirmed via a DRG assay and a neurite growth assay using stem cell derived interneurons and motor neurons. Finally, both primary and stem cell derived neurons were able to adhere, grow and extend neurites through the hydrogels when seeded within. Therefore, this HA hydrogel system

provides a promising platform to deliver biologically active NT-3 to the injured spinal cord and allow for improved axonal growth and regeneration.

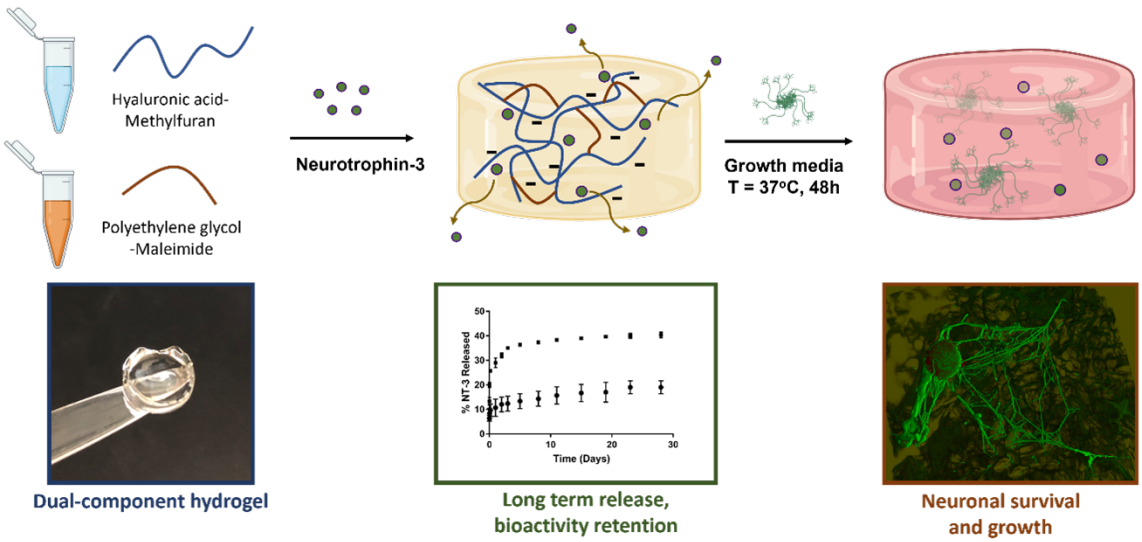

2.2 Introduction

The aims of this study were twofold: evaluating the feasibility of a hyaluronic acid hydrogel drug delivery system for neurotrophin-3 in vitro and determining the effect of sustained release of neurotrophin-3 from a hyaluronic acid hydrogel drug delivery system on neurons in vitro. Hydrogels have the potential to allow spatio-temporal control for the release of therapeutic agents such as growth factors due to their tunability, including functionalization, degradability and physical properties. The properties of these scaffolds can be tuned to provide similar mechanical properties to central nervous system tissue and a platform to control drug delivery (Lampe et al., 2013; Rehmann et al., 2017). The goal of this aim is to design HA hydrogels capable of releasing neurotrophin-3 in a sustained manner. It is vital to ensure that the encapsulation and release of NT-3 from the HA hydrogel does not affect its biological function. The dorsal root ganglion (DRG) assay is a common in vitro assay initially used to measure the bioactivity of nerve growth factor, but it

has also been applied to NT-3 (Genç et al., 2004; Stanwick et al., 2012; S. J. Taylor et al., 2004; Tuttle & Matthew, 1995). Here we used the DRG assay to confirm the bioactivity of the delivered NT-3 once the hydrogel system was tuned to provide its sustained release and ensuring that the HA system presents a beneficial platform for axonal growth.

In this work, we have tuned a hyaluronic acid-based scaffold to deliver biologically active NT-3 in vitro. We synthesized methylfuran-functionalized hyaluronic acid, crosslinked with polyethylene glycol-dimaleimide (PEG-diMal) and characterized the chemical and mechanical properties of the resulting hydrogels. We carried out release studies to evaluate the sustained release of bioactive molecules, including NT-3. Finally, we have also tested the biological activity of the NT-3 that is encapsulated and released using neurite outgrowth experiments from both primary neurons and stem cell-derived neurons in vitro. This study presents sustained delivery of NT-3 from HA-based hydrogels as a promising alternative to promote axonal growth.

2.3 Materials & Methods

2.3.1 HAmF synthesis

Hyaluronic acid was functionalized with methyl furan groups using (4-(4,6-dimethoxy-1,3,5-triazin-2-yl)-4-methyl-morpholinium chloride) to activate the carboxylates in HA followed by the addition of 5-methylfurfurylamine, leading to coupling with its primary amine. The resulting reaction mixture was dialyzed 24h later against deionized water for three days and the resulting material was lyophilized to recover the HAmF and stored at -20^{o}C. The degree of methylfuran functionalization was measured using NMR by dissolving the dry HAmF in deuterated water. Hydrogels were formed using a bifunctional maleimide poly-ethylene glycol crosslinker via a Diels-Alder reaction, a highly selective cycloaddition click reaction

between the maleimide and methylfuran. Both the HAmF and PEG-Mal were dissolved in phosphate buffer saline (PBS) at 7.4 pH and mixed in a tube at different ratios. The mixture was allowed to react in an incubator at 37°C. After 24h, the formed gels were frozen at -80°C in order to be lyophilized overnight. The resulting dry gels were resuspended in D_2O to measure mF-Mal coupling efficiency.

Methylfuran functionalized HA was synthesized as previously reported(Nimmo et al., 2011; Smith et al., 2018). Briefly, 400 mg HA (Creative PEGWorks, MW 250 kDa) were dissolved in 40 mL 2-(N-morpholino)ethanesulfonic acid (MES) buffer (pH 5.5) in a round bottom flask. 750 mg of 4- (4,6- dimethoxy-1,3,5-triazin-2-yl)-4- methylmorpholinium (DMTMM) (TCI America) were added to the solution and stirred for 10 min. 124.5 µL of 5-methylfurfurylamine were added dropwise, and the reaction was carried out for 72 hours under constant agitation with a magnetic stir bar. The solution was dialyzed against DI water for two days replacing the dialysis water after 24 hours, and the remaining product was lyophilized for two days to ensure removal of all water. The final product was collected as a white fibrous material and stored at -20 °C until further use. 15 mg/mL of HAmF was dissolved in deuterium oxide (Thermo) for 24 hours. H^1 NMR was used to characterize the product and calculate the degree of methylfuran substitution by dissolving HAmF in deuterated water at 10 mg/mL.

2.3.2 Hydrogel synthesis

Lyophilized HAmF was dissolved in phosphate buffer saline (PBS) buffer at pH 7.4 overnight at 11 mg/mL and crosslinked with PEG-diMal (MW 3150, Rapp Polymere) in PBS at 156 mg/mL and combined in different volume ratios of HAmF to PEG-diMal for final molar ratios of 1.5:1, 3:1 and 5:1 methylfuran to maleimide, respectively.

2.3.3 Quenching and NMR Analysis

To determine the amount of unreacted maleimides present in the scaffolds, the hydrogels were crosslinked for 24h before quenching either with pH 9 phosphate buffer (to prevent the methylfuran from reacting via ring-opening hydrolysis) or with a L-cysteine solution (for the free thiols to react with the leftover maleimide). The gels were then degraded with 2500U/mL hyaluronidase for 3 days, lyophilized and resuspended in deuterated water for NMR analysis. The amount of unreacted maleimide was calculated by measuring the ratio of unreacted methylfuran present in the samples and comparing it to the initial amount.

2.3.4 Rheology

The mechanical properties of the gels were measured using a Discovery Hybrid Rheometer. Gelation kinetics were investigated by running a time sweep for at least 3 hours, with an evaporation trap in place to minimize sample loss and a heating plate to keep the temperature constant at 37^{o}C. To investigate the swollen characteristics, lyophilized hydrogels were rehydrated in excess PBS for 24 hours, then the thin disks were placed in the rheometer. The samples were subjected to a frequency sweep followed by a strain sweep to ensure the values obtained were within the viscoelastic linear region.

Viscoelastic measurements were taken on a Hybrid Discovery Rheometer ® (TA Instruments). Gelation kinetics were examined by subjecting 0.6 mL of a pre-gel solution to a 4h time-sweep at 10 rad/s and 0.2% strain using a 40 mm cone geometry with a solvent trap to prevent sample evaporation. To measure the storage modulus after lyophilization and rehydration, hydrogels were prepared as mentioned and freeze dried for 24 hours, followed by rehydration in PBS over another 24 hours. These samples were analyzed using a 10 mm diameter parallel plate as the geometry and a strain sweep was applied for at least 200 minutes.

2.3.5 Spinal cord harvesting and testing

Fresh spinal cords were carefully harvested from euthanized rats. Using a scalpel, a longitudinal cut was made along the back of the rat exposing the spine. Clips were used to hold the skin apart while crushing and removing with rongeurs each individual vertebrae and bone covering it, allowing direct access to the spinal cord. After severing the nerve roots on both sides along the length of the spine, the spinal cord was collected by carefully lifting it up with forceps. The samples were placed immediately in PBS buffer in an ice bath and within 30 minutes of sample collection the spinal cord was sectioned in 1 mm thick slices and placed in the rheometer. A 10 mm diameter parallel plate geometry was used and a strain sweep was applied.

2.3.6 Loading experiments

To study the release kinetics of NT-3 from the hydrogels, 100 µL gels were prepared as described in low binding plastic tubes, quenched with pH 9 buffer and freeze dried, followed by rehydration in a solution containing 100 ng/mL NT-3 (Peprotech) and 1% bovine serum albumin (BSA) (ThermoFisher) to stabilize the growth factor. First, in order to confirm the uptake and release of protein into the scaffold during rehydration, a loading study was carried out. An excess solution of NT-3 in PBS at different concentrations was added to the dry gels, using either a PBS solution, a 1M NaCl PBS solution or a 2M NaCl PBS solution. 24 hours later the unswollen solution was removed and frozen at -20°C. The remaining hydrogel was cut into small 1 mm square pieces and placed in an elution buffer containing 137 mM NaCl, 0.1% Triton-X and 10 mg/mL heparin for another 24 hours at 4°C to extract the bound NT-3. The amount of NT-3 present in the samples was measured with an enzyme-linked immunosorption assay (ELISA) using a mouse anti-human NT-3 capture antibody and a biotinylated goat anti-human NT-3 detection antibody according to the

manufacturer's protocol (R&D Systems). A standard curve with known concentrations was prepared to calculate the amount of NT-3 present in each sample. The fraction of growth factor loaded was calculated by dividing the amount present in the gel by the total amount detected in the solution plus the gel. Release experiments were carried out in a similar way, loading the dry gels with an excess solution containing 100 ng/mL NT-3 in a PBS solution supplemented with 1% BSA. Following loading, 100 μL of 1% BSA PBS was added to each gel as a release solution and samples were collected at several time points, then frozen at -20°C for storage until analyzed using ELISA to measure the amount of NT-3 released and produce a release curve.

2.3.7 Release studies

Drug release studies were carried out *in vitro* using recombinant neurotrophin-3. Briefly, 200 μL gels were made in PBS in a 48 well plate, then frozen and lyophilized. Dry gels were rehydrated in a PBS solution containing 100 ng/mL NT-3 supplemented with 0.1% BSA to prevent protein adsorption to surfaces and overall loss and placed in an incubator at 37°C overnight. To start retrieving release samples, 0.5mL of PBS was added to each gel and release samples were collected at several time points while replenishing the PBS each time. Samples were quickly transferred to a -80°C freezer to be stored until the end of the study. An ELISA kit was used to measure the concentration of each sample by comparing them to a standard curve with known amounts of NT-3.

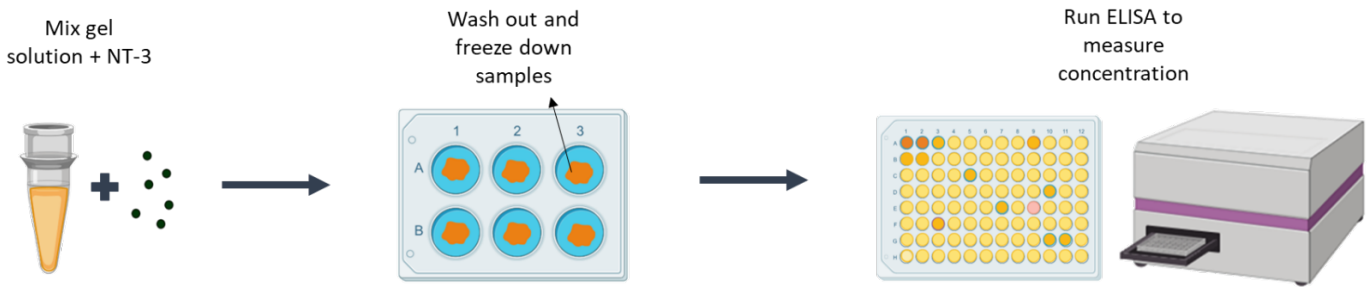

Figure 2.1. Release study methodology. Hydrogel solution and growth factors are mixed and incubated for an hour then placed in excess buffer. At select time points, release buffer samples are collected for final protein concentration determination via ELISA.

2.3.8 Dorsal Root Ganglion harvesting and culture

Fertilized chicken eggs from Texas A&M Poultry Science Department were incubated in an egg incubator (GQF Model 1500) for 7 to 9 days. At the day of collection, eggs were removed from the incubator and embryos were placed on a petri dish to be dissected under the microscope. Using two sets of forceps, the spine was cut and removed to expose the dorsal roots at both sides. DRGs were collected carefully and pooled in a smaller petri dish with warm neurobasal media.

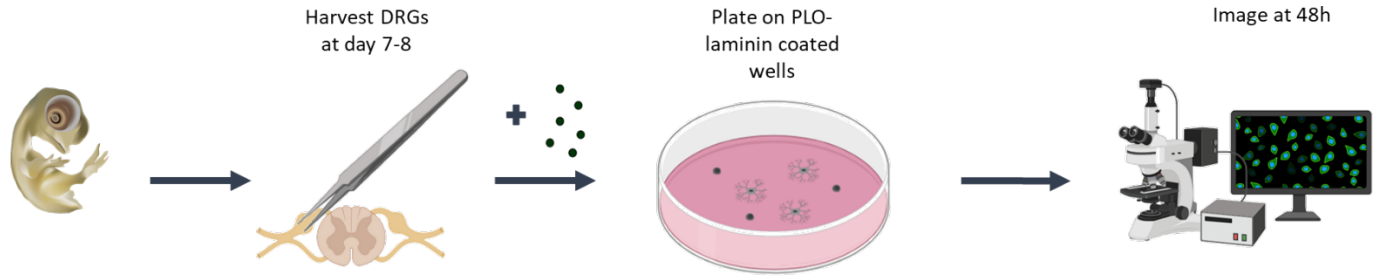

Figure 2.1. Dorsal root ganglion harvesting and seeding protocol. DRGs are obtained from day 7 chick embryos then plated on PLO-laminin coated wells, then grown for 48 hours.

2.3.9 V2a interneuron and motoneuron culture and preparation

<u>mESC Culture</u>

Fluorescent Hb9-PAC and Chx10-PAC mESCs cell lines were generated in previous work in our lab(Iyer et al., 2016; Mccreedy et al., 2014). Both cell lines were maintained in complete media (CM) containing (10% Fetal Bovine Serum (Invitrogen), 10% Newborn Calf Serum (Invitrogen), 132 μM beta mercaptoethanol (BME) (Sigma), 10,000 units/mL mouse leukemia inhibitory factor (Life Technologies) and passaged every 2–3 days at approximately 80% confluency. 1mL of 0.25% Trypsin-EDTA (Life Technologies) incubation at 37°C for 5 min was used to dissociate mESCs from the culture flask. This reaction was then quenched with fresh CM and cells were seeded into a new T25 flask coated with 0.1% gelatin (Sigma).

Stem Cell Differentiation and Selection Protocol

Motoneurons and V2a interneurons were generated from Hb9-PAC and Chx10-PAC mESCs as previously described(Brown et al., 2014; Iyer et al., 2016; McCreedy et al., 2012, 2014). Briefly, both were differentiated using a $2^{-}/4^{+}$ induction protocol, culturing approximately 1.5 x 10^{6} cells in suspension in agar coated petri dishes using DFK5 media, composed of DMEM/F12 (Life Technologies) with 5% Knockout Serum Replacement (Life Technologies), 1x Insulin-Transferrin-Selenium (Life Technologies), 50 μM nonessential amino acids (Life Technologies), 5 μM thymidine, 100 μM beta-mercaptoethanol (Sigma) and 15 μM of the following nucleosides: adenosine, cytosine, guanosine, and uridine (Life Technologies). As part of this process, mESCs aggregate into embryoid bodies. For motoneurons, at two and four days the media was replaced with fresh DFK5 media containing 2 μM of retinoic acid (RA; Sigma) and 600 nM of smoothened agonist (SAG; EMD Millipore). In the case of V2a's, the media was also changed at two days adding 10 nM RA and 1 μM purmorphamine (EMD Millipore), and at day 4 with DFK5 supplemented with 10 nM RA, 1 μM purmorphamine and 5 μM N-{N-(3,5-difluorophenacetyl-l-alanyl))-(S)-phenylglycine-t-

butyl-ester (DAPT; Sigma). At day 6, EBs were dissociated using 0.25% Trypsin-EDTA and quenched with complete media. After counting, approximately 3.5 x 10^6 cells were seeded onto laminin coated T25 flasks in "selection media", composed of half DFK5 and half neurobasal (NB) media supplemented with 4 μg/mL puromycin, 10 ng/mL of NT-3, BDNF and GDNF, 1x GlutaMAX and 1x B27.

Preparation of Motoneuron and V2a Interneuron Neuroaggregates

Two days after selection, motoneurons and V2a interneurons were lifted from the flasks using Accutase ® (Sigma) treatment for 20 minutes and 600,000 – 800,000 cells were transferred into a single well in a Aggrewell 400 (Stemcell Technologies) plate with 1200 microwells per well to get approximately aggregates with 500 – 600 cells per neuroaggregates. The well had been previously treated with anti-adherence rinsing solution to reduce surface tension and reduce cell adhesion. In both cases, the cells were cultured for two days in DFK5:NB media supplemented with 1x GlutaMAX, 1x B27 and 10 ng/mL of NT-3, GDNF and BDNF to drive neuroaggregate formation. At this time, neuroaggregates were lifted and collected for counting before seeding.

2.3.10 Quantitative-PCR

qRT-PCR was performed following differentiation and selection of V2a interneurons and motoneurons as previously described(Iyer et al., 2016). Briefly, cell lysates were collected for RNA extraction with a RNeasy kit (Qiagen) before selection, 1 and 2 days post-selection. An RNA-to cDNA kit was used to synthesize cDNA, which was combined with TaqMan Fast Advanced Master Mix (Applied Biosystems) and TaqMan Gene Expression Assays (Applied Biosystems). The gene of interest was targeted using a TrkC receptorTaqMan probe (ID: Mm00456222_m1, Thermo), and qRT-PCR was performed in a thermocycler with an initial 95°C for 20s then 40 cycles of 95 °C for 1s and 60 °C for 20s.

2.3.11 Biological activity assay

To confirm that the released NT-3 retained its biological activity, a dorsal root ganglion (DRG) assay was used. 24 well plates were coated with Poly-L-ornithine and incubated at 37^{o}C for 1 hour followed by 3 washes with HBSS buffer and coating with a 5 ug/mL laminin solution in HBSS for another hour. The laminin solution was removed before seeding the cells. Briefly, 5-8 dorsal root ganglion harvested from day 7 white leghorn chick embryos were individually picked with a pipette and placed in the wells with neurobasal media with 1% GlutaMAX, 1% penicillin-streptomycin, 2% B-27 supplement and 0.1 % BSA. During this time, the samples collected from the release experiment were thawed at room temperature, warmed up to 37^{o}C and finally 400 µL of differentiation media was added to each well. The DRGs were grown for 48h and imaged using bright-field microscopy with a 4x objective. The images were analyzed with ImageJ software to quantify the average neurite growth, which was calculated as the average radius of an annulus between the DRG body area and the outer ring of axonal extension. The results were compared to previously established correlations between NT-3 concentration in the media and average neurite extension to determine the retention of bioactivity of released NT-3 when compared to free NT-3 in media.

Total area of outgrowth

-

Area of DRG body

=

Average neurite extension area

$$r = \sqrt{\frac{area}{\pi}} = \text{average neural extension}$$

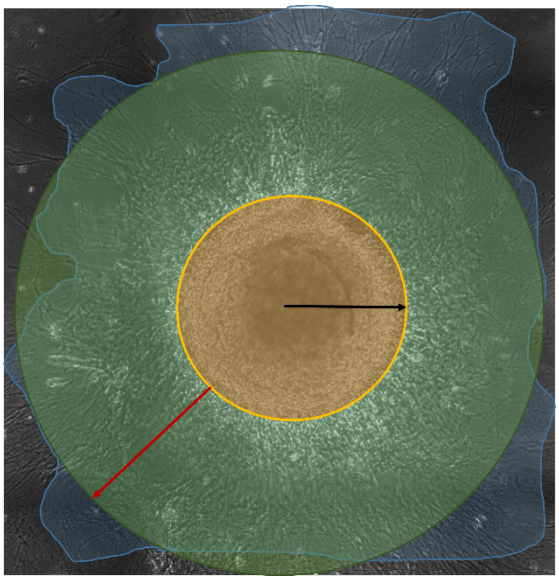

Figure 2.3. Axonal growth tracing method and equation. The blue area is initially traced across the edge of all axonal extensions. The area of the DRG body is subtracted and the average radius of outgrowth can be obtained.

Similarly, the effect of NT-3 on neurite outgrowth of V2a interneuron and motoneuron neuroaggregates were investigated as follows: laminin coated wells (5 µg/mL) were prepared before aggregate collection and 8 – 10 aggregates were seeded into each well of a 24-well plate supplemented with 0, 5, 10 or 20 ng/mL NT-3. The aggregates were grown for two days at 37°C and 5% CO_2 and imaged using fluorescent microscopy. Neurite extension was also quantified and analyzed.

2.3.12 Statistics

All in vitro data was analyzed using multiple comparison ANOVA with a Scheffé post-hoc test and a 95% confidence threshold, unless otherwise stated. Significance for each experiment was determined by comparing each group and condition to the respective controls. In the case of analyzing more than one condition against each other, Sidak's

multiple comparisons test was used, determining the mean difference and 95% confidence intervals to calculate the adjusted P-values and establish significant differences between groups.

2.4 Results

2.4.1 Synthesis of hyaluronic acid hydrogels

Previous work has demonstrated the benefits of using hyaluronic acid as a natural polymer for neural tissue applications due to its biocompatibility and suitability to be chemically tuned for different purposes. In this case, HAmF PEG-diMal hydrogels were successfully synthesized in two steps. Hyaluronic acid was first functionalized with methylfuran to provide a functional group for crosslinking (**Figure 2.4A**), then reacted with PEG-diMal in different molar ratios. In this reaction, the carboxylates of HA were activated by DMTMM to drive the coupling with the primary amine present in 5-methylfurfurylamine. The presence of methylfuran in the hyaluronic acid was confirmed via proton NMR (**Figure 2.4B**). The degree of functionalization was calculated by comparing the integration areas under the methylfuran proton peaks (6.26, 6.02 and 5.96 ppm) to the N-acetyl glucosamine of hyaluronic acid (2.01 ppm), resulting in degrees of substitution of 51% to 55%.

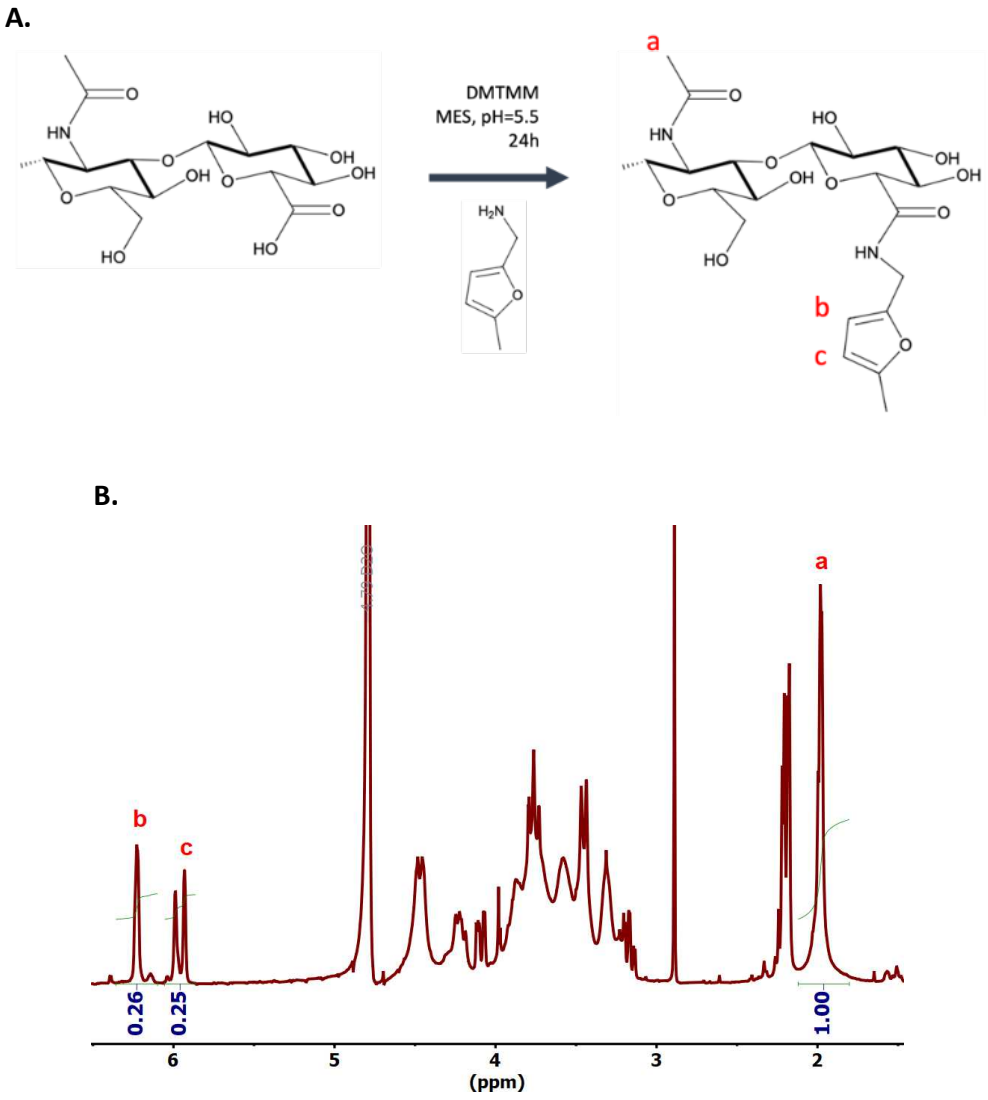

Figure 2.4. A) Hyaluronic acid functionalization reaction scheme. The carboxylic acid groups on the hyaluronic acid chain are activated and functionalized with methylfurfurylamine resulting in HA-methylfuran. The final product is dialyzed against DI water, lyophilized and collected as a white fibrous material. B) NMR spectra of HA-methylfuran. The proton peaks highlighted represent methylfuran (b and c) and the N-acetyl glucosamine of HA (a). The degree of functionalization is calculated from this data dividing the integration areas under the methylfuran peaks by the HA peak.

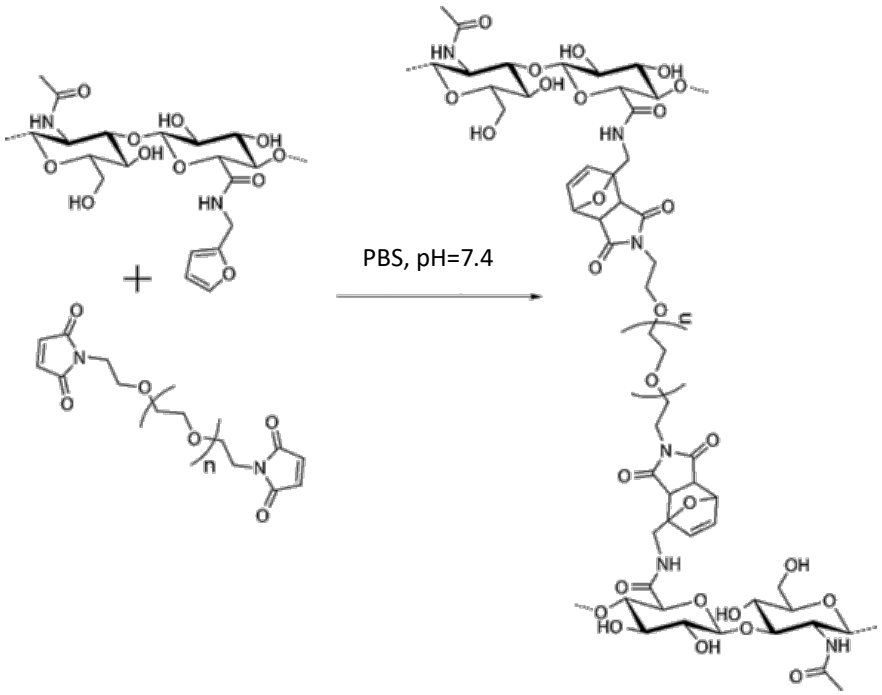

Figure 2.5. HAmF crosslinking with PEG-diMal Diels-Alder reaction scheme. The click reaction is carried out at 37 C in PBS buffer as a highly selective [4 + 2] cycloaddition between a diene and a dienophile, proceeding without the need for a catalyst.

The hydrogel was formed in a Diels-Alder click reaction, without the presence of a catalyst and any toxic byproducts (**Figure 2.5**). To mimic the *in vivo* environment, the crosslinking reaction and all the following steps were formed at physiological temperature and pH (37°C and pH 7.4, respectively).

2.4.2 Rheological characterization of hydrogel properties

One of the most relevant parameters for the design of biomaterials for specific tissues is stiffness. To optimize the reintegration with host tissue, it is crucial that no mechanical mismatch occurs, and that the stiffness of the material is equal or as close as possible to that of the tissue of interest. For this purpose, rheology experiments were carried out to study the final elastic modulus of the hydrogel as well as the gelation time. It was found that the hydrogel formed in approximately 15 minutes for all ratios (**Figure 2.6A**). The final storage

modulus of the gels could be tuned by modifying the molar ratio of the functional groups. Values in the range of 200 to 700 Pa were obtained for maleimide to methylfuran ratios of 1:5, 1:3 and 1:1.5, respectively. For the gels that were previously lyophilized and rehydrated, the storage modulus was 60 to 70% higher due to the hydrogel not fully swelling to the same volume. Freshly harvested rat spinal cords showed a similar storage modulus when measured under the same conditions as the gels, in the range of 560 to 890 Pa (**Figure 2.6B**). These values are in agreement with most of those reported for central nervous tissue, generally 100 – 1000 Pa(Cheng et al., 2008; Seidlits et al., 2010).

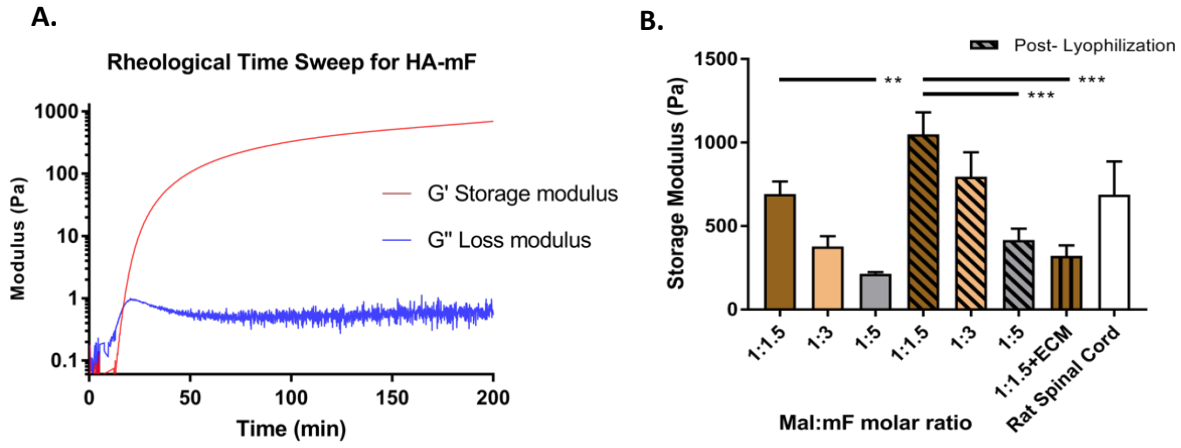

Figure 2.6. A) Rheological time sweep shows gelation kinetics for HAmF hydrogels. 700 μL of pre-gelled solution were placed on a rheometer and a four-hour time sweep was applied at 10 rad/s and 0.2% strain using a 40 mm cone geometry with a solvent trap to prevent sample evaporation. The gel started forming at 15 minutes (storage modulus crossing loss modulus) and it was fully formed after three hours. B) Final storage modulus of HAmF hydrogels at different Mal:mF ratios with and without lyophilization, in the presence of ECM and native rat spinal cord tissue (** = $p < 0.005$, *** = $p < 0.001$, $n>4$). Hydrogel values were taken when the storage modulus curve plateaued, spinal cord was measured within 15 minutes of harvesting to preserve physiological mechanical integrity.

2.4.3 Hydrogel quenching and protein loading

Hydrogels were formed as mentioned and left to crosslink for 24 hours, then crosslinking was quenched with a pH 9 PBS solution to hydrolyze unreacted maleimide groups. The quenched hydrogels were freeze-dried for 24 hours. This procedure prevents the maleimides from competitively reacting with NT-3, which was found to block effective binding to the capture antibody of the ELISA (**Figure 2.7A**). In this case, NT-3 was loaded onto the hydrogels by rehydrating the dry scaffolds in a 1% BSA PBS solution containing 10, 50, 100 or 250 ng/mL of NT-3. Even though no clear trend was observed, the percentage of NT-3 loaded onto the hydrogels ranged between a low end of 65% for 50 ng/mL and 83% of the initial theoretical loaded amount for 250 ng/mL. Based upon previous studies and data, 100 ng/mL was chosen as the target loading concentration(Johnson et al., 2009; L. Taylor et al., 2006; S. J. Taylor et al., 2004; Yang et al., 2010) (**Figure 2.7B**).

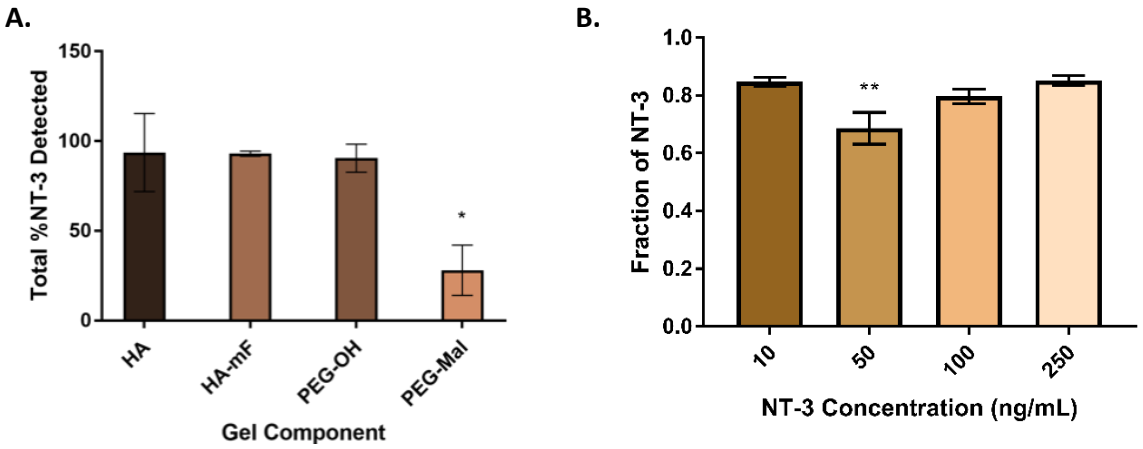

Figure 2.7. A) Amount of NT-3 detected in the presence of each component of the hydrogels after 24h. Both components of the hydrogel were tested separately with and without functional reactive groups to determine specific interactions with NT-3. PEG-Mal showed reduced levels of NT-3 detection, suggesting a competitive binding effect of NT-3 with maleimide reactive groups (* = $p<0.005$, n=3). B) Amount of NT-3 loaded onto the hydrogels based upon NT-3

concentration measured at 24h. The amount of NT-3 loaded was measured by degrading the hydrogel in the presence of hyaluronidase, heparin and NaCl (** = $p < 0.005$, n=4).

2.4.4 Modeling of release

To investigate the nanostructure of the material, calculations based upon polymer crosslinking parameters were used to gain an understanding of the pore size in the hydrogel network:

$$\frac{1}{M_c} = \frac{2}{M_n} = \frac{\left(\frac{v}{V_1}\right)\left[\ln\left(1 - v_{2,s}\right) + v_{2,s} + X_1 v_{2,s}^2\right]}{v_{2,r}\left[\left(\frac{v_{2,s}}{v_{2,r}}\right)^{1/3} - \frac{v_{2,s}}{v_{2,r}}\right]} \qquad \xi = v_{2,s}^{-1/3}\left(\frac{2C_n M_c}{M_r}\right)^{1/2} l = 38\ nm$$

$$D_\infty = \frac{kT}{6\pi\mu r_{se}} = \frac{RT}{6\pi\mu r_{se} N_A} = 1.57 \cdot 10^{-6}\ cm^2/s$$

$$\frac{D}{D_o} = \exp\left(-\frac{\pi}{4}\left(\frac{r_s + r_f}{\frac{\varepsilon}{2} + r_f}\right)^2\right) = 8.06 \cdot 10^{-7}\ cm^2/s$$

Mesh size calculations were done using experimentally measured swelling parameters and the Peppas equation to determine the average pore size of the gels (Peppas et al., 2000, 2006). To obtain the mesh size value, ξ, the first step is to calculate the average molecular weight between crosslinks, M_c. To obtain it, we used the molecular weight of the polymer chain, M_n (250,000 Da for our HA), the polymer volume fraction in the swollen and relaxed states, $v_{2,s}$ and $v_{2,r}$ respectively, obtained by measuring the weight of hydrogels that were swollen and relaxed. ν, the specific volume of bulk HA (0.764 cm^3/g), V_1, the molar volume

of the solvent (18 mol/cm^3), C_n, the characteristic ratio of HA (27) and χ_1, the Flory-Huggins interaction parameter for HA in water (0.439) were obtained and approximated from the literature (Wanselius et al., 2022; Martini et al., 2016; Baier Leach et al., 2003; Potenzone & Hopfinger, 1978). Similarly, M_r, the molecular weight of the HA repeat unit (415 g/mol) and l, the length of a glycosidic oxygen bond (0.52 nm) were used to calculate an average pore diameter (ξ) of 38 nm was found. We approximated the size of NT-3 using the Stokes-Einstein equation where k is Boltzmann's constant, T is the temperature, and η is the solvent viscosity and found the average hydrodynamic radius of NT-3, r_{se}, to be 3 nm (Butte et al., 1998; Kolbeck et al., 1994). This would suggest that the mechanism of release should be purely diffusional as the growth factor has enough space to exit the hydrogel when swollen. However, the delivery profile showed otherwise, introducing the possibility that the release was being slowed or prevented by other forces present in the hydrogel system.

2.4.5 In vitro NT-3 release from hydrogels

To further investigate the release mechanism, 100 ng/mL NT-3 was encapsulated in the gels, and these were placed in release buffers containing 0 M, 1 M and 2 M NaCl. 24 hours later, the amount of NT-3 released and that bound to the gels was measured **(Figure 2.8A)**. When using a loading solution containing salt, the amount of NT-3 that was taken up by the hydrogel was reduced. For the NT-3 released onto the PBS solution, 80% of it was still bound to the hydrogel. As the salt concentration increased, so did the amount of NT-3 released, with 25% released in 1M NaCl and almost 90% in 2M NaCl. NT-3 has an isoelectric point of 9.4(Maisonpierre et al., 1990), and the carboxylates present in the backbone of the HA chains have a pKa of 3-4, so at a pH of 7.4 the growth factor is positively charged while the hydrogel presents an overall negative charge. Furthermore, a basic sequence present in

the C-terminus of the growth factor may also contribute to the electrostatic binding between NT-3 and HA's carboxylic acid groups(S. J. Taylor et al., 2004). Therefore, a higher salt concentration may cause the disruption of the ionization in the HA backbone, leading to weaker electrostatic interactions between the gel and the NT-3 and resulting in a lower loading fraction. It is suggested that the presence of electrostatic interactions between the molecule and the polymer may be the reason for the entrapment of NT-3 and may effectively slow down the release over a longer period of time. To determine if this was the case, a release study was conducted over 4 weeks to compare the delivery of NT-3 *in vitro* in a PBS buffer with that in an elution buffer, containing 1M NaCl and 10 mg/mL heparin (**Figure 2.8B**).

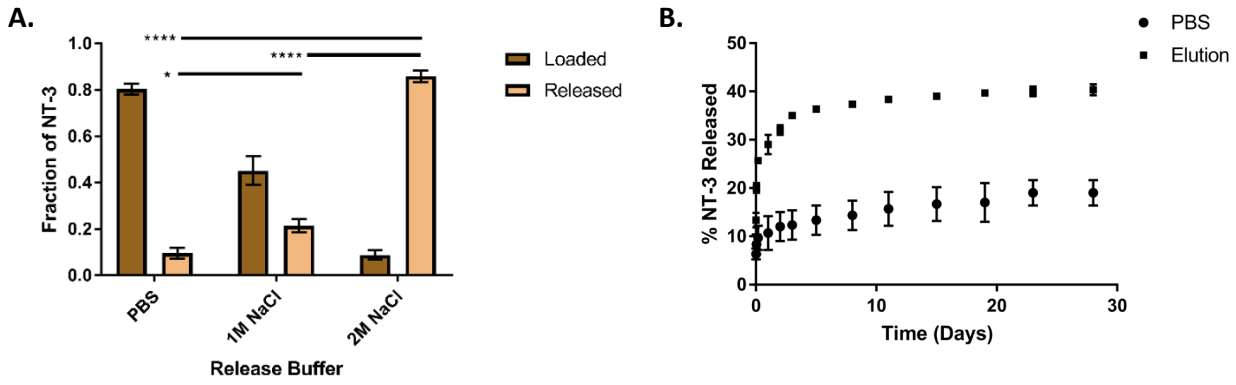

Figure 2.8. A) Fraction of NT-3 released and bound to the hydrogels at 24h in the presence of PBS, 1M NaCl and 2M NaCl. Hydrogels were placed in excess PBS buffer with BSA and the concentration of released NT-3 was measured. Loaded refers to NT-3 still bound to the hydrogel, measured by degrading it in the presence of hyaluronidase, heparin and NaCl. Higher salt concentrations led to unbinding of NT-3 from the hydrogel (* = $p < 0.05$, **** = $p < 0.0001$, n=3). B) Release profile of 100 ng/mL NT-3 from a HAmF hydrogel over 4 weeks in the presence of PBS or elution buffer containing 1M NaCl and 10mg/mL heparin.

The release profile was typical of an affinity-based delivery system, with a slight burst release of 10-15% of the total loaded within the first hour. During the following 28 days, small amounts of NT-3 were detected in the release buffer, resulting in only 25% of the total NT-3 loaded being released. Exposing the hydrogels to the elution buffer resulted in the amount of NT-3 release almost doubling, to 42% of the NT-3 initially loaded. This suggests that the presence of electrostatic interactions trap the molecules and either the loss of binding or the degradation of the gels are the main drivers of NT-3 release. If injected *in vivo*, the presence of hyaluronidases and the excess shear would likely lead to quicker degradation, reduced viscosity and therefore we would expect a higher amount of growth factor released over the same 4 weeks.

2.4.6 In vitro DRG axonal growth assay

As the release profile seemed to be promising for the sustained delivery of NT-3, the biological activity of the released growth factor was analyzed. The DRG assay provides a simple and established platform to study the effect of different therapeutic agents on neurons *in vitro* **(Figure 2.9)**. The laminin concentration for the coating of the plate had to be tuned to a level sufficient to provide an attractive substrate for cell adhesion but not too high to allow axonal growth (high levels can cause entrapment).

To confirm that the growth factor bioactivity was maintained after being released from the hydrogel, samples were collected from release media and added to DRGs in culture to compare with free NT-3 in media. Following the release curves, the NT-3 concentration at 24h was assumed to be between 8 and 12 ng/mL, which should be sufficient to elicit a significant enhancement of neurite growth. It was found that the released NT-3 elicited axonal growth that was statistically different from the 0 ng/mL negative control, and not

significantly different from the 10 ng/mL positive control, suggesting that most of the bioactivity was retained (**Figure 2.10**).

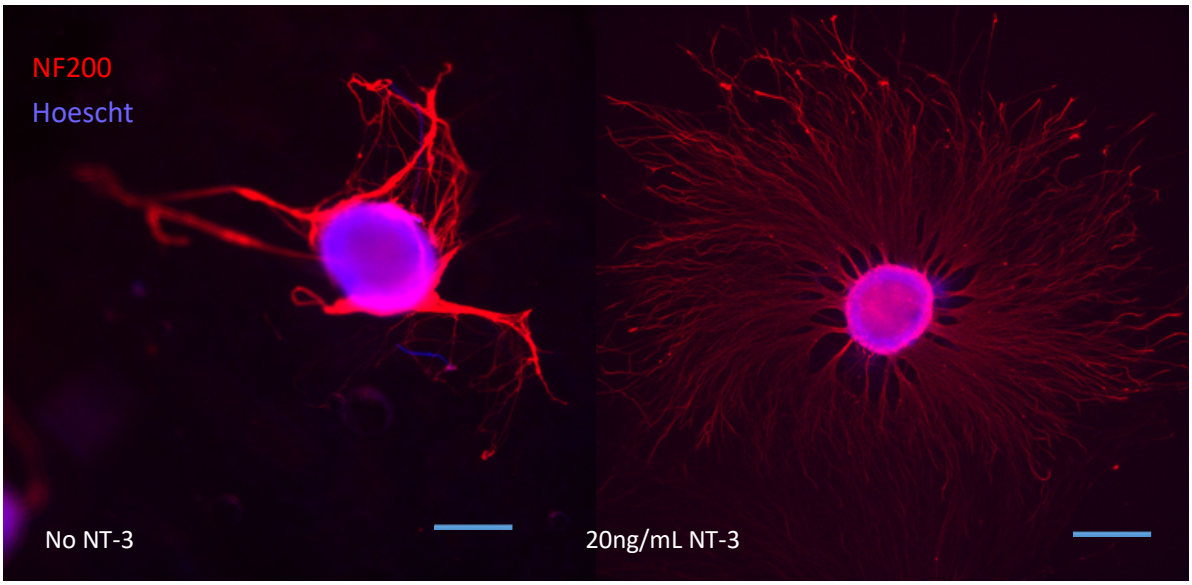

Figure 2.9. DRG neurons seeded on laminin coated wells in the presence of no NT-3 or 10 ng/mL NT-3. Images were taken on a fluorescent microscope with a 4x objective (scale bar = 200 mm). Staining indicates axonal processes (NF200) and cell nuclei (Hoescht).

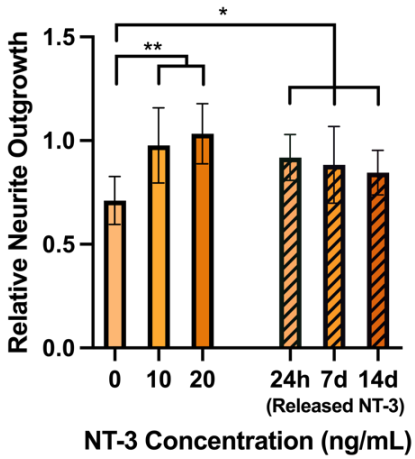

Figure 2.10. Average neurite extension in the presence of NT-3 normalized to 10 ng/mL. The growth was calculated by measuring the overall area of axonal extension, subtracting the cell body and applying the formula of a circle to find the average radius (* = $p < 0.05$, ** = $p < 0.005$, n=4).

2.4.7 V2a Interneuron and Motoneuron Axonal Growth Assay

Because DRGs are clusters of peripheral sensory neurons, they do not adequately represent all cell populations present in the spinal cord. For this reason, mESC-derived interneurons and motoneurons were investigated to confirm that NT-3 can improve neuronal growth using similar *in vitro* bioactivity studies. Both cell populations were differentiated and aggregates of 800 -1000 neurons were formed before seeding (**Figure 2.11A**). In the relevant concentration windows, NT-3 was shown to increase neurite outgrowth for both V2a interneurons and motoneurons and this growth was concentration dependent, with 10 ng/mL being sufficient to elicit a significant improvement and 20 ng/mL showing almost a 25% increase over the lower concentration (**Figure 2.11B**).

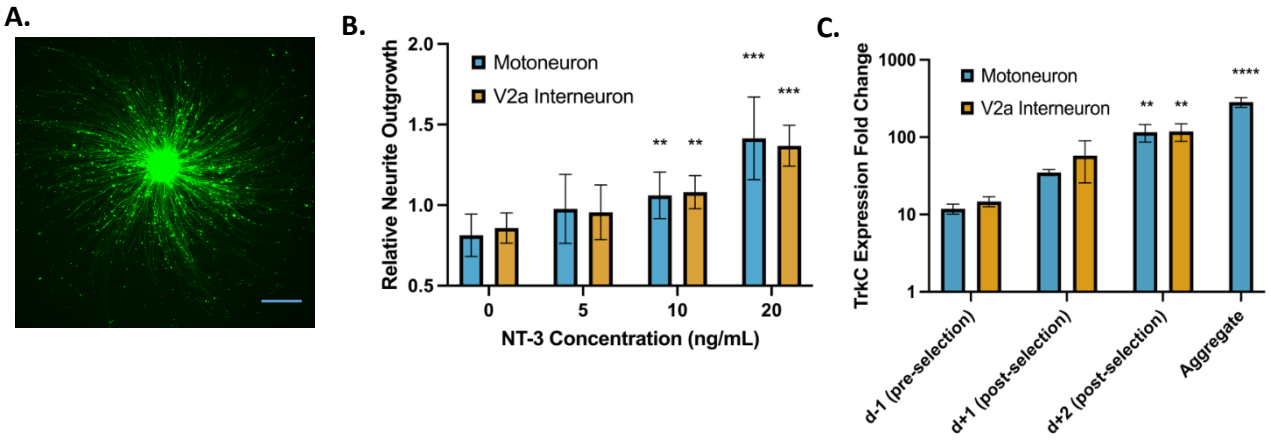

Figure 2.11. A) V2a interneuron aggregate seeded on laminin coated well in the presence of 20 ng/mL NT-3 (scale bar = 200 mm). B) Normalized neurite outgrowth from V2a interneuron and motoneuron neuroaggregates in the presence of NT-3. (** = $p<0.005$, *** = $p<0.001$, n=3 for at least 10 neuroaggregates per group). C) TrkC receptor expression for motoneuron and V2a interneuron quantified using qRT-PCR expressed as TrkC fold change relative to the ESC control for each cell line (** = $p < 0.005$, **** = $p < 0.0001$, n>3).

Quantitative PCR was used to study the presence of TrkC receptor and expression in both neuronal cell types. Motoneurons and V2a interneurons expressed significantly higher levels of TrkC when compared to ESC controls (**Figure 2.11C**). This expression was dependent upon the day samples were collected, with levels increasing one and two days post selection in both cases. This makes sense as during the differentiation protocol, the amount of differentiated motoneurons or interneurons should be higher following selection (addition of puromycin), and we expect that cell population to express higher levels of TrkC compared to pre- or unselected neurons.

2.4.8 Growth of DRGs and V2a Interneuron Aggregates Seeded in HAmF Hydrogels

Although it is commonly used as a scaffold material, HA does not inherently support the adhesion and growth of neurons, so it is often functionalized with ECM components, such as laminin and fibronectin or binding peptides, including IKVAV and RGD, respectively (Ishihara et al., 2018; Lampe et al., 2013; J. Park et al., 2010). To further confirm that the HAmF hydrogels were conducive to neuronal survival and growth, V2a interneuron aggregates were seeded within the HAmF hydrogels, and two days post-seeding over 75% of cells were found to be viable in hydrogels supplemented with growth factors. As expected, when laminin was added to the gels, the cell viability increased to over 85% (**Figure 2.12A**). To further confirm that the HAmF hydrogels were conducive to neuronal survival and growth, both DRGs and V2a interneuron aggregates were seeded within the HAmF hydrogels, stained and imaged two days post-seeding with beta-tubulin (TUJ-1), a neuronal marker and neurofilament (NF200), which stains axons (**Figure 2.12B**). Both cell populations adhered to the scaffolds in the presence of 5 mg/mL laminin and extended robust axonal processes through the pores of the hydrogel. We encapsulated the DRGs and

aggregates by adding them to the pre-gelled hydrogel solution in media. The presence of laminin improved the adhesion of the neurons to the scaffold and the growth factors provided the necessary cues to enhance axonal growth. We observed that the DRGs grew neurites and axonal extensions through the pores of the scaffold, reaching 5 to 10 times the length of the cell body.

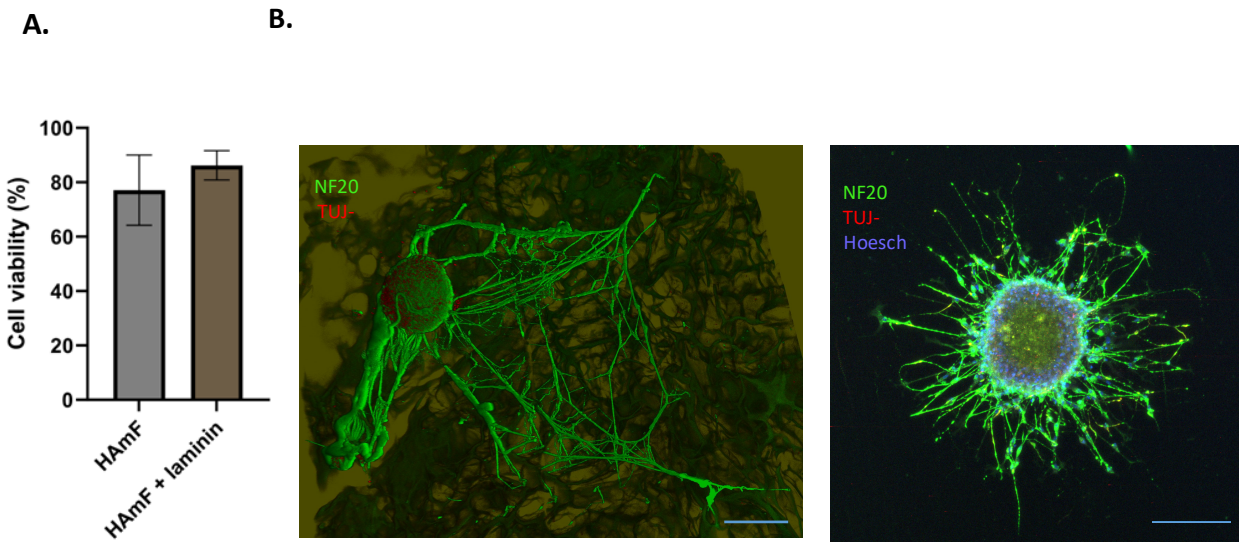

Figure 2.12. A) D) Cell viability of V2a interneuron aggregates inside of the HAmF hydrogels ($p = 0.0568$, ns, error bars = SD). B) 3D confocal image of DRG seeded inside of HAmF PEG-diMal hydrogel supplemented with 5 µg/mL laminin and 20 ng/mL NT-3 (scale bar = 200 µm) C) Stacked confocal image of V2a interneuron aggregate seeded inside of HAmF PEG-diMal hydrogel supplemented with 5 µg/mL laminin and 20 ng/mL NT-3 (scale bar = 200 µm).

2.5 Discussion

HAmF hydrogels were previously used to transplant both V2a interneurons and astrocyte-derived ECM; however, their ability to be used as a drug delivery platform had not been investigated. In this work, hyaluronic acid hydrogels were shown to provide sustained

delivery of biologically active NT-3 following encapsulation and release for over 28 days. We found the mechanism to be controlled by electrostatic interactions between the negatively charged hydrogel chains and positively charged NT-3. Compared to other methods, this affinity-based system does not require extra complexity in the form of microparticles, binding motifs, or transplantation of transgenic cells overexpressing a specific protein. In the case of encapsulating molecules in micro/nanoparticles, the process often results in exposure to various stresses that negatively impact neurotrophin stability (Stanwick et al., 2012).

In many studies demonstrating controlled release of neurotrophic factors from hydrogels or particle systems, there is very little emphasis on biological activity. As a crucial element to effective drug delivery, this is often overcome by significantly increasing the loading concentrations to compensate for the partial loss of bioactivity. HAmF PEG-diMal hydrogels provide a simple matrix capable of protecting protein stability over multiple weeks allowing for lower protein concentrations and minimizing the potential side effects when used as a clinical therapy. Furthermore, the biomechanical properties of the gels were studied using rheology and showed that the storage modulus of the gels was in a physiologically relevant range when compared to native rat spinal cord tissue (0.1 – 1 kPa).

To validate the use of NT-3 as a therapeutic approach to the CNS, we tested its effect on relevant cells specific to the spinal cord. Both V2a interneurons and motoneurons were studied and found to express the NT-3 targeted TrkC receptor using qPCR. Further bioactivity experiments showed that NT-3 significantly enhances neurite outgrowth for both cell types in vitro. We found that the hydrogels were a suitable platform for neuron growth, with relatively high cell viability levels even in the absence of cell-adhesion molecules such as laminin. V2a interneurons and DRGs presented axonal projections through the scaffold

pores, suggesting that HAmF hydrogels provide a conducive environment for cell survival and growth.

The main limitation of this study is the lack of in vivo release data. Based on the characteristics of the hydrogels, if injected in vivo, the presence of hyaluronidases and the excess shear would likely lead to quicker degradation, reduced viscosity and therefore we would expect a higher amount of growth factor released over the same 4 weeks. Other groups have shown both in vitro release and in vivo delivery of NT-3 to the spinal cord over similar time periods ranging between 2 and 6 weeks39,60–62. We only tested the biological activity of released NT-3 after 14 days and not 28 days due to the limited sensitivity of the bioactivity assay and the NT-3 loading concentration needed to test the potency after 4 weeks of release. However, our system shows strong retention of biological activity at the two-week time frame, which is relevant to the acute and subacute phases of SCI.

2.6 Conclusion

We have synthesized HAmF PEG-diMal hydrogels and tuned them to achieve a sustained delivery of NT-3 over a period of 4 weeks. The neurotrophin remains biologically active as shown by DRG outgrowth studies, and the gels allow for adhesion and growth of neuroaggregates when supplemented with laminin and other ECM proteins. Furthermore, the hydrogels match the mechanical properties of native spinal cord from rats, are injectable and crosslink at body temperature.

Here, we demonstrated sustained release of bioactive NT-3 from a hyaluronic acid hydrogel. The release of NT-3 was found to be controlled by electrostatic interactions between the growth factor and the backbone of the polymer, slowing down the delivery and providing

long term release over a period of 28 days. Additionally, the biological activity of released NT-3 was confirmed using both primary neurons and stem cell derived neuron populations suggesting a protective and stabilizing role of HAmF for at least 14 days. The gels were also shown to provide a platform for cell survival and growth, and these effects were enhanced when the scaffold was functionalized with laminin. This system introduces a novel neurotrophin delivering platform that matches the mechanical properties of the central nervous system and has the potential to aid regeneration after SCI.

Chapter 3

PEG-Based Microparticles for Controlled Release of Insulin-Like Growth Factor 1

3.1 Abstract

In this work, we aimed to evaluate the effect of insulin-like growth factor (IGF-1) delivery from polyethylene-glycol diacrylate (PEG-DA) microparticles (MPs). Here, we have developed PEG-DA based MPs using varying levels of acrylic acid (AA) as a comonomer. The particles were synthesized via precipitation polymerization under UV light, yielding microparticles 2-3 μm in diameter with a relatively low polydispersity index. Both insulin and IGF-1 were encapsulated in the PEG-DA particles via incubation, and formulations with a higher acrylic acid content resulted in higher loading efficiency. Release studies showed IGF-1 being released in a sustained manner over 4 weeks, and the conditions with high AA displaying the slowest release, suggesting the presence of binding interactions between the positively charged IGF-1 and negatively charged particles containing AA. The released IGF-1 was tested in dorsal root ganglion (DRG) assays and found to retain its biological activity for up to two weeks after delivery. Furthermore, IGF-1's trophic effect was tested in stem cell derived V2a interneurons and found to have a synergistic effect when combined with neurotrophin-3. To assess the potential of a combinatory approach with the system developed in chapter 2, IGF-1 releasing MPs were encapsulated within hyaluronic acid-methylfuran (HAmF) hydrogels and showed promise as a dual delivery system. The dual encapsulation of IGF-1 within the MPs and the embedding of MPs within the HAmF scaffold drove down the release rate and resulted in a slower, sustained release when compared to the IGF-1

encapsulated in the matrix. Overall, the PEG-DA MPs developed herein deliver bioactive IGF-1 for a period of weeks and hold potential to enable axonal growth of injured neurons via sustained release.

3.2 Introduction

The proper locomotor function of the central nervous system is lost during spinal cord injury (SCI), when the axonal pathways extending from the brainstem are severed. Targeting these damaged neuronal circuits and promoting their regeneration and regrowth is a promising therapeutic approach. IGF-1 is a growth factor implicated in cellular function, somatic development, metabolic homeostasis and most notably for regulating growth (Ciucci et al., 2007; Mullen et al., 2015; Musarò et al., 2007). In the CNS, IGF-1 has been shown to play a role in neuroprotection and have a trophic effect, attenuating motor neuron apoptosis and cell death (Tsai et al., 2012). The combination of IGF-1 and osteopontin has been shown to increase corticospinal tract axon growth *in vitro* and in a complete SCI model in adult rats (Anderson et al., 2018; Özdinler & Macklis, 2006). The effect of IGF-1 is believed to be mediated mainly via the IGF-1 receptor (IGF-1R), which is highly expressed neurons, and downstream via the PI3-kinase/Akt pathway (Laurino et al., 2005). This receptor also acts as a modulator of signaling endosome trafficking, and its inhibition has been shown to improve deficits in motor neurons *in vitro* and in a mouse model of amyotrophic lateral sclerosis (Fellows et al., 2020). Other studies have shown that IGF-1R activation plays a critical role in growth cone assembly and therefore is important in axonal formation (Dupraz et al., 2013). It also has been reported to mediate enriched environment effects during visual cortical development (Ciucci et al., 2007). The downregulation of IGF-1R in mature neurons and the decreased growth factor levels following SCI are implicated in the limited regenerative ability

of adult mammals. Because of its neuroprotective effect, controlled delivery of IGF-1 presents a promising target for axon growth.

Sustained, local delivery of t to the spinal cord can be achieved using tailored drug delivery systems. Biomaterials, including hydrogels and particulate systems, have been extensively explored as drug carriers to the spinal cord (Ansorena et al., 2013; Elliott Donaghue et al., 2016; Johnson et al., 2009; Ziemba & Gilbert, 2017). However, during delivery system fabrication, growth factors are often exposed to disruptive conditions including organic solvents, extended light exposure, sonication, and other stresses. This exposure may lead to denaturation of the proteins, resulting in decreased biological activity. Prioritizing bioactivity in drug delivery systems will enable more effective therapies and allow for lower loading concentrations, resulting in fewer unwanted side effects and lower costs. Loading of neurotrophic factors onto poly(lactic-coglycolic acid) (PLGA) nanoparticles via short-range electrostatic interactions enabled adsorption and long-term release of the proteins without encapsulation, taking advantage of affinity binding (Pakulska et al., 2016; Vulic et al., 2015). PEG-diacrylate microparticles have been previously synthesized using precipitation photopolymerization (Flake et al., 2011). Both visible and UV light were used to crosslink the polymers, forming small particles with relatively high aggregation but low polydispersity. Furthermore, the zeta potential of the microparticles could be controlled by varying the content of the comonomer, acrylic acid. Previous work from our group has demonstrated that hyaluronic acid (HA) hydrogels are an ideal candidate for clinical applications due to its similar mechanical properties and sustained affinity-based release of bioactive neurotrophin-3 from (Ramos Ferrer et al., 2023). The charge differences between the carboxylates on the HA chain and the positively charged NT-3 enabled release of the growth factor over 4 weeks. The hydrogels matched the mechanical properties of native rat

spinal cord tissue and allowed adhesion and growth of dorsal root ganglion cells and mouse embryonic stem cell derived motoneurons and V2a interneurons.

In this work, we explored the potential of modifying these PEG-DA based microparticles to enable sustained release of IGF-1 by taking advantage of electrostatic interactions between the MPs and cationic proteins. First, we investigated the effect of copolymerization of microparticles with acrylic acid on IGF-1 loading and delivery. The particles were also embedded within HA scaffolds to further characterize the release profile. Finally, the cytotoxicity and biological activity of IGF-1 were tested using primary neurons and mouse embryonic stem cell derived interneurons *in vitro*, as well as in combination with NT-3 as a potential approach to increase axonal growth and neuronal regeneration.

3.3 Materials & Methods

3.3.1 Polyethylene Glycol-Diacrylate (PEG-DA) microparticle synthesis

Polyethylene-glycol microparticles were synthesized via precipitation photopolymerization of polyethylene glycol-diacrylate (Flake et al., 2011) with certain modifications. 3% w/v PEG-diacrylate (MW 3500), 10 μM of Irgacure 2959 or lithium phenyl(2,4,6-trimethylbenzoyl) phosphinate (LAP) as a photoinitiator, acrylic acid as a comonomer at 0, 40 or 80 mol% relative to PEG-diacrylate and 500 mM of sodium sulfate were combined at room temperature. The mixed solution was exposed to UV light at 2.5 mW/cm^2 and a wavelength of 365nm for times ranging between 30 seconds and 1 minute. Following polymerization, the microparticles were buffer exchanged to remove the remaining salt in solution via centrifugation at 8000 rpm for 5 minutes.

3.3.2 Microparticle characterization

10 µL of microparticle solution were placed on top of a microscope slide and covered with a glass coverslip to reduce motion and drying of the samples. Images were taken at 4x, 10x and 20x magnification in a Nikon Ti2 Microscope using phase contrast imaging. Particle size was determined using ImageJ by measuring the average diameter of each individual microparticle for at least 10 representative images in 3 distinct replicates.

Polydispersity index (PDI), as a measure of quality with respect to size distribution, was calculated using the following equation:

$$PDI = (\frac{StDev}{Mean})^2$$

For PDIs under 0.1, a particle solution is assumed to be monodisperse.

3.3.3 IGF-1 encapsulation and loading

PEG-DA microparticles were prepared as mentioned in section 3.3.1. Stock solutions of human recombinant insulin (Sigma-Aldrich) and IGF-1 (STEMCELL Technologies) were made in PBS supplemented with 0.1% BSA at 20 mg/mL and 1 mg/mL, respectively. Briefly, 10 mg of microparticles per sample were prepared and resuspended in 200 µL of PBS with 100 µg insulin or 10 µg IGF-1. The solutions were allowed to equilibrate for 24 hours at 4 ^{o}C. For an indirect measurement, 100 µl of loading solution were removed to measure the amount of free protein. The theoretical loading can be calculated using the non-encapsulated amount and the original known mass of protein added to the microparticles. For a direct measurement, the remaining microparticles were degraded over two hours with 200 µl DMSO and 600 µl of 0.2M NaOH solution added to each sample. The amount of protein in the microparticles was also measured using the same Pierce BCA or Micro BCA assay kit (ThermoFisher).

3.3.4 Long term release of IGF-1 from PEG-DA microparticles

To investigate the drug release characteristics of IGF-1 from PEG-DA microparticles, a four-week long release study was conducted. PEG-DA microparticles were synthesized as previously mentioned, and 60 mg each of 3 different formulations were prepared: PEG-DA, and PEG-DA with 40 or 80 mol% acrylic acid relative to PEG-diacrylate. 15 mg of microparticles per sample (all conditions tested in quadruplicate) were incubated in 200 µl PBS with 15 ug IGF-1 for 24 hours at 4 ^{o}C. Once the growth factor was loaded, microparticle solutions were centrifuged to remove the remaining IGF-1 that had not fully bound to the particles. The samples were then resuspended in 500 µl PBS as a release buffer and 200 µL samples were collected at the following time points: 1, 3, 5, 7, 10, 14, 21 and 28 days. The release buffer was replenished with 200 µL fresh PBS to keep the total volume constant. Following the collection of the last sample, MPs were degraded in 200 µL DMSO and 600 µL of 0.2M NaOH for 6 hours to extract the remaining growth factor. Sample concentrations were measured using a MicroBCA assay kit (ThermoFisher) comparing readings at 562 nm to that of a standard curve.

Alternatively, to understand the mechanism of a potential dual-release system, PEG-DA microparticles were loaded with IGF-1 and encapsulated in HAmF hydrogels. PEG-DA microparticles were prepared, incubated for 24 hours with 20 µg IGF-1 to load the growth factor and centrifuged to obtain a pellet. 60 mg each of 3 different formulations were prepared: PEG-DA, PEG-DA with 40 or 80 mol% acrylic acid relative to PEG-diacrylate. HAmF hydrogels were prepared by mixing HAmF at 11 mg/mL and PEG-diMal at 156 mg/mL. The microparticles were added to the HAmF solution before adding the crosslinker. The total volume of each hydrogel was 200 µL. Four separate conditions were tested, one with each microparticle formulation and one with free IGF-1 added to the gels, all in

quadruplicate. The hydrogels were allowed to crosslink and form for 3 hours. Next, 500 µL of PBS were added to each tube as the release buffer and 200 µL samples were collected from this buffer at the following time points: 24 hours, 4 days, 7 days, 10 days, 14 days, 21 days and 28 days. After removing each sample, the buffer was replenished with 200 µL of fresh PBS. At the end of the experiment, the hydrogels were degraded with 2500 U/mL of hyaluronidase, 10 mg/mL heparin and 137 mM NaCl to determine the leftover amount of growth factor. A Micro-BCA assay kit was used to measure the growth factor concentration in each sample by comparing each reading at 562 nm to that of an IGF-1 standard curve of known concentrations. Using these results, a release curve over time was plotted.

3.3.5 Cytotoxicity of PEG-DA microparticles

V2a interneuron aggregates were prepared as mentioned in 2.3.9. PEG-DA microparticles with and without acrylic acid were synthesized and freeze dried. Following sterilization, 10 mg of particles /1 mL of media were added to each well of a 48 well plate containing 20-30 V2a aggregates. Samples were run in quadruplicate. DFK5:NB media supported with B-27, GlutaMax and 10 ng/mL NT-3, BDNF and GDNF was used. 24 hours later, a cytotoxicity kit was used to determine the live/dead percentage. Briefly, calcein AM and ethidium homodimer were added to each well and incubated for 1 hour at 37^{o}C. The wells were gently washed with fresh PBS and replaced with fresh media for imaging. Microscope images at 10x were taken of each aggregate in both fluorescent channels. Images were prepared for analysis by splitting the channels and the fluorescent area of live and dead cells was determined in ImageJ. The % of alive cells was calculated by dividing the area of live cells by the total area of cells.

3.3.6 Biological activity of IGF-1 *in vitro*

The bioactivity of IGF-1 on neurons was assayed similarly to that of NT-3 (Section 2.3.8 and 2.3.9). V2a interneuron aggregates were prepared as in section 2.3.9. At least 15 aggregates were seeded into a well of a 24 well plate, in quadruplicate, using NB:DFK5 media supplemented with 1% GlutaMAX, 1% B27 and the following conditions: 10 ng/mL of NT-3, GDNF and BDNF as the growth factor positive control, or 0, 25, 50, 100 ng/mL IGF-1. For the combination study, 20 ng/mL NT-3 and 50 ng/mL IGF-1 as well as 10 ng/mL NT-3 and 25 ng/mL IGF-1 were tested together to investigate synergistic effects of both growth factors. 2 days after seeding, the aggregates were imaged using fluorescent microscopy due to their inherent fluorescence with a TdTomato reporter. The average radius of axonal extension was measured and analyzed on ImageJ software.

Released IGF-1 Bioactivity on DRGs

Briefly, microparticles were formed with 40% mol acrylic acid relative to PEG-DA in a concentration of 3% in neurobasal (NB) media. 250 ng/mL IGF-1 was loaded onto the MPs over 24 hours of incubation at 4°C. Samples of 300 µL were prepared in triplicate and at the selected timepoints, namely 24 hours, 7 days and 14 days following encapsulation of the growth factor, the MPs were centrifuged, and the supernatant collected. For the released IGF-1 bioactivity study, DRGs were harvested from day 7 White Broiler chicken embryos as covered in section 2.3.8. Approximately 5 DRGs were pooled and placed in a well of a 12 well plate, with at least 4 wells in each condition. Fresh media was prepared using NB supplemented with 1% GlutaMAX, 1% penicillin-streptomycin, 2% B-27 supplement and 0.1 % BSA. For the negative control, no growth factors were added, for the GF control, 10 ng/mL NT-3, GDNF and BDNF were added, and 50 ng/mL IGF-1 was used as the positive control. For the released samples, the collected media with IGF-1 was used and adjusted to

the total volume of the NB solution. 48 hours post-seeding, images were taken using phase microscopy. Average neurite extension from the DRGs was measured using ImageJ and normalized to the GF control between experiments.

Western Blot

V2a interneurons were exposed to 20 ng/mL NT-3, 50 ng/mL IGF-1 or both for one hour. Cell lysates were obtained by trypsinizing and collecting the cells in ice cold RIPA buffer (1 mL per $1x10^7$ cells), centrifuging and collecting the supernatant. The protein concentration was quantified using a bicinchoninic acid (BCA) assay (Pierce) and a dilution of protein concentration standards. Based on the results of the BCA, 20 μg of protein lysate were loaded into each well of a 4% Mini-PROTEAN TGX Stain-Free protein gel (BioRad), and the proteins were separated using gel electrophoresis at 200 mV. The proteins were then transferred to Immun-Blot PVDF membranes (BioRad). The membranes were blocked in EveryBlot Blocking Buffer (BioRad) for 1 h followed by an overnight incubation with primary antibody. Primary antibodies for Erk1/2 and p-ERK1/2 (Cell Signaling Technology, Boston, MA), were used at a 1:1000 dilution. The following day, the membranes were washed five times with TBS containing 0.1% Triton-X (TBS-T). The membranes were then incubated with secondary antibody at a 1:10000 dilution (Cell Signaling) for 1 h followed by an additional five washes with TBS-T. The blots were then developed using SuperSignal West Pico Plus chemiluminescence substrate (ThermoFisher) for 5 minutes before imaging on a GelDoc imaging system (BioRad). Molecular weight was determined by comparison to Precision Plus Protein Standards (BioRad). The blots for ERK1/2 and p-ERK1/2 were developed on the same blot by stripping the antibodies with 0.2M glycine in DI water at pH 2.2 with 0.1% Tween-20 for 20 minutes before reapplying the primary antibody.

3.4 Results

3.4.1 Formation and characterization of PEG-DA microparticles

PEG-DA microparticles with or without acrylic acid were photopolymerized in the presence of two photoinitiators: Irgacure 2959 and LAP. 500 mM sodium sulfate was added before UV exposure to aid in phase separation and was found to be the optimal salt concentration.

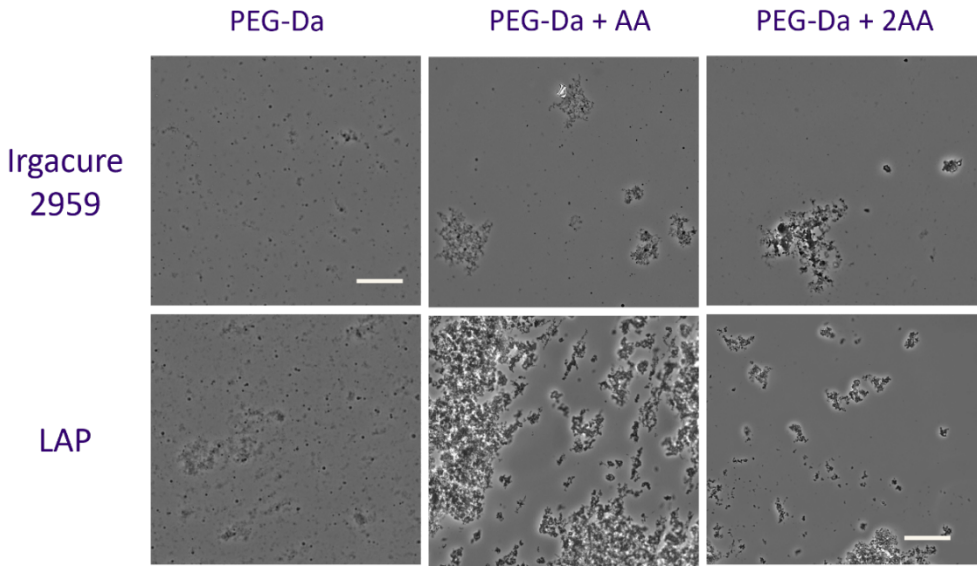

Figure 3.1. Representative images of PEG-Diacrylate microparticles with 0%, 40% or 80% mol acrylic acid relative to PEG-DA in the presence of photoinitiator Irgacure 2959 or lithium phenyl-2,4,6-trimethylbenzoylphosphinate (scale bar = 50 μm).

The microparticles were formed rapidly, with less than 30 seconds of exposure to a 365 nm wavelength UV lamp. Longer time exposures drove the reaction to significant particle aggregation so we kept reaction times to 30 seconds in all subsequent experiments. We also

observed that using LAP was more efficient than Irgacure 2959 due to its poor water-solubility, so only LAP was used for the remainder of the study.

There were no notable differences in shape or size for the MPs, even though the conditions with acrylic acid tended to aggregate more than those without **(Figure 3.1)**. However, this aggregation was easy to disrupt by gently pipetting up and down the MPs in solution. Regardless of the formulation, all MPs ranged in diameter between 2 and 3 μm **(Figure 3.2 and Table 3.1)**. In the case of the particles with 80 mol% AA relative to PEG-DA, the size was slightly larger, likely due to a higher concentration of initial monomer. Based on our preliminary experiments and previous work, the only factor that altered particle size was initial PEG-DA molecular weight (Flake et al., 2011). We used only 3500 MW PEG-DA so we did not expect the differences in formulation to significantly alter the size and morphology of the MPs.

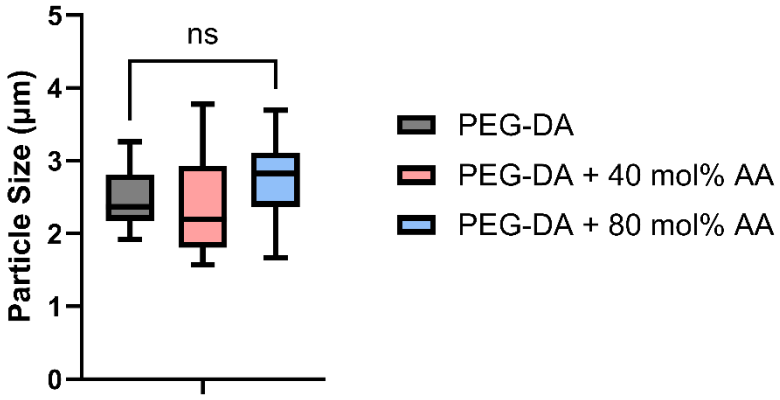

Figure 3.2. Average microparticle size for PEG-Diacrylate with 0%, 40% or 80% mol acrylic acid relative to PEG-DA in the presence of LAP as a photoinitiator (* = p< 0.05, ** = p< 0.01, *** = p< 0.001).

The polydispersity index ranged from 0.094 for PEG-DA with 40 mol% relative acrylic acid with Irgacure as the photoinitiator, to a low of 0.022 in the case of 80 mol% acrylic acid

relative to PEG-DA in the presence of LAP. All measured values fell within the monodispersed range, with PDI under 0.1. This low degree of polydispersity suggests that the precipitation polymerization reaction produces a highly homogenous mix of particles.

Table 3.1. Average microparticle size and polydispersity index for PEG-Diacrylate formulations

	Irgacure 2959		LAP	
	Size (μm)	PDI	Size (μm)	PDI
PEG-DA	2.486	0.027	2.327	0.071
PEG-DA + 40 mol% AA	2.277	0.094	2.192	0.043
PEG-DA + 80 mol% AA	2.740	0.023	2.795	0.022

3.4.2 Loading of insulin via incubation

Following characterization, we tested the potential of these PEG-DA based MPs to encapsulate proteins. We used insulin as a control protein based on its similar size but different isoelectric point to IGF-1. At pH 7.4, insulin is negatively charged, while IGF-1 is electropositive. We tested all formulations by fabricating, washing and drying the particles, then loading insulin or IGF-1 by incubating the protein with MPs over 24 hours. We then measured the % loaded indirectly, by measuring the remaining unloaded insulin or IGF-1 in solution after spinning down and removing the supernatant, and directly, by degrading the MPs in DMSO and NaOH before reading out the protein concentration. In the case of

insulin, we found no clear trend or correlation between the different conditions, with loading concentrations between 37 and 51% for all groups **(Figure 3.3A)**.

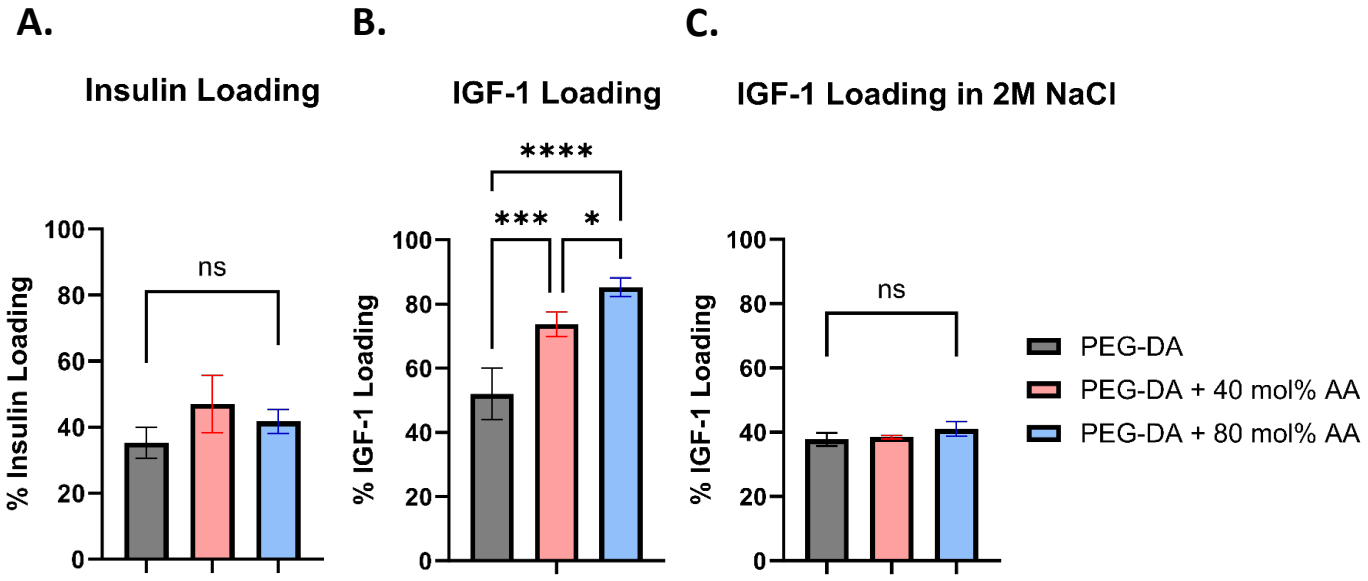

Figure 3.3. Percentage loading for PEG-Diacrylate with 0%, 40% or 80% mol acrylic acid relative to PEG-DA in the presence of LAP as a photoinitiator of A) 100 µg insulin and B) 10 µg IGF-1 per condition. Error bars denote standard error of the mean (* = p< 0.05, *** = p< 0.001, **** = p< 0.0001).

However, when we tested the same MPs with IGF-1 we saw differences in loading in between our three MP formulations. As the amount of acrylic acid increased, we observed significantly higher IGF-1 loading, going from ~50% to over 80% for the group with the high AA concentration **(Figure 3.3B).** One of the main reasons why this trend was present is the difference in protein properties. Insulin, with an isoelectric point of 5.4 and 5.7 kDa size, and IGF-1 with pI= 8.5 and a molecular weight of 7.6 kDa, present different loading behavior. We attribute this differential loading to the different protein charge in the PBS solution. IGF-1, is positively charged at physiological pH, while the acrylate groups present in the PEG-DA MPs yield an overall negative charge over the particles. This behavior was

not present in the case of insulin, suggesting that its low isoelectric point and negative charge are not sufficient to drive protein encapsulation. To further characterize this behavior, we loaded IGF-1 in the presence of 2M NaCl to shield the microparticle charges. We found that in this case, the overall amount encapsulated was reduced in all conditions and there were no differences in loading between the MP formulations **(Figure 3.3C).** More specifically, in the case of the 80 mol% AA condition, the fraction of IGF-1 loaded decreased from 0.85 to 0.4, confirming that a high salt concentration disrupts the electrostatic interactions present. Using a high salt concentration effectively neutralized the charge differences between each of the formulations and equalized the final loading percentage regardless of acrylic acid content. The system here provides a tunable loading platform for positively charged or cationic proteins by exploiting affinity binding.

3.4.3 Release of IGF-1 from PEG-DA microparticles

Once we confirmed the MPs' ability to encapsulate growth factors, we investigated the release profile of IGF-1 over a period of 4 weeks. As expected, based on the loading experiments, we observed slower protein release as the acrylic acid concentration increased among each group **(Figure 3.4)**. With less than 20% of growth factor released after 24 hours in all conditions, we observed no significant burst release, with the MPs displaying the characteristic release curve of a sustained release system. In the case of only PEG-DA, almost 60% of the loaded IGF-1 was released in the first 7 days. However, when 40 or 80% mol acrylic acid relative to PEG-DA was used, that number dropped to 50 and 40% released, respectively. During the remainder of the study, IGF-1 was slowly delivered reaching 80% and 60% of the total amount loaded in both 40 and 80% mol AA formulations. In this case, similar to what we observed during encapsulation, we found a direct correlation between

binding and acrylic acid content, suggesting the presence of stronger interactions when the charge difference between MPs and IGF-1 is larger.

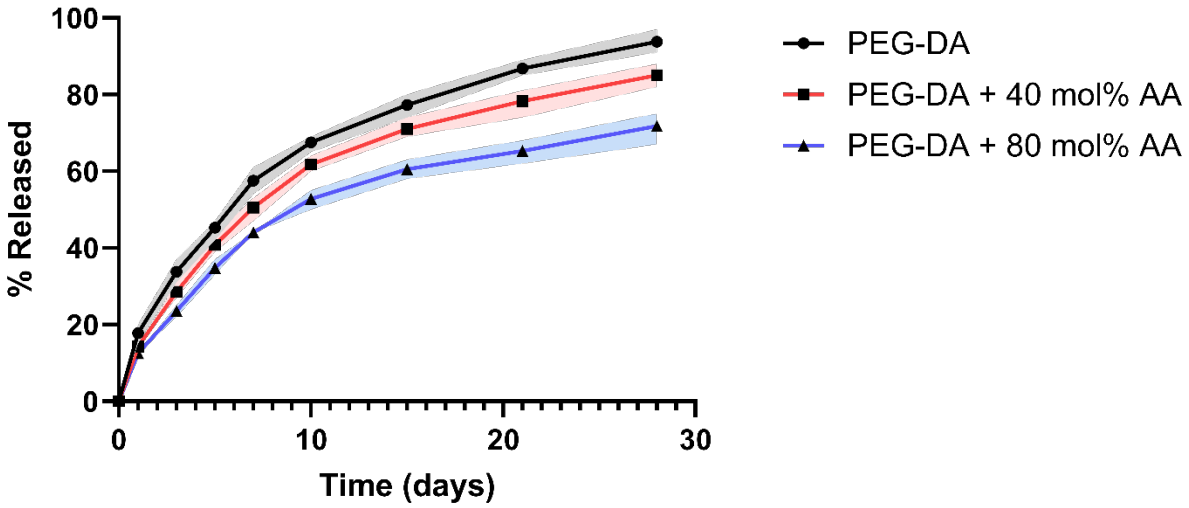

Figure 3.4. Release curves of IGF-1 from PEG-Diacrylate microparticles with 0%, 40% or 80% mol acrylic acid relative to PEG-DA. Each condition contained 15 mg of microparticles and was previously loaded with 15 µg of IGF-1 that was released into PBS buffer (n=4).

3.4.4 Release of IGF-1 from PEG-DA microparticles in hyaluronic acid hydrogels

We then aimed to combine both the HA hydrogel system developed in Chapter 2 with the PEG-DA MPs to assess the feasibility of a dual-delivery platform. MPs under the same conditions as in the solution study in 3.4.3 were prepared and encapsulated within the HA hydrogels via crosslinking at 37 ^{o}C. Hydrogels were placed in excess PBS buffer and the concentration of IGF-1 was determined at each time point. As expected, encapsulating the MPs within the scaffold drove down the release rate in all three formulations **(Figure 3.5)**.

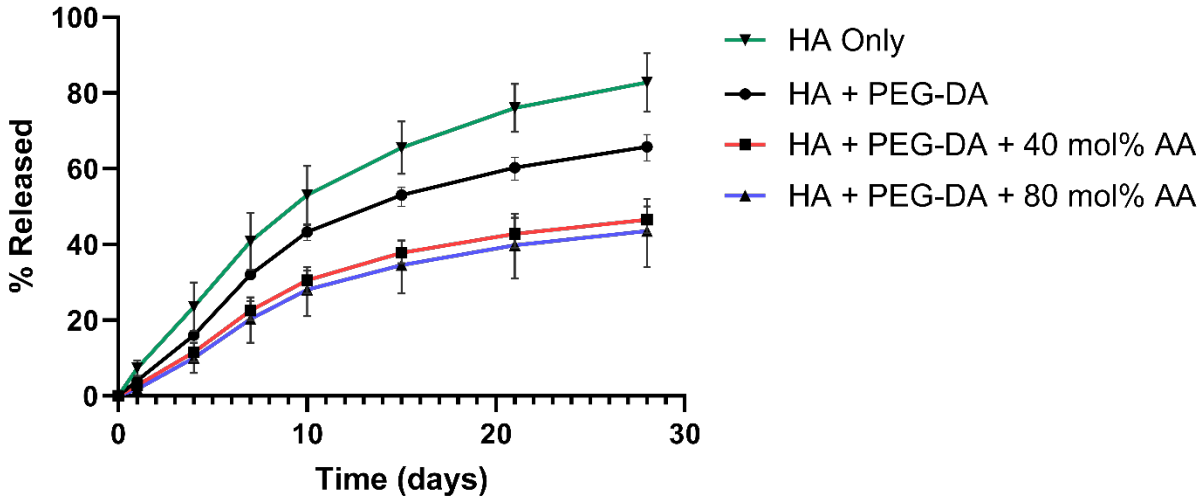

Figure 3.5. Release curves of IGF-1 released from PEG-Diacrylate microparticles with 0%, 40% or 80% mol acrylic acid relative to PEG-DA embedded in a hyaluronic acid hydrogel. Each condition contained 15 mg of microparticles and was previously loaded with 15 µg of IGF-1 that was released into PBS buffer (n=4).

In the case of only PEG-DA, the total amount released at the end of the 4 weeks decreased to just over 60%, and for both AA conditions the final amount delivered was ~40% of the loaded IGF-1. In the case of just HA, the growth factor had a faster release and 80% of its initial concentration was delivered by the end of the study. Physically, the entrapment of the particles within the hydrogel pores is one of the drivers of the decreased release rate. Since IGF-1, like NT-3, is positively charged at pH 7.4, and the hydrogel's carboxylates give it an overall negative charge, the same type of electrostatic interaction we found in section 2.4.5 are likely still present. However, NT-3 is almost four times larger than IGF-1, so we would still expect IGF-1 to diffuse out of the hydrogel faster than the neurotrophin.

3.4.5 Cytotoxicity of PEG-DA microparticles on V2a interneuron aggregates

Even though we expected our PEG-DA based microparticles to be biocompatible with cells and specifically neurons, we tested their cytotoxicity using a live/dead assay. In the presence of 10 mg MPs/ 1 mL media, there was no statistically significant difference between the control and the microparticles, independent of the acrylic acid content and overall MP formulation **(Figure 3.6)**. All cell viability percentages, measured as the number of live cells over the total amount of cells (live plus dead), ranged from 87% to 93%, results that confirm the biocompatibility in vitro of the PEG-DA MPs and suggest that they could likely be a viable candidate to be implanted *in vivo* without a significant cytotoxic response.

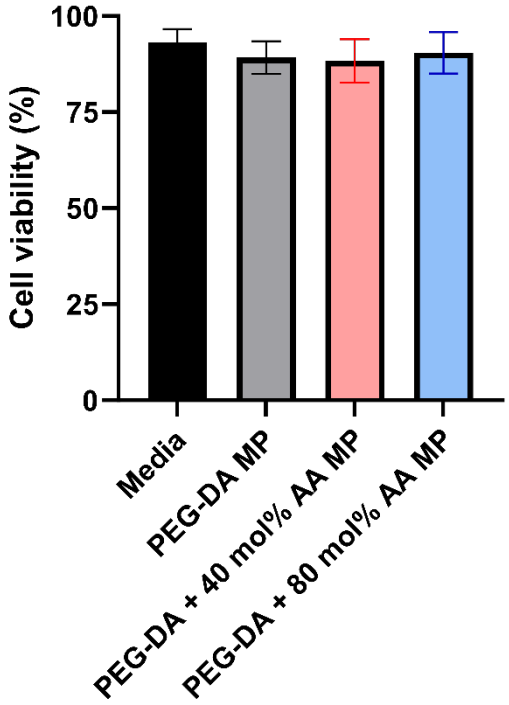

Figure 3.6. Cell viability of V2a interneuron aggregates treated with PEG-DA microparticles with 0 mol%, 40 mol% or 80 mol% AA as a percentage of total cells present in each condition.

3.4.6 Biological activity of IGF-1 on DRGs and V2A interneurons

To study the effect of IGF-1 on neurite growth *in vitro*, we designed a similar DRG bioactivity assay to that reported in section 2.4.6 but using IGF-1 instead of the usual

neurotrophins. After a literature search, very few instances of IGF-1 bioactivity assays with neurons were found (Pan et al., 2019; Salie & Steeves, 2005). We harvested DRGs from chick embryos and seeded them in laminin-coated wells. We also collected the release samples into NB media containing IGF-1 delivered from the PEG-DA MPs. We supplemented each DRG condition using either the released IGF-1 at 24h, 7 days or 14 days and analyzed the neurite length. Fresh IGF-1 at a concentration of 50 ng/mL was used to compare the released samples and no IGF-1 was used as the negative control. All measurements were normalized to the growth factor control, containing 10 ng/mL each of NT-3, BDNF and GDNF. At the 24-hour time point, the average neurite length was almost the same as that of fresh IGF-1 **(Figure 3.7)**. Based on the initial loading of 250 ng/mL and ~20% of it being released based on the release curves, the IGF-1 seemed to retained all its bioactivity by day 1, and most of it by days 7 and 14.The growth elicited by the release samples from day 14 showed statistically significant difference with the control and no difference with the fresh, 24 hour and 7 day samples. Since a therapy of this type would be the most beneficial during the subacute phase of SCI, sustained release over two weeks would be a promising approach to enhance and promote axonal regeneration.

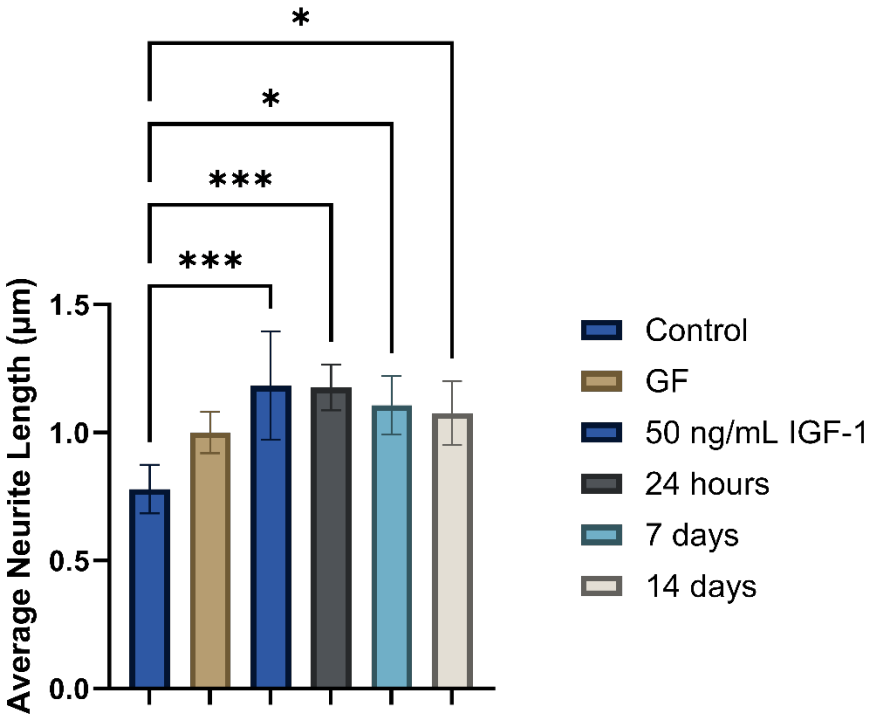

Figure 3.7. Average neurite outgrowth from DRGs in the presence of NB media (control), 10 ng/mL NT-3, GDNF, BDNF (GF), 50 ng/mL IGF-1, released IGF-1 from PEG-DA MPs at 24 hours, 7 days and 14 days. (*** = $p<0.001$, **** = $p<0.0001$, n=3 for at least 10 neuroaggregates per group).

We then aimed to study the effect of IGF-1 on mouse embryonic stem cell derived V2a interneuron aggregates. As explained in section 2.4.7, DRGs are located in the peripheral nervous system and do not accurately represent the neuron population present on the spinal cord, so utilizing these types of neurons yields a more translatable result. Several conditions were prepared from 0 to 100 ng/mL IGF-1 to test the cells response to the growth factor, aiming to establish a correlation between IGF-1 concentration and neurite extension (Figure 3.8). The neurite extension was higher at 10 and 25 ng/mL IGF-1 but not significantly different from the control, and it peaked at 50 ng/mL **(Figure 3.8)**. The growth at 100 ng/mL was lower than 50 ng/mL, suggesting that the cells response to IGF-1 plateaus at this concentration.

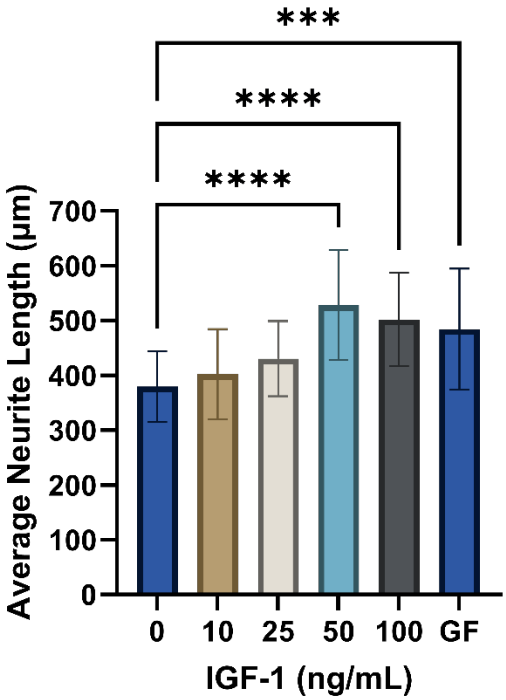

Figure 3.8. Average neurite outgrowth from V2a interneuron neuroaggregates in the presence of 0, 10, 25, 50 or 100 ng/mL IGF-1, or 10 ng/mL NT-3, GDNF, BDNF (GF). (*** = $p<0.001$, **** = $p<0.0001$, n=3 for at least 30 neuroaggregates per group).

This data is in agreement with other studies reporting a biphasic response to neurotrophic factors, where a specific dosage yields an optimal response and a higher concentration results in a reduced response , potentially through the saturation of the neurotrophin cell surface receptors (Cao & Shoichet, 2003; S. J. Taylor et al., 2004).

3.4.7 Synergistic effect of NT-3 and IGF-1

Next, we explored whether the combination of IGF-1 with NT-3 would be capable of improving the axonal growth that each of the growth factors could achieve individually. For this, we used V2a interneuron aggregates and added the growth factors concentrations that yielded the highest growth in each of the respective studies, 20 ng/mL for NT-3 and 50 ng/mL in the case of IGF-1. We found that the combination of both molecules resulted in a

significantly higher neurite length than each of them separately **(Figure 3.9)**. We also observed a similar enhancing effect of the cocktail even when both concentrations were cut in half, using 10 ng/mL NT-3 and 25 ng/mL for IGF-1. This suggests the presence of a synergistic effect between the growth factors when acting in combination with each other. Even though IGF-1 signals through the IGF-1 receptor, a tyrosine kinase, and NT-3 mainly through TrkC, a tropomyosin receptor, both growth factors share the downstream signaling pathways phosphoinositide-3 kinase (PI3K)-AKT and RAS-mitogen activated protein kinase (MAPK) (Hisaoka et al., 2002; C. Liu et al., 2019; Ma & Bai, 2012). We hypothesized that sharing these common pathways played a role in the synergistic effect observed in the combined treatment in neurons. The negligible difference between the 20 - 50 ng/mL and 10 - 25 ng/mL can be attributed to saturation of these common signaling pathways.

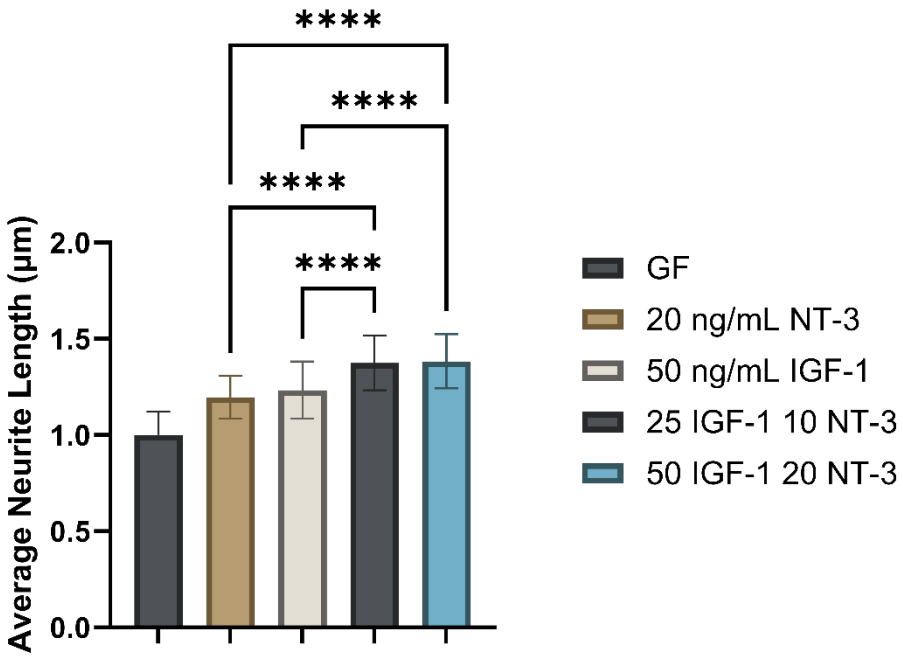

Figure 3.9. Average neurite outgrowth from V2a interneuron neuroaggregates in the presence of 20 ng/mL NT-3, 50 ng/mL IGF-1 or both. (*** = p<0.001, **** = p<0.0001, n=3 for at least 30 neuroaggregates per group).

To further investigate this behavior, we measured phosphorylation levels of ERK 1/2, extracellular-signal regulated kinases 1 and 2. Based on previous data from our group, we expected higher expression levels within 60 to 90 minutes after growth factor exposure (Willerth & Sakiyama-Elbert, 2009). For this reason, we cultured V2a interneurons and exposed them to NT-3, IGF-1 or both for 60 minutes and then collected the cell lysate to measure protein expression via Western Blot **(Figure 3.10A)**. Densitometry calculations based on band intensity after protein loading normalization showed significantly higher ERK phosphorylation for both conditions in which NT-3 and IGF-1 were combined **(Figure 3.10B)**. This data confirms that both growth factors share a downstream signaling pathway and the activation of this pathway, likely via TrkC and IGF1-R activation. Phosphorylation of ERK increased by IGF-1 and NT-3 stimulation, highlighting the potential of the combination of these growth factors as an axonal growth approach, which had been reported previously (Kaspar et al., 2003; R. Li et al., 2016; Menu et al., 2004; Zhang et al., 2011).

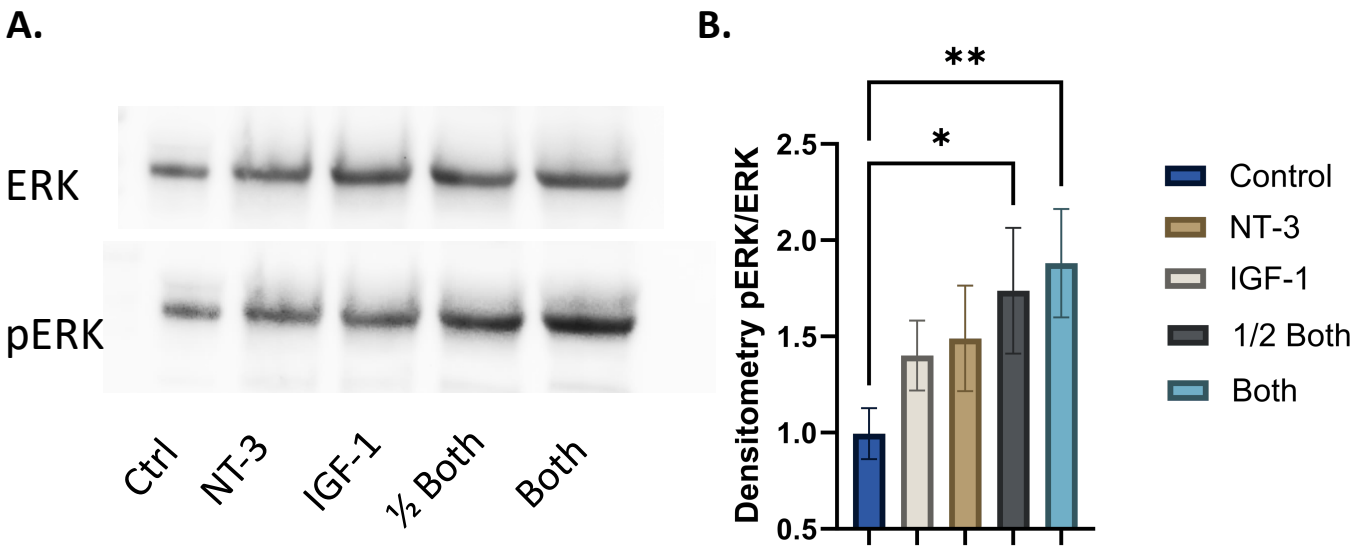

Figure 3.10. A) Phosphorylation of ERK in V2a interneuron cell lysates previously exposed to growth factors measured via Western Blot B) Densitometry of Western Blot data calculated as pERK/ERK and normalized to the control. N=3 (* = p< 0.05, ** = p< 0.01).

3.5 Discussion

Regrowth of lost axonal circuitry has long been a promising therapeutic approach to promote functional recovery following SCI. Insulin-like growth factor-1 has been shown to have a trophic effect, increasing axonal growth both *in vitro* and *in vivo* and even improving locomotor function scores in preclinical models of SCI in rodents (Özdinler & Macklis, 2006; Q. Zhao et al., 2023). Even though many neuroregenerative agents have been extensively explored, there is still room for improvement in the drug delivery methods used. Microparticles provide a highly tunable platform to have temporal and spatial control over the release rate of therapeutic agents. Parameters such as size, charge, material choice, degradability and biocompatibility are all critical when designing and developing drug release systems. Novel approaches can exploit non-specific binding mechanisms to control loading and release, including electrostatic interactions.

The precipitation polymerization of PEG-DA reported here produced microparticles of similar size and polydispersity regardless of formulation, with changes in photoinitiator or acrylic acid content barely affecting the average diameter. Based on previous data, the main size determinant parameter that could be exploited is the molecular weight of the initial PEG-DA (Flake et al., 2011). The underlying model that describes the mechanism of nucleation and production of monodisperse particles was first reported 70 years ago (LaMer & Dinegar, 1950). This model set up the theoretical basis for other microparticle production methods, including the precipitation polymerization used here. According to La Mer, particle formation occurs in two steps: nucleation and growth. In the initial nucleation step, phase separation occurs when small clusters of atoms or molecules assemble to form a nucleus. Supersaturation of the polymer is necessary for nucleation to occur, and we controlled this by adding relatively high salt concentrations. Growth of newly formed

particles proceeds in the absence of nucleation of new particles via addition of more molecules to the existing clusters. This step is limited by diffusion, depending on the rate at which molecules can diffuse to the surface of the nucleus and attach themselves to it. Therefore, a key assumption of this model is that all particles that were nucleated at the same time grow at equal rates, resulting in low polydispersity.

The ability to encapsulate and release IGF-1 from the 2 – 3 μm in diameter MPs developed here was tested. We found a direct correlation between AA content and loading percentage, suggesting the presence of electrostatic interactions between the positively charged IGF-1 molecules and the electronegative acrylate groups in the MPs. This trend was not found in the case of insulin being loaded, likely due to its positive charge at physiological pH not driving the same affinity binding. In the case of drug release, we observed a similar behavior with an inverse correlation between the release rate and the amount of AA in the MPs, with the total amount of IGF-1 released after 28 days decreasing from 94% to 71% when the PEG-DA was copolymerized with 80 mol% AA. Therefore, the release rate might be tuned by varying simple parameters in formulation, namely acrylic acid content and initial protein concentration. We also encapsulated IGF-1 loaded MPs within HAmF hydrogels, effectively adding another limiting factor for diffusion and further slowing down the release rate. Furthermore, the MPs exhibited very low cytotoxicity, presenting a promising platform to deliver growth factors.

While NT-3 and IGF-1 have both been found to be effective individually, the combined action of NT-3 and IGF-1 had not been extensively reported. Here we found that the combination of optimal dosages of both growth factors had a synergistic effect on neurite outgrowth in chick DRGs and mESC-derived V2a interneuron aggregates. The optimal concentration of NT-3 *in vitro* was previously determined, and in this work, we conducted a

similar experiment with IGF-1. Individually, 20 ng/mL NT-3 and 50 ng/mL IGF-1 resulted in the highest neurite outgrowth, and the combination of both significantly increased the average neurite length. However, using half of the concentration for each growth factor (10 ng/mL NT-3 and 25 ng/mL IGF-1) did not decrease the growth, resulting in average lengths comparable to the higher concentration condition. This suggests that we can use smaller amounts of protein without affecting the overall axon-growth promoting effect.

3.6 Conclusion

In this work, we demonstrated the feasibility of using PEG-DA based microparticles as a drug delivery platform for growth factors and other proteins. We synthesized the MPs via precipitation polymerization in three different formulations, with varying levels of acrylic acid to alter the overall charge of the particles without significantly affecting the individual size and morphology. We found that through affinity binding, the growth factor IGF-1 could be encapsulated and released in a sustained manner over a period of 4 weeks. The release could be further slowed down by incorporating the particles within the HAmF scaffolds developed in chapter 2. The MPs showed very little cytotoxicity and the encapsulated IGF-1 retained its bioactivity up to two weeks post-loading, as shown by axonal growth assays in both primary DRG neurons and mESC-derived V2a interneurons. Furthermore, we found a synergistic effect between NT-3 and IGF-1 on neurite outgrowth, using lower than the optimal concentrations for each growth factor individually.

Chapter 4

Discussion

4.1 Summary of findings and implications of the study

Neural tissue engineering has emerged as a promising field over the past decades, striving to regenerate the central nervous system (CNS) using stem cell biology, gene therapy, biomaterials, and drug delivery approaches. The Sakiyama-Elbert lab works on all these areas with the goal of studying spinal cord injury (SCI) and other injuries in the peripheral nervous system. This work has aimed to develop drug delivery strategies to target the spinal cord by focusing on neurotrophin-3 (NT-3) and insulin-like growth factor 1 (IGF-1) as growth factors to promote axonal regeneration. We chose these two growth factors due to their trophic, growth promoting effect shown both *in vitro* and *in vivo* (Elliott Donaghue et al., 2016; Musarò et al., 2007; Rao et al., 2018; S. J. Taylor & Sakiyama-Elbert, 2006; Q. Zhao et al., 2023). While there are several therapeutic approaches to treat spinal cord injury including increasing axonal growth, reducing inflammation, and remodeling the local microenvironment to promote cell survival and regrowth, we focused on promoting axonal regeneration via sustained delivery of NT-3 and IGF-1.

The first aim was to develop and evaluate a hydrogel-based drug delivery system capable of controlled, sustained release of biologically active NT-3 with the goal of increasing axonal regeneration following SCI. The hyaluronic acid hydrogel was functionalized with methylfuran and crosslinked with polyethylene glycol-dimaleimide (PEG-Mal) via Diels-Alder click chemistry, resulting in biocompatible, tunable scaffolds that form in under 3 hours allowing for cell and protein encapsulation. We showed that the

stiffness of the gels could be tuned by controlling the ratio of methylfuran to maleimide, allowing us to formulate gels that match the native spinal cord tissue. The loading and release of NT-3 from the hydrogels was likely driven by electrostatic interactions, resulting in sustained delivery of the growth factor over 28 days. We tested the bioactivity of the released NT-3 using a dorsal root ganglion (DRG) assay, measuring neurite outgrowth and correlating it to the NT-3 concentration. However, since DRGs are part of the peripheral nervous system (PNS), we also explored the effect of NT-3 on neurons more representative of the SCI. We took advantage of our previously developed protocols to obtain specific neuron populations from mouse embryonic stem cells, namely the puromycin selectable motoneuron and V2a interneuron cell lines (Iyer et al., 2016; McCreedy et al., 2014). NT-3 also resulted in increased neurite outgrowth *in vitro* in aggregates formed for both V2a interneurons and motoneurons. The expression of the principal NT-3 receptor, TrkC, in these cells was confirmed using qPCR. Finally, the cell viability of V2a interneuron aggregates seeded on hydrogels with and without laminin showed that the hydrogels are not cytotoxic and enable cell adhesion and growth.

In the second part of this thesis, we modified previously synthesized PEG-DA based microparticles (MPs) from the Elbert lab with the goal of delivering IGF-1 (Flake et al., 2011). Based on the affinity binding we observed in the first aim, we explored the potential of exploiting the same interactions to slow down the release of IGF-1 from PEG-DA microparticles. Three different formulations were developed with varying acrylic acid content as a comonomer to modify the overall particle charge: 0%, 40% and 80% mol relative to PEG-DA. We showed that the precipitation polymerization occurred rapidly in less than 30 seconds, and the average size and polydispersity of the particles remained relatively constant regardless of AA content and choice of photoinitiator. We loaded several

concentrations of IGF-1 onto the MPs via incubation, and observed differential loading directly correlated to the amount of AA present. On the other hand, when insulin was loaded, the same trend was not present. Since AA drives the MPs to be negatively charged, the positively charged IGF-1 showed higher loading as the AA content increased, while insulin, with an isoelectric point of 5.3 - 5.4, did not display the same behavior likely due to its negative charge at physiological pH. We conducted release studies over a period of 4 weeks, where the release rate of IGF-1 could also be controlled by the formulation and AA content. Additionally, the MPs were encapsulated within hyaluronic acid methylfuran (HAmF) hydrogels to obtain release curves. As expected, free IGF-1 diffused faster than IGF-1 encapsulated in the PEG-DA MPs, where the release was effectively slowed down. The biological activity of released IGF-1 was confirmed by the same DRG assay used previously. PEG-DA MPs were found to be non-cytotoxic regardless of formulation.

Here, we designed and demonstrated the potential of a hyaluronic acid hydrogel scaffold and a polyethylene-glycol diacrylate microparticle system as suitable methods to deliver bioactive NT-3 and IGF-1 via non-specific electrostatic interactions. Both systems are capable of long-term release and offer a protective role to the encapsulated growth factors which retain their biological activity. We reported for the first-time affinity binding between cationic proteins, in this case NT-3, and hyaluronic acid, and similarly between IGF-1 and PEG-diacrylate. We observed a strong correlation between increased growth factor loading and slower drug release over time, and the overall charge differences between the proteins and the scaffold matrices. These data suggest the presence of local, nonspecific electrostatic interactions that enable controlled loading and tunable release rates via modification of the drug delivery system. We tuned the mechanical properties of the gel to match the stiffness of native rat spinal cord, HA hydrogels supported neuronal adhesion and

growth, and exposure to the microparticles resulted in very low cytotoxicity. Additionally, we report a synergistic effect between NT-3 and IGF-1, mediated by the MAPK downstream signaling pathway measured via the phosphorylation of ERK1/2. For these reasons, these systems hold potential to be used as a therapy for SCI, especially in the subacute phase of the injury. We confirmed the biological activity of the released factors 14 days after encapsulation, suggesting that their delivery during the initial stages of the injury would be the most optimal.

4.2 Limitations and future directions

Translation of novel therapeutic approaches for SCI including biomaterial and cell transplantation, drug delivery systems and gene therapy remains a significant challenge due to the multifaceted characteristics of the condition and individual variability of the injuries. As we have aimed to emphasize through the introduction, the CNS lacks inherent ability to spontaneously regenerate. Local extracellular and intracellular mechanisms that initially aim to isolate the injury site and localize the damage to a specific, enclosed area, end up resulting in increased inflammation, reduced infiltration and create a physical barrier that is not conducive to cell and axonal growth. There is a lack of robust methods to efficiently deliver neurotrophins and other trophic factors to the injury site, in the necessary time frames to drive regeneration. Polymeric systems, including hydrogels and particulates, hold the potential to encapsulate and control the release of proteins through a high degree of tunability that allows to finely design and modulate both physical and chemical parameters. Both systems developed here displayed excellent encapsulation and growth factor release capabilities via affinity release. We exploited short-range, nonspecific, electrostatic interactions between the cationic proteins and negatively charged scaffolds in both cases to enhance binding and drive sustained release over a period of 4 weeks. In the case of the HA

hydrogel, the negatively charged carboxylates present in the polymeric backbone offer an ideal binding site that could be tuned by varying the crosslinker ratio. In the case of PEG-DA microparticles, we carried out precipitation polymerization using acrylic acid as a comonomer, tuning the overall charge independently of particle size and allowing us to control the amount of IGF-1 loaded and released based on the amount of AA copolymerized.

For the purposes of this work, we aimed to develop effective and relatively simple drug delivery systems in terms of formulation, design, and synthesis. However, further modifications to the HA hydrogel could be made, incorporating specific biochemical cues to further promote cell adhesion and survival or reduce inflammation. For example, adding small concentrations of IKVAV, RGD and other peptides has been shown to increase cell adhesion and promote growth and neurogenesis (Deister et al., 2007; D'Souza et al., 1988; Farrukh et al., 2017; Pierschbacher & Ruoslahti, 1984; Ruoslahti & Pierschbacher, 1987). These specific peptides, derived from laminin and fibronectin, respectively, have been extensively studied and characterized, enabling relatively easy conjugation to hydrogels and other biomaterials. We confirmed that incubating the hydrogels in laminin increased DRG adhesion, but other proteins and peptides may have a more optimal effect. One area where our group is particularly suited to explore is incorporating astrocyte-derived ECM. Work from Russell Thompson and more recently by Sangamithra Vardhan has showed a differential response following SCI to ECM derived from protoplasmic or fibrous astrocytes (Thompson et al., 2018). Protoplasmic astrocytes commonly reside in the grey matter, while fibrous are present in the white matter. We have characterized the composition of the ECM derived from both astrocyte populations specifically derived from engineered mouse embryonic stem cells. Protoplasmic astrocyte-derived ECM resulted in higher axonal growth, reduced glial scar size and lower macrophage and microglia infiltration compared to

fibrous-derived. Future studies in our laboratory will include incorporating specific proteins and peptides from astrocyte-derived ECM into the HAmF hydrogels to enhance growth of axons depending on the target cell population. For example, the hydrogels could be synthesized in different layers, with one layer including grey matter ECM proteins targeting V2a interneurons and another with white matter ECM proteins, promoting axonal growth and synapse formation of bulbospinal or corticospinal tract neurons, which in the spinal cord are present in the white matter.

Because all the work shown here was *in vitro*, to confirm the translation potential of HA hydrogels and PEG-DA microparticles as growth factor delivering systems for SCI *in vivo* studies should be carried out. Future studies in our lab will explore combining the most promising biochemical cues from protoplasmic astrocyte-derived ECM devised by proteomics along with the hydrogel and microparticle drug delivery system. The *in vivo* study should assay toxicity of both polymeric systems as well as the growth factors. A contusion or dorsal hemisection SCI model in rodents would provide a robust environment to study the effect of dual release of IGF-1 and NT-3 on axonal growth and functional recovery following injury. The study design parameters are critical, and should include testing both drug delivery systems independently, with and without growth factors to ensure that the controls account for non-specific effects. Based on the presence of hyaluronidase and other enzymes in the spinal cord, we would expect the hydrogels to have a slightly faster degradation rate, resulting in release of more growth factor. Since we only saw ~40% of NT-3 loaded to release in vitro over 4 weeks, there should still be sufficient growth factor to compensate for the faster delivery. Electrophysiological measurements, anatomical tracing and immunohistochemistry should also be conducted to investigate neuronal activity and cell identity and morphology.

NT-3 and IGF-1 were the two growth factors that we chose to focus on in this study, but there are many other proteins and molecules that may have an equal or higher beneficial effect on axonal growth and regeneration. Several other growth factors could be loaded into MPs with different formulations to drive specific release rates based on the therapeutic needs of the target application. For example, delivering simultaneously an anti-inflammatory agent early on with most of the drug released within the first few hours, followed by a longer, sustained release of a neuroregenerative factor such as NT-3 or IGF-1 could be accomplished with these two platforms. The tunability of both systems allows to customize the concentration of growth factor loaded and released for at least a month.

Another area that is worth exploring following this work is cell transplantation. We have shown that both primary neurons and stem cell derived V2a interneurons and motoneurons can adhere onto, grow, and extend axonal processes through the HA scaffolds. We previously reported the transplantation of V2a interneurons with HA gels and showed an increase in neuronal processes, both within the site of injury and around it (Thompson et al., 2018). The corticospinal tract has gained increased attention due to its role in motor function, with its upper motoneurons relaying movement related information to the spinal cord from the cerebral cortex. Other groups have shown that graft transplantation of neural progenitor cells driven toward a spinal cord, caudalized fate, resulted in robust corticospinal projection and axon regeneration (Kadoya et al., 2016; Kumamaru et al., 2019). As previously discussed, IGF-1 enhances axonal outgrowth of corticospinal motoneurons via IGF-1R and its downstream signaling pathways (Özdinler & Macklis, 2006). I propose that a combinatory approach that includes neuronal transplantation with sustained IGF-1 and NT-3 delivery would result in significant axonal regrowth following a spinal cord lesion. The cells engrafted would repopulate damaged or dead cells due to the injury, while the growth

factors would provide trophic support to promote axonal extension and growth of both transplanted neurons and surviving host cells around the lesion site.

4.3 Contributions

This work would not have been possible without continuous collaboration with other lab members and external committee members. Thomas Willems helped with the initial hydrogel study design and provided critical insight and feedback on hydrogel formulation and drug release studies. Dr. Nicholas White and Sangamithra Vardhan provided expertise in stem cell culture and troubleshooting of qPCR, immunocytochemistry, and blot assays. Alaynah Murphy helped with hydrogel characterization, including swelling and rehydration studies.

References

Abune, L., & Wang, Y. (2021). Affinity Hydrogels for Protein Delivery. *Trends in Pharmacological Sciences*, *42*(4), 300–312. https://doi.org/10.1016/j.tips.2021.01.005

Allen, S. J., Watson, J. J., Shoemark, D. K., Barua, N. U., & Patel, N. K. (2013). GDNF, NGF and BDNF as therapeutic options for neurodegeneration. *Pharmacology & Therapeutics*, *138*(2), 155–175. https://doi.org/10.1016/J.PHARMTHERA.2013.01.004

Anderson, M. A., Burda, J. E., Ren, Y., Ao, Y., O'Shea, T. M., Kawaguchi, R., Coppola, G., Khakh, B. S., Deming, T. J., & Sofroniew, M. V. (2016). Astrocyte scar formation aids central nervous system axon regeneration. *Nature*, *532*(7598), Article 7598. https://doi.org/10.1038/nature17623

Anderson, M. A., O'Shea, T. M., Burda, J. E., Ao, Y., Barlatey, S. L., Bernstein, A. M., Kim, J. H., James, N. D., Rogers, A., Kato, B., Wollenberg, A. L., Kawaguchi, R., Coppola, G., Wang, C., Deming, T. J., He, Z., Courtine, G., & Sofroniew, M. V. (2018). Required growth facilitators propel axon regeneration across complete spinal cord injury. *Nature*, *561*(7723), 396–400. https://doi.org/10.1038/s41586-018-0467-6

Angeli, C. A., Boakye, M., Morton, R. A., Vogt, J., Benton, K., Chen, Y., Ferreira, C. K., & Harkema, S. J. (2018). Recovery of Over-Ground Walking after Chronic Motor Complete Spinal Cord Injury. *New England Journal of Medicine*, *379*(13), 1244–1250. https://doi.org/10.1056/NEJMoa1803588

Ansorena, E., De Berdt, P., Ucakar, B., Simón-Yarza, T., Jacobs, D., Schakman, O., Jankovski, A., Deumens, R., Blanco-Prieto, M. J., Préat, V., & Rieux, A. des. (2013). Injectable alginate hydrogel loaded with GDNF promotes functional recovery in a hemisection model of spinal cord injury. *International Journal of Pharmaceutics*, *455*(1–2), 148–158. https://doi.org/10.1016/J.IJPHARM.2013.07.045

Atkinson, P. P., & Atkinson, J. L. D. (1996). Spinal Shock. *Mayo Clinic Proceedings*, *71*(4), 384–389. https://doi.org/10.4065/71.4.384

Austin, J. W., Kang, C. E., Baumann, M. D., DiDiodato, L., Satkunendrarajah, K., Wilson, J. R., Stanisz, G. J., Shoichet, M. S., & Fehlings, M. G. (2012). The effects of intrathecal injection of a hyaluronan-based hydrogel on inflammation, scarring and neurobehavioural outcomes in a rat model of severe spinal cord injury associated with arachnoiditis. *Biomaterials*, *33*(18), 4555–4564. https://doi.org/10.1016/j.biomaterials.2012.03.022

Bahney, J., & Von Bartheld, C. S. (2018). The Cellular Composition and Glia-Neuron Ratio in the Spinal Cord of a Human and a Non-Human Primate: Comparison with other Species and Brain Regions. *Anatomical Record (Hoboken, N.J. : 2007)*, *301*(4), 697–710. https://doi.org/10.1002/ar.23728

Baier Leach, J., Bivens, K. A., Patrick Jr., C. W., & Schmidt, C. E. (2003). Photocrosslinked hyaluronic acid hydrogels: Natural, biodegradable tissue engineering scaffolds. *Biotechnology and Bioengineering*, *82*(5), 578–589. https://doi.org/10.1002/bit.10605

Bartlett, R. D., Choi, D., & Phillips, J. B. (2016). Biomechanical properties of the spinal cord: Implications for tissue engineering and clinical translation. *Regenerative Medicine*, *11*(7), 659–673. https://doi.org/10.2217/rme-2016-0065

Baumann, M. D., Kang, C. E., Stanwick, J. C., Wang, Y., Kim, H., Lapitsky, Y., & Shoichet, M. S. (2009). An injectable drug delivery platform for sustained combination therapy. *Journal of Controlled Release*, *138*(3), 205–213. https://doi.org/10.1016/J.JCONREL.2009.05.009

Blanco, E., Shen, H., & Ferrari, M. (2015). Principles of nanoparticle design for overcoming biological barriers to drug delivery. *Nature Biotechnology*, *33*(9), 941–951. https://doi.org/10.1038/nbt.3330

Brown, C. R., Butts, J. C., McCreedy, D. A., & Sakiyama-Elbert, S. E. (2014). Generation of v2a interneurons from mouse embryonic stem cells. *Stem Cells and Development*, *23*(15), 1765–1776. https://doi.org/10.1089/scd.2013.0628

Burdick, J. A., Ward, M., Liang, E., Young, M. J., & Langer, R. (2006). Stimulation of neurite outgrowth by neurotrophins delivered from degradable hydrogels. *Biomaterials*, *27*(3), 452–459. https://doi.org/10.1016/j.biomaterials.2005.06.034

Burnside, E. R., & Bradbury, E. J. (2014). Review: Manipulating the extracellular matrix and its role in brain and spinal cord plasticity and repair. *Neuropathology and Applied Neurobiology*, *40*(1), 26–59. https://doi.org/10.1111/nan.12114

Butte, M. J., Hwang, P. K., Mobley, W. C., & Fletterick, R. J. (1998). *Crystal Structure of Neurotrophin-3 Homodimer Shows Distinct Regions Are Used To Bind Its Receptors †, ‡*. https://doi.org/10.1021/bi9812540

Cao, X., & Shoichet, M. S. (2003). Investigating the synergistic effect of combined neurotrophic factor concentration gradients to guide axonal growth. *Neuroscience*, *122*(2), 381–389. https://doi.org/10.1016/j.neuroscience.2003.08.018

Cheng, S., Clarke, E. C., & Bilston, L. E. (2008). Rheological properties of the tissues of the central nervous system: A review. *Medical Engineering & Physics*, *30*(10), 1318–1337. https://doi.org/10.1016/J.MEDENGPHY.2008.06.003

Cheng, S., Clarke, E. C., & Bilston, L. E. (2009). The effects of preconditioning strain on measured tissue properties. *Journal of Biomechanics*, *42*(9), 1360–1362. https://doi.org/10.1016/j.jbiomech.2009.03.023

Ciucci, F., Putignano, E., Baroncelli, L., Landi, S., Berardi, N., & Maffei, L. (2007). Insulin-Like Growth Factor 1 (IGF-1) Mediates the Effects of Enriched Environment (EE) on Visual Cortical Development. *PLOS ONE*, *2*(5), e475. https://doi.org/10.1371/journal.pone.0000475

Czervionke, L. F., Daniels, D. L., Ho, P. S., Yu, S. W., Pech, P., Strandt, J. A., Williams, A. L., & Haughton, V. M. (1988). The MR appearance of gray and white matter in the cervical spinal cord. *American Journal of Neuroradiology*, *9*(3), 557–562.

Davies, J. E., Pröschel, C., Zhang, N., Noble, M., Mayer-Pröschel, M., & Davies, S. J. A. (2008). Transplanted astrocytes derived from BMP- or CNTF-treated glial-restricted precursors have opposite effects on recovery and allodynia after spinal cord injury. *Journal of Biology*. https://doi.org/10.1186/jbiol85

Deister, C., Aljabari, S., & Schmidt, C. E. (2007). Effects of collagen 1, fibronectin, laminin and hyaluronic acid concentration in multi-component gels on neurite extension. *Journal of Biomaterials Science, Polymer Edition*, *18*(8), 983–997. https://doi.org/10.1163/156856207781494377

Delplace, V., Obermeyer, J., & Shoichet, M. S. (2016). Local Affinity Release. *ACS Nano*, *10*(7), 6433–6436. https://doi.org/10.1021/acsnano.6b04308

Designed Research; J, X. L. S. R. (2018). *NT3-chitosan enables de novo regeneration and functional recovery in monkeys after spinal cord injury*. https://doi.org/10.1073/pnas.1804735115

Ding, Y., & Chen, Q. (2022). mTOR pathway: A potential therapeutic target for spinal cord injury. *Biomedicine & Pharmacotherapy*, *145*, 112430. https://doi.org/10.1016/j.biopha.2021.112430

Dizdaroglu, M., Jaruga, P., Birincioglu, M., & Rodriguez, H. (2002). Free radical-induced damage to DNA: mechanisms and measurement. *Free Radic. Biol. Med. Jun*, *32*(11), 1102–1115.

D'Souza, S. E., Ginsberg, M. H., Burke, T. A., Lam, S. C.-T., & Plow, E. F. (1988). Localization of an Arg-Gly-Asp Recognition Site Within an Integrin Adhesion Receptor. *Science*, *242*(4875), 91–93. https://doi.org/10.1126/science.3262922

Dupraz, S., Grassi, D., Karnas, D., Guil, A. F. N., Hicks, D., & Quiroga, S. (2013). The Insulin-Like Growth Factor 1 Receptor Is Essential for Axonal Regeneration in Adult Central Nervous System Neurons. *PLOS ONE*, *8*(1), e54462. https://doi.org/10.1371/journal.pone.0054462

Eleftheriadou, I., Manolaras, I., Irvine, E. E., Dieringer, M., Trabalza, A., & Mazarakis, N. D. (2016). αCAR IGF-1 vector targeting of motor neurons ameliorates disease progression in ALS mice. *Annals of Clinical and Translational Neurology*, *3*(10), 752–768. https://doi.org/10.1002/acn3.335

Elliott Donaghue, I., Tator, C. H., & Shoichet, M. S. (2015). Sustained delivery of bioactive neurotrophin-3 to the injured spinal cord. *Biomaterials Science*, *3*(1), 65–72. https://doi.org/10.1039/C4BM00311J

Elliott Donaghue, I., Tator, C. H., & Shoichet, M. S. (2016). Local Delivery of Neurotrophin-3 and Anti-NogoA Promotes Repair After Spinal Cord Injury. *Tissue Engineering Part A*, *22*(9–10), 733–741. https://doi.org/10.1089/ten.tea.2015.0471

Farrukh, A., Ortega, F., Fan, W., Marichal, N., Paez, J. I., Berninger, B., Campo, A. del, & Salierno, M. J. (2017). Bifunctional Hydrogels Containing the Laminin Motif IKVAV Promote Neurogenesis. *Stem Cell Reports*, *9*(5), 1432–1440. https://doi.org/10.1016/j.stemcr.2017.09.002

Fellows, A. D., Rhymes, E. R., Gibbs, K. L., Greensmith, L., & Schiavo, G. (2020). IGF1R regulates retrograde axonal transport of signalling endosomes in motor neurons. *EMBO Reports*, *21*(3), e49129. https://doi.org/10.15252/embr.201949129

Fernández-Cabada, T., & Ramos-Gómez, M. (2019). A Novel Contrast Agent Based on Magnetic Nanoparticles for Cholesterol Detection as Alzheimer's Disease Biomarker. *Nanoscale Research Letters*, *14*(1), 36. https://doi.org/10.1186/s11671-019-2863-8

Flake, M. M., Nguyen, P. K., Scott, R. A., Vandiver, L. R., Willits, R. K., & Elbert, D. L. (2011). Poly(ethylene glycol) Microparticles Produced by Precipitation Polymerization in Aqueous Solution. *Biomacromolecules*, *12*(3), 844–850. https://doi.org/10.1021/bm1011695

Geissler, S. A., Sabin, A. L., Besser, R. R., Gooden, O. M., Shirk, B. D., Nguyen, Q. M., Khaing, Z. Z., & Schmidt, C. E. (2018). Biomimetic hydrogels direct spinal progenitor cell differentiation and promote functional recovery after spinal cord injury. *Journal of Neural Engineering*, *15*(2), 025004. https://doi.org/10.1088/1741-2552/aaa55c

Genç, B., Özdinler, P. H., Mendoza, A. E., & Erzurumlu, R. S. (2004). A Chemoattractant Role for NT-3 in Proprioceptive Axon Guidance. *PLoS Biology*, *2*(12), e403. https://doi.org/10.1371/journal.pbio.0020403

Haggerty, A. E., Marlow, M. M., & Oudega, M. (2017). Extracellular matrix components as therapeutics for spinal cord injury. *Neuroscience Letters*, *652*, 50–55. https://doi.org/10.1016/j.neulet.2016.09.053

Hammarlund, M., Nix, P., Hauth, L., Jorgensen, E. M., & Bastiani, M. (2009). Axon regeneration requires a conserved MAP kinase pathway. *Science (New York, N.Y.)*, *323*(5915), 802–806. https://doi.org/10.1126/science.1165527

Harrow-Mortelliti, M., Reddy, V., & Jimsheleishvili, G. (2023). Physiology, Spinal Cord. In *StatPearls*. StatPearls Publishing. http://www.ncbi.nlm.nih.gov/books/NBK544267/

Hausmann, O. N. (2003). Post-traumatic inflammation following spinal cord injury. *Spinal Cord*, *2003;41(7):369-378*.

Hellenbrand, D. J., Reichl, K. A., Travis, B. J., Filipp, M. E., Khalil, A. S., Pulito, D. J., Gavigan, A. V., Maginot, E. R., Arnold, M. T., Adler, A. G., Murphy, W. L., & Hanna, A. S. (2019). Sustained interleukin-10 delivery reduces inflammation and improves motor function after spinal cord injury. *Journal of Neuroinflammation*, *16*(1), 93. https://doi.org/10.1186/s12974-019-1479-3

Herculano-Houzel, S. (2017). Numbers of neurons as biological correlates of cognitive capability. *Current Opinion in Behavioral Sciences*, *16*, 1–7. https://doi.org/10.1016/j.cobeha.2017.02.004

Hisaoka, M., Sheng, W. Q., Tanaka, A., & Hashimoto, H. (2002). Gene expression of TrKC (NTRK3) in human soft tissue tumours. *Journal of Pathology*, *197*(5), 661–667. https://doi.org/10.1002/path.1138

Hou, S., Xu, Q., Tian, W., Cui, F., Cai, Q., Ma, J., & Lee, I. S. (2005). The repair of brain lesion by implantation of hyaluronic acid hydrogels modified with laminin. *Journal of Neuroscience Methods*, *148*(1), 60–70. https://doi.org/10.1016/j.jneumeth.2005.04.016

Hu, X., Gao, Z., Tan, H., Wang, H., Mao, X., & Pang, J. (2019). An Injectable Hyaluronic Acid-Based Composite Hydrogel by DA Click Chemistry With pH Sensitive Nanoparticle for Biomedical Application. *Frontiers in Chemistry*, *7*. https://doi.org/10.3389/fchem.2019.00477

Ishihara, J., Ishihara, A., Fukunaga, K., Sasaki, K., White, M. J. V., Briquez, P. S., & Hubbell, J. A. (2018). Laminin heparin-binding peptides bind to several growth factors and enhance diabetic wound healing. *Nature Communications*, *9*(1), 2163. https://doi.org/10.1038/s41467-018-04525-w

Iyer, N. R., Huettner, J. E., Butts, J. C., Brown, C. R., & Sakiyama-Elbert, S. E. (2016). Generation of highly enriched V2a interneurons from mouse embryonic stem cells. *Experimental Neurology*, *277*, 305–316. https://doi.org/10.1016/J.EXPNEUROL.2016.01.011

Iyer, N. R., Wilems, T. S., & Sakiyama-Elbert, S. E. (2017). Stem cells for spinal cord injury: Strategies to inform differentiation and transplantation. *Biotechnology and Bioengineering*, *114*(2), 245–259. https://doi.org/10.1002/bit.26074

Jain, N. B., Ayers, G. D., Peterson, E. N., Harris, M. B., Morse, L., O'Connor, K. C., & Garshick, E. (2015). Traumatic spinal cord injury in the United States, 1993-2012. *JAMA*, *313*(22), 2236–2243. https://doi.org/10.1001/jama.2015.6250

Javvaji, P. K., Dhali, A., Francis, J. R., Kolte, A. P., Roy, S. C., Selvaraju, S., Mech, A., & Sejian, V. (2021). IGF-1 treatment during in vitro maturation improves developmental potential of ovine oocytes through the regulation of PI3K/Akt and apoptosis signaling. *Animal Biotechnology*, *32*(6), 798–805. https://doi.org/10.1080/10495398.2020.1752703

Jessen, N. A., Munk, A. S. F., Lundgaard, I., & Nedergaard, M. (2015). The Glymphatic System: A Beginner's Guide. *Neurochemical Research*, *40*(12), 2583–2599. https://doi.org/10.1007/s11064-015-1581-6

Johnson, P. J., Parker, S. R., & Sakiyama-Elbert, S. E. (2009). Controlled release of neurotrophin-3 from fibrin-based tissue engineering scaffolds enhances neural fiber sprouting following subacute spinal cord injury. *Biotechnology and Bioengineering*, *104*(6), 1207–1214. https://doi.org/10.1002/bit.22476

Johnson, P. J., Tatara, A., Shiu, A., & Sakiyama-Elbert, S. E. (2010). Controlled Release of Neurotrophin-3 and Platelet-Derived Growth Factor from Fibrin Scaffolds Containing Neural Progenitor Cells Enhances Survival and Differentiation into Neurons in a Subacute Model of SCI. *Cell Transplantation*, *19*(1), 89–101. https://doi.org/10.3727/096368909X477273

Kadoya, K., Lu, P., Nguyen, K., Lee-Kubli, C., Kumamaru, H., Yao, L., Knackert, J., Poplawski, G., Dulin, J. N., Strobl, H., Takashima, Y., Biane, J., Conner, J., Zhang, S.-C., & Tuszynski, M. H. (2016). Spinal cord reconstitution with homologous neural

grafts enables robust corticospinal regeneration. *Nature Medicine*, *22*(5), 479–487. https://doi.org/10.1038/nm.4066

Kaspar, B. K., Lladó, J., Sherkat, N., Rothstein, J. D., & Gage, F. H. (2003). Retrograde Viral Delivery of IGF-1 Prolongs Survival in a Mouse ALS Model. *Science*, *301*(5634), 839–842. https://doi.org/10.1126/science.1086137

Keefe, K. M., Sheikh, I. S., & Smith, G. M. (2017). Targeting Neurotrophins to Specific Populations of Neurons: NGF, BDNF, and NT-3 and Their Relevance for Treatment of Spinal Cord Injury. *International Journal of Molecular Sciences*, *18*(3). https://doi.org/10.3390/ijms18030548

Khademhosseini, A., & Langer, R. (2007). Microengineered hydrogels for tissue engineering. *Biomaterials*, *28*(34), 5087–5092. https://doi.org/10.1016/j.biomaterials.2007.07.021

Koffler, J., Zhu, W., Qu, X., Platoshyn, O., Dulin, J. N., Brock, J., Graham, L., Lu, P., Sakamoto, J., Marsala, M., Chen, S., & Tuszynski, M. H. (2019). Biomimetic 3D-printed scaffolds for spinal cord injury repair. *Nature Medicine*, *25*, 263–269. https://doi.org/10.1038/s41591-018-0296-z

Kolbeck, R., Jungbluth, S., & Barde, Y. -A. (1994). Characterisation of Neurotrophin Dimers and Monomers. *European Journal of Biochemistry*, *225*(3), 995–1003. https://doi.org/10.1111/j.1432-1033.1994.0995b.x

Kumamaru, H., Lu, P., Rosenzweig, E. S., Kadoya, K., & Tuszynski, M. H. (2019). Regenerating Corticospinal Axons Innervate Phenotypically Appropriate Neurons within Neural Stem Cell Grafts. *Cell Reports*. https://doi.org/10.1016/j.celrep.2019.01.099

Labouyrie, E., Dubus, P., Groppi, A., Mahon, F. X., Ferrer, J., Parrens, M., Reiffers, J., De Mascarel, A., & Merlio, J. P. (1999). Expression of neurotrophins and their receptors in human bone marrow. *American Journal of Pathology*, *154*(2), 405–415. https://doi.org/10.1016/S0002-9440(10)65287-X

LaMer, V. K., & Dinegar, R. H. (1950). Theory, Production and Mechanism of Formation of Monodispersed Hydrosols. *Journal of the American Chemical Society*, *72*(11), 4847–4854. https://doi.org/10.1021/ja01167a001

Lampe, K. J., Antaris, A. L., & Heilshorn, S. C. (2013). Design of three-dimensional engineered protein hydrogels for tailored control of neurite growth. *Acta Biomaterialia*, *9*(3), 5590–5599. https://doi.org/10.1016/j.actbio.2012.10.033

Lasfargues, J. E., Custis, D., Morrone, F., Carswell, J., & Nguyen, T. (1995). A model for estimating spinal cord injury prevalence in the United States. *Paraplegia*, *33*(2), 62–68. https://doi.org/10.1038/sc.1995.16

Lau, L. W., Cua, R., Keough, M. B., Haylock-Jacobs, S., & Yong, V. W. (2013). Pathophysiology of the brain extracellular matrix: A new target for remyelination. *Nature Reviews Neuroscience*, *14*(10), Article 10. https://doi.org/10.1038/nrn3550

Laurino, L., Wang, X. X., de la Houssaye, B. A., Sosa, L., Dupraz, S., Cáceres, A., Pfenninger, K. H., & Quiroga, S. (2005). PI3K activation by IGF-1 is essential for the regulation of membrane expansion at the nerve growth cone. *Journal of Cell Science*, *118*(16), 3653–3662. https://doi.org/10.1242/jcs.02490

Lee, K. Y., & Mooney, D. J. (2001). Hydrogels for Tissue Engineering. *Chemical Reviews*, *101*(7), 1869–1880. https://doi.org/10.1021/cr000108x

Li, J., & Mooney, D. J. (2016). Designing hydrogels for controlled drug delivery. *Nature Reviews Materials*, *1*(12), Article 12. https://doi.org/10.1038/natrevmats.2016.71

Li, R., Wu, Y., & Jiang, D. (2016). NT-3 attenuates the growth of human neuron cells through the ERK pathway. *Cytotechnology*, *68*(4), 659–664. https://doi.org/10.1007/s10616-014-9813-1

Liu, C., Liu, S., Wang, S., Sun, Y., Lu, X., Li, H., & Li, G. (2019). IGF-1 Via PI3K/Akt/S6K Signaling Pathway Protects DRG Neurons with High Glucose-induced Toxicity. *Open Life Sciences*, *14*, 502–514. https://doi.org/10.1515/biol-2019-0056

Liu, K., Lu, Y., Lee, J. K., Samara, R., Willenberg, R., Sears-Kraxberger, I., Tedeschi, A., Park, K. K., Jin, D., Cai, B., Xu, B., Connolly, L., Steward, O., Zheng, B., & He, Z. (2010). PTEN deletion enhances the regenerative ability of adult corticospinal neurons. *Nature Neuroscience*, *13*(9), 1075–1081. https://doi.org/10.1038/nn.2603

Lorach, H., Galvez, A., Spagnolo, V., Martel, F., Karakas, S., Intering, N., Vat, M., Faivre, O., Harte, C., Komi, S., Ravier, J., Collin, T., Coquoz, L., Sakr, I., Baaklini, E., Hernandez-Charpak, S. D., Dumont, G., Buschman, R., Buse, N., … Courtine, G. (2023). Walking naturally after spinal cord injury using a brain–spine interface. *Nature*, *618*(7963), Article 7963. https://doi.org/10.1038/s41586-023-06094-5

Lu, D. C., Niu, T., & Alaynick, W. A. (2015). Molecular and cellular development of spinal cord locomotor circuitry. *Frontiers in Molecular Neuroscience*, *8*(June), 1–18. https://doi.org/10.3389/fnmol.2015.00025

Ma, X., & Bai, Y. (2012). IGF-1 activates the P13K/AKT signaling pathway via upregulation of secretory clusterin. *Molecular Medicine Reports*, *6*(6), 1433–1437. https://doi.org/10.3892/mmr.2012.1110

Maisonpierre, P. C., Belluscio, L., Squinto, S., Nancy, Y., Furth, M. E., Lindsay, R. M., & Yancopoulos, G. D. (1990). Neurotrophin-3: Related to Neurotrophic Factor. *Science*, *247*(10), 1446–1451.

Martini, M., Hegger, P. S., Schädel, N., Minsky, B. B., Kirchhof, M., Scholl, S., Southan, A., Tovar, G. E. M., Boehm, H., & Laschat, S. (2016). Charged Triazole Cross-Linkers for Hyaluronan-Based Hybrid Hydrogels. *Materials*, *9*(10), 810. https://doi.org/10.3390/ma9100810

Matson, K. J. E., Russ, D. E., Kathe, C., Hua, I., Maric, D., Ding, Y., Krynitsky, J., Pursley, R., Sathyamurthy, A., Squair, J. W., Levi, B. P., Courtine, G., & Levine, A. J. (2022). Single cell atlas of spinal cord injury in mice reveals a pro-regenerative signature in spinocerebellar neurons. *Nature Communications*, *13*(1), Article 1. https://doi.org/10.1038/s41467-022-33184-1

Mattucci, S., Speidel, J., Liu, J., Kwon, B. K., Tetzlaff, W., & Oxland, T. R. (2019). Basic biomechanics of spinal cord injury—How injuries happen in people and how animal models have informed our understanding. *Clinical Biomechanics*, *64*, 58–68. https://doi.org/10.1016/j.clinbiomech.2018.03.020

Mccreedy, D. A., Brown, C. R., Butts, J. C., Xu, H., Huettner, J. E., & Sakiyama-Elbert, S. E. (2014). A new method for generating high purity motoneurons from mouse embryonic stem cells. *Biotechnology and Bioengineering*, *111*(10), 2041–2055. https://doi.org/10.1002/bit.25260

McCreedy, D. A., Brown, C. R., Butts, J. C., Xu, H., Huettner, J. E., & Sakiyama-Elbert, S. E. (2014). A new method for generating high purity motoneurons from mouse embryonic stem cells. *Biotechnology and Bioengineering*, *111*(10), 2041–2055. https://doi.org/10.1002/bit.25260

McCreedy, D. A., Rieger, C. R., Gottlieb, D. I., & Sakiyama-Elbert, S. E. (2012). Transgenic enrichment of mouse embryonic stem cell-derived progenitor motor neurons. *Stem Cell Research*, *8*(3), 368–378. https://doi.org/10.1016/j.scr.2011.12.003

Menu, E., Kooijman, R., Valckenborgh, E. V., Asosingh, K., Bakkus, M., Camp, B. V., & Vanderkerken, K. (2004). Specific roles for the PI3K and the MEK–ERK pathway in IGF-1-stimulated chemotaxis, VEGF secretion and proliferation of multiple myeloma cells: Study in the 5T33MM model. *British Journal of Cancer*, *90*(5), 1076. https://doi.org/10.1038/sj.bjc.6601613

Mullen, L. M., Best, S. M., Ghose, S., Wardale, J., Rushton, N., & Cameron, R. E. (2015). Bioactive IGF-1 release from collagen–GAG scaffold to enhance cartilage repair in vitro. *Journal of Materials Science: Materials in Medicine*, *26*(1), 2. https://doi.org/10.1007/s10856-014-5325-y

Musarò, A., Dobrowolny, G., & Rosenthal, N. (2007). The neuroprotective effects of a locally acting IGF-1 isoform. *Experimental Gerontology*, *42*(1), 76–80. https://doi.org/10.1016/j.exger.2006.05.004

Nakamura, M., Houghtling, R. A., MacArthur, L., Bayer, B. M., & Bregman, B. S. (2003). Differences in cytokine gene expression profile between acute and secondary injury in adult rat spinal cord. *Experimental Neurology*, *184*(1), 313–325. https://doi.org/10.1016/S0014-4886(03)00361-3

Namiki, J., Kojima, A., & Tator, C. H. (2000). Effect of brain-derived neurotrophic factor nerve growth factor and neurotrophin-3 on functional recovery and regeneration after spinal cord injury in adult rats. *Journal of Neurotrauma*, *17*(12), 1219–1231. https://doi.org/10.1089/neu.2000.17.1219

Nance, E., Pun, S. H., Saigal, R., & Sellers, D. L. (2022). Drug delivery to the central nervous system. *Nature Reviews Materials*, *7*(4), Article 4. https://doi.org/10.1038/s41578-021-00394-w

Nathan, P. W., & Smith, M. C. (1955). Long descending tracts in man. I. Review of present knowledge. *Brain: A Journal of Neurology*, *78*(2), 248–303. https://doi.org/10.1093/brain/78.2.248

National Spinal Cord Injury Statistical Center, Facts and Figures at a Glance. Birmingham, AL: University of Alabama at Birmingham, 2019. (n.d.).

National Spinal Cord Injury Statistical Center, Traumatic Spinal Cord Injury Facts and Figures at a Glance. Birmingham, AL: University of Alabama at Birmingham. (2023).

Nguyen, L. H., Gao, M., Lin, J., Wu, W., Wang, J., & Chew, S. Y. (2017). Three-dimensional aligned nanofibers-hydrogel scaffold for controlled non-viral drug/gene delivery to direct axon regeneration in spinal cord injury treatment. *Scientific Reports*, *7*(1), 42212. https://doi.org/10.1038/srep42212

Nih, L. R., Gojgini, S., Carmichael, S. T., & Segura, T. (2018). Dual-function injectable angiogenic biomaterial for the repair of brain tissue following stroke. *Nature Materials*, *17*(7), 642–651. https://doi.org/10.1038/s41563-018-0083-8

Nimmo, C. M., Owen, S. C., & Shoichet, M. S. (2011). Diels-alder click cross-linked hyaluronic acid hydrogels for tissue engineering. *Biomacromolecules*, *12*(3), 824–830. https://doi.org/10.1021/bm101446k

O'Shea, T. M., Burda, J. E., & Sofroniew, M. V. (2017). Cell biology of spinal cord injury and repair. *The Journal of Clinical Investigation*, *127*(9), 3259–3270. https://doi.org/10.1172/JCI90608

Oudega, M., Hao, P., Shang, J., Haggerty, A. E., Wang, Z., Sun, J., Liebl, D. J., Shi, Y., Cheng, L., Duan, H., Sun, Y. E., Li, X., & Lemmon, V. P. (2019). Validation study of neurotrophin-3-releasing chitosan facilitation of neural tissue generation in the severely injured adult rat spinal cord. *Experimental Neurology*, *312*, 51–62. https://doi.org/10.1016/j.expneurol.2018.11.003

Ozawa, H., Matsumoto, T., Ohashi, T., Sato, M., & Kokubun, S. (2004). Mechanical properties and function of the spinal pia mater. *Journal of Neurosurgery: Spine*, *1*(1), 122–127. https://doi.org/10.3171/spi.2004.1.1.0122

Özdinler, P. H., & Macklis, J. D. (2006). IGF-I specifically enhances axon outgrowth of corticospinal motor neurons. *Nature Neuroscience*, *9*(11), 1371–1381. https://doi.org/10.1038/nn1789

Pakulska, M. M., Ballios, B. G., & Shoichet, M. S. (2012). Injectable hydrogels for central nervous system therapy. *Biomedical Materials*, *7*(2), 024101. https://doi.org/10.1088/1748-6041/7/2/024101

Pakulska, M. M., Elliott Donaghue, I., Obermeyer, J. M., Tuladhar, A., McLaughlin, C. K., Shendruk, T. N., & Shoichet, M. S. (2016). Encapsulation-free controlled release: Electrostatic adsorption eliminates the need for protein encapsulation in PLGA nanoparticles. *Science Advances*, *2*(5), e1600519. https://doi.org/10.1126/sciadv.1600519

Pan, S., Qi, Z., Li, Q., Ma, Y., Fu, C., Zheng, S., Kong, W., Liu, Q., & Yang, X. (2019). Graphene oxide-PLGA hybrid nanofibres for the local delivery of IGF-1 and BDNF in spinal cord repair. *Artificial Cells, Nanomedicine, and Biotechnology*, *47*(1), 650–663. https://doi.org/10.1080/21691401.2019.1575843

Papa, S., Rossi, F., Vismara, I., Forloni, G., & Veglianese, P. (2019). Nanovector-Mediated Drug Delivery in Spinal Cord Injury: A Multitarget Approach. *ACS Chemical Neuroscience*, *10*(3), 1173–1182. https://doi.org/10.1021/acschemneuro.8b00700

Park, J., Lim, E., Back, S., Na, H., Park, Y., & Sun, K. (2010). Nerve regeneration following spinal cord injury using matrix metalloproteinase-sensitive, hyaluronic acid-based biomimetic hydrogel scaffold containing brain-derived neurotrophic factor. *Journal of Biomedical Materials Research - Part A*, *93*(3), 1091–1099. https://doi.org/10.1002/jbm.a.32519

Park, K. K., Liu, K., Hu, Y., Smith, P. D., Wang, C., Cai, B., Xu, B., Connolly, L., Kramvis, I., Sahin, M., & He, Z. (2008). Promoting Axon Regeneration in the Adult CNS by Modulation of the PTEN/mTOR Pathway. *Science*, *322*(5903), 963–966. https://doi.org/10.1126/science.1161566

Patterson, J., & Hubbell, J. A. (2010). Enhanced proteolytic degradation of molecularly engineered PEG hydrogels in response to MMP-1 and MMP-2. *Biomaterials*, *31*(30), 7836–7845. https://doi.org/10.1016/j.biomaterials.2010.06.061

Peppas, N. A., Bures, P., Leobandung, W., & Ichikawa, H. (2000). Hydrogels in pharmaceutical formulations. *European Journal of Pharmaceutics and Biopharmaceutics*, *50*(1), 27–46. https://doi.org/10.1016/S0939-6411(00)00090-4

Peppas, N. A., Hilt, J. Z., Khademhosseini, A., & Langer, R. (2006). Hydrogels in biology and medicine: From molecular principles to bionanotechnology. *Advanced Materials*, *18*(11), 1345–1360. https://doi.org/10.1002/adma.200501612

Pierschbacher, M. D., & Ruoslahti, E. (1984). Cell attachment activity of fibronectin can be duplicated by small synthetic fragments of the molecule. *Nature*, *309*(5963), 30–33. https://doi.org/10.1038/309030a0

Potenzone, R., & Hopfinger, A. J. (1978). Conformational Analysis of Glycosaminoglycans. III. Conformational Properties of Hyaluronic Acid and Sodium Hyaluronate. *Polymer Journal*, *10*(2), 181–199. https://doi.org/10.1295/polymj.10.181

Ramer, M. S., Bishop, T., Dockery, P., Mobarak, M. S., O'Leary, D., Fraher, J. P., Priestley, J. V., & McMahon, S. B. (2002). Neurotrophin-3-mediated regeneration and recovery of proprioception following dorsal rhizotomy. *Molecular and Cellular Neuroscience*, *19*(2), 239–249. https://doi.org/10.1006/mcne.2001.1067

Ramos Ferrer, P., Vardhan, S., & Sakiyama-Elbert, S. (2023). Sustained neurotrophin-3 delivery from hyaluronic acid hydrogels for neural tissue regeneration. *Journal of Biomedical Materials Research. Part A*. https://doi.org/10.1002/jbm.a.37596

Rao, J.-S., Zhao, C., Zhang, A., Duan, H., Hao, P., Wei, R.-H., Shang, J., Zhao, W., Liu, Z., Yu, J., Fan, K. S., Tian, Z., He, Q., Song, W., Yang, Z., Sun, Y. E., & Li, X. (2018). NT3-chitosan enables de novo regeneration and functional recovery in monkeys after spinal cord injury. *Proceedings of the National Academy of Sciences*, *115*(24), E5595–E5604. https://doi.org/10.1073/pnas.1804735115

Rehmann, M. S., Skeens, K. M., Kharkar, P. M., Ford, E. M., Maverakis, E., Lee, K. H., & Kloxin, A. M. (2017). Tuning and Predicting Mesh Size and Protein Release from

Step Growth Hydrogels. *Biomacromolecules*, *18*(10), 3131–3142. https://doi.org/10.1021/acs.biomac.7b00781

Rexed, B. (1952). The cytoarchitectonic organization of the spinal cord in the cat. *The Journal of Comparative Neurology*, *96*(3), 414–495. https://doi.org/10.1002/cne.900960303

Rizwan, M., Yahya, R., Hassan, A., Yar, M., Azzahari, A. D., Selvanathan, V., Sonsudin, F., & Abouloula, C. N. (2017). pH Sensitive Hydrogels in Drug Delivery: Brief History, Properties, Swelling, and Release Mechanism, Material Selection and Applications. *Polymers*, *9*(4), Article 4. https://doi.org/10.3390/polym9040137

Rose, J. C., Gehlen, D. B., Haraszti, T., Köhler, J., Licht, C. J., & De Laporte, L. (2018). Biofunctionalized aligned microgels provide 3D cell guidance to mimic complex tissue matrices. *Biomaterials*, *163*, 128–141. https://doi.org/10.1016/J.BIOMATERIALS.2018.02.001

Ruoslahti, E., & Pierschbacher, M. D. (1987). New Perspectives in Cell Adhesion: RGD and Integrins. *Science*, *238*(4826), 491–497. https://doi.org/10.1126/science.2821619

Rutka, J. T., Apodaca, G., Stern, R., & Rosenblum, M. (1988). The extracellular matrix of the central and peripheral nervous systems: Structure and function. *Journal of Neurosurgery*, *69*(2), 155–170. https://doi.org/10.3171/jns.1988.69.2.0155

Salie, R., & Steeves, J. D. (2005). IGF-1 and BDNF promote chick bulbospinal neurite outgrowth in vitro. *International Journal of Developmental Neuroscience*, *23*(7), 587–598. https://doi.org/10.1016/j.ijdevneu.2005.07.003

Sau, S., Alsaab, H. O., Bhise, K., Alzhrani, R., Nabil, G., & Iyer, A. K. (2018). Multifunctional nanoparticles for cancer immunotherapy: A groundbreaking approach for

reprogramming malfunctioned tumor environment. *Journal of Controlled Release*, *274*(January), 24–34. https://doi.org/10.1016/j.jconrel.2018.01.028

Savio, T., & Schwab, M. E. (1989). Rat CNS white matter, but not gray matter, is nonpermissive for neuronal cell adhesion and fiber outgrowth. *Journal of Neuroscience*, *9*(4), 1126–1133. https://doi.org/10.1523/JNEUROSCI.09-04-01126.1989

Seidlits, S. K., Khaing, Z. Z., Petersen, R. R., Nickels, J. D., Vanscoy, J. E., Shear, J. B., & Schmidt, C. E. (2010). The effects of hyaluronic acid hydrogels with tunable mechanical properties on neural progenitor cell differentiation. *Biomaterials*, *31*(14), 3930–3940. https://doi.org/10.1016/J.BIOMATERIALS.2010.01.125

Seliktar, D., Zisch, A. H., Lutolf, M. P., Wrana, J. L., & Hubbell, J. A. (2004). MMP-2 sensitive, VEGF-bearing bioactive hydrogels for promotion of vascular healing. *Journal of Biomedical Materials Research Part A*, *68A*(4), 704–716. https://doi.org/10.1002/jbm.a.20091

Shibata, T., Tashiro, S., Shibata, S., Shinozaki, M., Shindo, T., Hashimoto, S., Kawai, M., Kitagawa, T., Ago, K., Matsumoto, M., Nakamura, M., Okano, H., & Nagoshi, N. (2023). Rehabilitative Training Enhances Therapeutic Effect of Human iPSC-Derived Neural Stem/Progenitor Cells Transplantation in Chronic Spinal Cord Injury. *Stem Cells Translational Medicine*, *12*(2), 83–96. https://doi.org/10.1093/stcltm/szac089

Silver, J., & Miller, J. H. (2004). Regeneration beyond the glial scar. *Nature Reviews Neuroscience*, *5*(2), Article 2. https://doi.org/10.1038/nrn1326

Smith, L. J., Taimoory, S. M., Tam, R. Y., Baker, A. E. G., Binth Mohammad, N., Trant, J. F., & Shoichet, M. S. (2018). Diels–Alder Click-Cross-Linked Hydrogels with Increased Reactivity Enable 3D Cell Encapsulation. *Biomacromolecules*, *19*(3), 926–935. https://doi.org/10.1021/acs.biomac.7b01715

Stanwick, J. C., Baumann, M. D., & Shoichet, M. S. (2012). Enhanced neurotrophin-3 bioactivity and release from a nanoparticle-loaded composite hydrogel. *Journal of Controlled Release*, *160*(3), 666–675. https://doi.org/10.1016/J.JCONREL.2012.03.024

Sun, F., Park, K. K., Belin, S., Wang, D., Lu, T., Chen, G., Zhang, K., Yeung, C., Feng, G., Yankner, B. A., & He, Z. (2011). Sustained axon regeneration induced by co-deletion of PTEN and SOCS3. *Nature*, *480*(7377), 372–375. https://doi.org/10.1038/nature10594

Tan, S., Faull, R. L. M., & Curtis, M. A. (2023). The tracts, cytoarchitecture, and neurochemistry of the spinal cord. *The Anatomical Record*, *306*(4), 777–819. https://doi.org/10.1002/ar.25079

Tang, S., Liao, X., Shi, B., Qu, Y., Huang, Z., Lin, Q., Guo, X., & Pei, F. (2014). The Effects of Controlled Release of Neurotrophin-3 from PCLA Scaffolds on the Survival and Neuronal Differentiation of Transplanted Neural Stem Cells in a Rat Spinal Cord Injury Model. *PLoS ONE*, *9*(9), e107517. https://doi.org/10.1371/journal.pone.0107517

Tay, A., Sohrabi, A., Poole, K., Seidlits, S., & Di Carlo, D. (2018). A 3D Magnetic Hyaluronic Acid Hydrogel for Magnetomechanical Neuromodulation of Primary Dorsal Root Ganglion Neurons. *Advanced Materials*, *30*(29), 1800927. https://doi.org/10.1002/adma.201800927

Taylor, L., Jones, L., Tuszynski, M. H., & Blesch, A. (2006). Neurotrophin-3 gradients established by lentiviral gene delivery promote short-distance axonal bridging beyond cellular grafts in the injured spinal cord. *Journal of Neuroscience*, *26*(38), 9713–9721. https://doi.org/10.1523/JNEUROSCI.0734-06.2006

Taylor, S. J., McDonald, J. W., & Sakiyama-Elbert, S. E. (2004). Controlled release of neurotrophin-3 from fibrin gels for spinal cord injury. *Journal of Controlled Release*, *98*(2), 281–294. https://doi.org/10.1016/J.JCONREL.2004.05.003

Taylor, S. J., & Sakiyama-Elbert, S. E. (2006). Effect of controlled delivery of neurotrophin-3 from fibrin on spinal cord injury in a long term model. *Journal of Controlled Release*, *116*(2), 204–210. https://doi.org/10.1016/j.jconrel.2006.07.005

Thompson, R. E., Pardieck, J., Smith, L., Kenny, P., Crawford, L., Shoichet, M. S., & Sakiyama-Elbert, S. (2018). Effect of hyaluronic acid hydrogels containing astrocyte-derived extracellular matrix and/or V2a interneurons on histologic outcomes following spinal cord injury. *Biomaterials*, *162*, 208–223. https://doi.org/10.1016/J.BIOMATERIALS.2018.02.013

Tsai, L.-K., Chen, Y.-C., Cheng, W.-C., Ting, C.-H., Dodge, J. C., Hwu, W.-L., Cheng, S. H., & Passini, M. A. (2012). IGF-1 delivery to CNS attenuates motor neuron cell death but does not improve motor function in type III SMA mice. *Neurobiology of Disease*, *45*(1), 272–279. https://doi.org/10.1016/j.nbd.2011.06.021

Tsaryk, R., Gloria, A., Russo, T., Anspach, L., De Santis, R., Ghanaati, S., Unger, R. E., Ambrosio, L., & Kirkpatrick, C. J. (2015). Collagen-low molecular weight hyaluronic acid semi-interpenetrating network loaded with gelatin microspheres for cell and growth factor delivery for nucleus pulposus regeneration. *Acta Biomaterialia*, *20*, 10–21. https://doi.org/10.1016/J.ACTBIO.2015.03.041

Tuszynski, M. H., & Steward, O. (2012). Concepts and Methods for the Study of Axonal Regeneration in the CNS. *Neuron*, *74*(5), 777–791. https://doi.org/10.1016/j.neuron.2012.05.006

Tuttle, R., & Matthew, W. D. (1995). Neurotrophins affect the pattern of DRG neurite growth in a bioassay that presents a choice of CNS and PNS substrates. *Development*, *121*(5), 1301–1309.

Urferl, R., Tsoulfas2', P., Soppet2, D., Escandon4, E., Parada2', L. F., & Presta, L. G. (1994). The binding epitopes of neurotrophin-3 to its receptors trkC and gp75 and the design of a multifunctional human neurotrophin. In *The EMBO Journal* (Vol. 13, Issue 24, pp. 5896–5909).

Vandenabeele, F., Creemers, J., & Lambrichts, I. (1996). Ultrastructure of the human spinal arachnoid mater and dura mater. *Journal of Anatomy*, *189*(Pt 2), 417–430.

Vulic, K., Pakulska, M. M., Sonthalia, R., Ramachandran, A., & Shoichet, M. S. (2015). Mathematical model accurately predicts protein release from an affinity-based delivery system. *Journal of Controlled Release*, *197*, 69–77. https://doi.org/10.1016/j.jconrel.2014.10.032

Wagner, A. M., Gran, M. P., & Peppas, N. A. (2018). Designing the new generation of intelligent biocompatible carriers for protein and peptide delivery. *Acta Pharmaceutica Sinica B*, *8*(2), 147–164. https://doi.org/10.1016/j.apsb.2018.01.013

Wang, N. X., & von Recum, H. A. (2011). Affinity-Based Drug Delivery. *Macromolecular Bioscience*, *11*(3), 321–332. https://doi.org/10.1002/mabi.201000206

Wanselius, M., Rodler, A., Searle, S. S., Abrahmsén-Alami, S., & Hansson, P. (2022). Responsive Hyaluronic Acid–Ethylacrylamide Microgels Fabricated Using Microfluidics Technique. *Gels*, *8*(9), Article 9. https://doi.org/10.3390/gels8090588

Waxman, S. G. (1989). Demyelination in spinal cord injury. *Journal of the Neurological Sciences*, *91*(1–2), 1–14.

Wheeler-Kingshott, C. A. M., Hickman, S. J., Parker, G. J. M., Ciccarelli, O., Symms, M. R., Miller, D. H., & Barker, G. J. (2002). Investigating Cervical Spinal Cord Structure Using Axial Diffusion Tensor Imaging. *NeuroImage*, *16*(1), 93–102. https://doi.org/10.1006/nimg.2001.1022

Wichmann, T. O., Damkier, H. H., & Pedersen, M. (2022). A Brief Overview of the Cerebrospinal Fluid System and Its Implications for Brain and Spinal Cord Diseases. *Frontiers in Human Neuroscience*, *15*. https://www.frontiersin.org/articles/10.3389/fnhum.2021.737217

Wilems, T. S., & Sakiyama-Elbert, S. E. (2015). Sustained dual drug delivery of anti-inhibitory molecules for treatment of spinal cord injury. *Journal of Controlled Release*, *213*, 103–111. https://doi.org/10.1016/J.JCONREL.2015.06.031

Willerth, S. M., & Sakiyama-Elbert, S. E. (2009). Kinetic Analysis of Neurotrophin-3–Mediated Differentiation of Embryonic Stem Cells into Neurons. *Tissue Engineering Part A*, *15*(2), 307–318. https://doi.org/10.1089/ten.tea.2008.0071

Wolf, K. J., & Kumar, S. (2019). Hyaluronic Acid: Incorporating the Bio into the Material. *ACS Biomaterials Science & Engineering*. https://doi.org/10.1021/acsbiomaterials.8b01268

Wuttke, T. V., Markopoulos, F., Padmanabhan, H., Wheeler, A. P., Murthy, V. N., & Macklis, J. D. (2018). Developmentally primed cortical neurons maintain fidelity of differentiation and establish appropriate functional connectivity after transplantation. *Nature Neuroscience*, *21*(April). https://doi.org/10.1038/s41593-018-0098-0

Xu, L., Qiu, L., Sheng, Y., Sun, Y., Deng, L., Li, X., Bradley, M., & Zhang, R. (2018). Biodegradable pH-responsive hydrogels for controlled dual-drug release. *Journal of Materials Chemistry B*, *6*(3), 510–517. https://doi.org/10.1039/C7TB01851G

Yang, Z., Duan, H., Mo, L., Qiao, H., & Li, X. (2010). The effect of the dosage of NT-3/chitosan carriers on the proliferation and differentiation of neural stem cells. *Biomaterials*, *31*(18), 4846–4854. https://doi.org/10.1016/J.BIOMATERIALS.2010.02.015

Yoon, H. Y., Selvan, S. T., Yang, Y., Kim, M. J., Yi, D. K., Kwon, I. C., & Kim, K. (2018). Engineering nanoparticle strategies for effective cancer immunotherapy. *Biomaterials*, *178*, 597–607. https://doi.org/10.1016/j.biomaterials.2018.03.036

Yu, F., Cao, X., Li, Y., Zeng, L., Yuan, B., & Chen, X. (2014). An injectable hyaluronic acid/PEG hydrogel for cartilage tissue engineering formed by integrating enzymatic crosslinking and Diels–Alder "click chemistry." *Polymer Chemistry*, *5*(3), 1082–1090. https://doi.org/10.1039/C3PY00869J

Zhang, Y., Moerkens, M., Ramaiahgari, S., de Bont, H., Price, L., Meerman, J., & van de Water, B. (2011). Elevated insulin-like growth factor 1 receptor signaling induces antiestrogen resistance through the MAPK/ERK and PI3K/Akt signaling routes. *Breast Cancer Research*, *13*(3), R52. https://doi.org/10.1186/bcr2883

Zhao, Q., Su, H., Jiang, W., Luo, H., Pan, L., Liu, Y., Yang, C., Yin, Y., Yu, L., & Tan, B. (2023). IGF-1 Combined with OPN Promotes Neuronal Axon Growth in Vitro Through the IGF-1R/Akt/mTOR Signaling Pathway in Lipid Rafts. *Neurochemical Research*. https://doi.org/10.1007/s11064-023-03971-3

Zhao, Y., Ji, T., Wang, H., Li, S., Zhao, Y., & Nie, G. (2014). Self-assembled peptide nanoparticles as tumor microenvironment activatable probes for tumor targeting and imaging. *Journal of Controlled Release*, *177*, 11–19. https://doi.org/10.1016/j.jconrel.2013.12.037

Zheng, B., & Tuszynski, M. H. (2023). Regulation of axonal regeneration after mammalian spinal cord injury. *Nature Reviews Molecular Cell Biology*, 1–18. https://doi.org/10.1038/s41580-022-00562-y

Zhou, L., Baumgartner, B. J., Hill-Felberg, S. J., McGowen, L. R., & Shine, H. D. (2003). Neurotrophin-3 expressed in situ induces axonal plasticity in the adult injured spinal cord. *Journal of Neuroscience*, *23*(4), 1424–1431. https://doi.org/10.1523/jneurosci.23-04-01424.2003

Ziemba, A. M., & Gilbert, R. J. (2017). Biomaterials for Local, Controlled Drug Delivery to the Injured Spinal Cord. *Frontiers in Pharmacology*, *8*, 245. https://doi.org/10.3389/fphar.2017.00245

Zipser, C. M., Cragg, J. J., Guest, J. D., Fehlings, M. G., Jutzeler, C. R., Anderson, A. J., & Curt, A. (2022). Cell-based and stem-cell-based treatments for spinal cord injury: Evidence from clinical trials. *The Lancet Neurology*, *21*(7), 659–670. https://doi.org/10.1016/S1474-4422(21)00464-6

Zuidema, J. M., Dumont, C. M., Wang, J., Batchelor, W. M., Lu, Y.-S., Kang, J., Bertucci, A., Ziebarth, N. M., Shea, L. D., & Sailor, M. J. (2020). Porous Silicon Nanoparticles Embedded in Poly(lactic-co-glycolic acid) Nanofiber Scaffolds Deliver Neurotrophic Payloads to Enhance Neuronal Growth. *Advanced Functional Materials*, *30*(25), 2002560. https://doi.org/10.1002/adfm.202002560